Elsevier Editorial System(tm) for Energy Conversion and Management

Manuscript Draft

Manuscript Number: ECM-D-18-05037R1

Title: Performance analysis and optimization of a combined cooling and power system using low boiling point working fluid driven by engine waste heat

Article Type: Original research paper

Section/Category: 1. Energy Conservation and Efficient Utilization

Keywords: Internal combustion engine; Brayton cycle; Waste heat recovery; Dual-pressure organic Rankine cycle; Ejector refrigeration cycle; Optimization

Corresponding Author: Dr. Jiangfeng Wang, Ph.D.

Corresponding Author's Institution: Xi'an Jiaotong University

First Author: Wenge Huang

Order of Authors: Wenge Huang; Jiangfeng Wang, Ph.D.; Jiaxi Xia; Pan Zhao, Ph.D.; Yiping Dai

Abstract: This paper develops a combined cooling and power system, which consists of a carbon dioxide Brayton cycle, a dual-pressure organic Rankine cycle and an ejector refrigeration cycle, to recover waste heat from exhaust gas and jacket water in internal combustion engines. Thermodynamic models of the system are performed and exergoeconomic methods are used to calculate the levelized exergy cost of the component products. Effects of seven parameters, including Brayton cycle turbine inlet temperature and inlet pressure, organic Rankine cycle turbine high-pressure side and low-pressure side inlet temperature and ejector primary inlet pressure, are evaluated. Single-objective optimization is carried out by means of genetic algorithm to obtain the minimum levelized exergy cost of system product. Results show that the increase of pressure at Brayton cycle turbine inlet and high-pressure and low-pressure side of the organic Rankine cycle turbine inlet contributes to the decrease of levelized exergy cost of the system product. Optimization results show that minimum levelized exergy cost for system product is 53.25 $ (MWh)-1. When system product levelized exergy cost is minimum, system net power output, cooling capacity and exergy efficiency are 374.37 kW, 188.63 kW and 37.31%, respectively.

Dear Editor:

We are sending a manuscript entitled “Performance analysis and optimization of a combined cooling and power system using low boiling point working fluid driven by engine waste heat”, which we should like to submit for publication in Energy Conversion and Management. We investigate a combined cooling and power system driven by exhaust gas and jacket water from an internal combustion engine. The mathematical model of the system is established to simulate the cycles under steady-state conditions. A parametric analysis of seven key parameters is conducted to examine their effects on the thermodynamic and exergoeconomic performance of the system. An optimization is conducted by genetic algorithm to obtain better system performance.

We declare that the manuscript has not been previously published, is not currently submitted for review to any other journal and will not be submitted elsewhere before one decision is made. Its publication is approved by all authors. If accepted, it will not be published elsewhere in the same form, in English or in any other language.

We appreciate your consideration of our manuscript, and we look forward to receiving comments from the reviewers.

Sincerely,

Jiangfeng Wang (on behalf of the authors’ team)

Institute of Turbomachinery

Cover letter

Shaanxi Engineering Laboratory of Turbomachinery and Power Equipment

State Key Laboratory of Multiphase Flow in Power Engineering

School of Energy and Power Engineering

Xi'an Jiaotong University, Xi'an, China

Highlights

A combined cooling and power system driven by engine exhaust gas and jacket water is proposed.

Thermodynamic and exergoeconomic performance of the system are analyzed.

Optimization for the combined cooling and power system is conducted by genetic algorithm.

Performance analysis and optimization of a combined cooling and power system using low boiling point working fluid driven by engine waste heat

Wenge Huang, Jiangfeng Wang*, Jiaxi Xia, Pan Zhao, Yiping Dai

Institute of Turbomachinery, Shaanxi Engineering Laboratory of Turbomachinery and Power Equipment, State Key Laboratory of Multiphase Flow in Power Engineering, School of Energy and Power Engineering, Xi'an Jiaotong University, Xi'an 710049, China

Corresponding author: Jiangfeng Wang

Mailing address:

Institute of Turbomachinery, Shaanxi Engineering Laboratory of Turbomachinery and Power Equipment, State Key Laboratory of Multiphase Flow in Power Engineering, School of Energy and Power Engineering

Xi'an Jiaotong University, Xi'an 710049, China

E-mail address: jfwang@mail.xjtu.edu.cn (JF Wang).

Performance analysis and optimization of a combined cooling and power system using low boiling point working fluid driven by engine waste heat

Wenge Huang, Jiangfeng Wang*, Jiaxi Xia, Pan Zhao, Yiping Dai

Institute of Turbomachinery, Shaanxi Engineering Laboratory of Turbomachinery and Power Equipment, State Key Laboratory of Multiphase Flow in Power Engineering, School of Energy and Power Engineering, Xi'an Jiaotong University, Xi'an 710049, China

Abstract

This paper develops a combined cooling and power system to recover waste heat from exhaust gas and jacket water in internal combustion engines using low boiling point fluid as working fluid. The system consists of a CO_2 Brayton cycle (CBC), a dual-pressure organic Rankine cycle (DORC) and an ejector refrigeration cycle (ERC). Comprehensive thermodynamic and exergoeconomic models of the system are performed and seven key parameters are selected to analyze the system performance. To obtain a better performance of the system, single-objective optimization is carried out by means of genetic algorithm with system product levelized exergy cost as the objective function. Results show that the increase of the BC turbine inlet temperature and inlet pressure can cause the increase of the system net power output. In both the high-pressure side and low-pressure side of the DORC, the increase of the ORC turbine inlet temperature causes the increase of the levelized exergy cost while the increase of the ORC turbine inlet pressure does the opposite. The increase of the

ejector primary inlet pressure causes the increase of system capital cost. Optimization shows that minimum levelized exergy cost for system product is 53.25 \$ $(MWh)^{-1}$ with exergy efficiency of 37.31%.

Keyworks:

Internal combustion engine

Brayton cycle

Waste heat recovery

Dual-pressure organic Rankine cycle

Ejector refrigeration cycle

Optimization

Nomenclature

A	area, m^2	ρ	density, kg m^{-3}
BC	Brayton cycle	μ	dynamic viscosity, m^2 s^{-1}
B_o	boiling number	η	efficiency, %
c	average cost per unit of exergy, \$ $(MWh)^{-1}$	δ	thickness, m
c_p	specific heat, kJ kg^{-1} K^{-1}	*Subscribe*	
C	cost rate, \$ $year^{-1}$	1-31	state points
CBC	CO_2 Brayton cycle	g1-g3	state points
CCP	combined cooling and power	w1-w3	state points
CRF	capital recovery factor	Bt	Brayton cycle turbine
CEPCI	chemical engineering plant cost index	BM	bare module
D	diameter, m	cond	condenser

DORC	dual-pressure organic Rankine cycle	comp	compressor
e	exergy, kJ kg^{-1}	D	destruction
E	exergy flow rate, kJ s^{-1}	elec	electricity
E_y	exergy flow rate per year, kJ year^{-1}	es	equivalent diameter
ERC	ejector refrigeration cycle	ev	evaporation/evaporator
F	multiplying factor	ex	exergy
f	friction factor	F	fuel
G	mass flow rate, kg s^{-1}	g	exhaust gas
h	enthalpy, kJ kg^{-1}	gh	gas heater
H	depth, m	he	heat exchanger
i_{eff}	interest rate	L	loss
l	length, m	l	liquid
M	mass flow rate, kg s^{-1}	M	material
n	lifetime, year	Ot	ORC turbine
Nu	Nusselt number	P	product
P	pressure, MPa	p1	pump 1
Pr	Prandtl number	p2	pump 2
Pt	center distance between tubes, m	p3	pump 3
P_r	reduced pressure	p4	pump 4
Q	heat transfer rate, kW	pf	primary flow
Q_{cool}	cooling capacity, kW	prec	precooler
q_m	average imposed wall heat flux, W m^{-2}	preh	preheater

r_f	enthalpy of vaporization, kJ kg^{-1}	s	shell
T	temperature, K	t	tube
U	overall heat transfer coefficient, W m^{-2} K^{-1}	th	thermal
W	power, kW	turb	turbine
W_y	annually power, MWh $year^{-1}$	vg	vapor generator
x	vapor quality	w	tube wall
Z	annually levelized cost value, \$ $year^{-1}$		
z	capital cost, K\$		
Greek symbol			
α	convection heat transfer coefficient, W m^{-2} K^{-1}		
λ	heat conductivity, W m^{-1} K^{-1}		

1. Introduction

Nowadays, internal combustion engines (ICEs) are the major motive power source in energy field. ICEs are used widely in transport, construction, agriculture, etc. Over 50% of the total transportation fuel is consumed by internal combustion engines. In a typical ICE, only 30-45% of the fuel energy is converted into effective power output, while the remaining energy is discharged to environment via exhaust gas, jacket water and other means, including charge air and lubrication [1]. Thus, technologies utilizing waste heat from ICEs have been investigated by a number of researchers.

Compared to other methods, organic Rankine cycle (ORC) is recognized as a well proven and highly efficient waste heat recovery technology [2,3]. Coupling the ORC

with the internal combustion engines is getting increasing interest of researchers. A volume of work was conducted to examine the potential of waste heat recovery from ICE with the help of ORC. Kalyan et al. [4] designed a system using ORC to generate power from exhaust gas in a low temperature combustion engine. Wei et al. [5] integrated an ORC system with a heavy-duty diesel engine to recover the waste heat. Srinivasan et al. [6] designed an ORC waste heat recovery system to improve the efficiency of the gas engine. Tian et al. [7] designed an ORC power generation system using engine exhaust gas as heat source.

Attention was mainly focused on the exhaust gas when people explored waste heat recovery from ICEs at early stage. ORC-based waste recovery systems mentioned above only absorbed heat from engine exhaust gas. However, there is a large amount energy exists in engine jacket water for its large mass flow rate and relatively high temperature (about 90℃). ORC-based power generation systems absorbed heat both form exhaust gas and jacket water were introduced by researchers. Vaja and Gambarotta [8] examined three different ORC cycles including a simply cycle, a preheating cycle and a regenerative cycle. Cycle preheated by jacket water was able to increase the system efficiency by about 12.5%. Rosset et al. [9] compared different ORC cycle configurations which converted waste heat from exhaust gas, from jacket water and from both. Calculation results revealed that the dual-source cycle provided the highest net power output.

To achieve a better performance for the waste heat recovery system, many studies try to improve the configurations of ORCs. Zhang et al. [10] developed a novel

system driven by waste heat in an ICE with a dual-loop ORC. The high-temperature cycle absorbed heat from the exhaust gas and the low-temperature cycle recovered heat from the high-temperature cycle and the jacket water. Yang et al. [11] modeled a dual-loop ORC system driven by waste heat in ICE. High-temperature cycle absorbed heat from the exhaust gas and low-temperature cycle absorbed heat from secondary exhaust gas and the jacket water. Ge et al. [12] designed a dual-loop ORC system to recover waste heat using different working fluids. Zeotropic mixture was used to recover high-temperature exhaust gas and R600a/R601a mixture was used to absorb heat in low-temperature jacket water. Systems integrated with complicated organic Rankine cycles were developed by many researchers [13-15].

Thermal stability of the organic working fluid should be considered when developing organic Rankine cycles to recovery waste heat from engine exhaust gas. Organic-based fluids would decompose under high-temperature and high-pressure conditions [16]. The low decomposition temperature of organic working fluid in ORC is about 200-300℃ while the temperature of engine exhaust gas can be more than 500℃. For all the studies mentioned above, the organic working fluid absorbs heat directly form the high-temperature exhaust gas, causing the potential of working fluid decomposition. Though an intermediate loop with thermal oil can be added between the ORC and the exhaust gas to avoid the decomposition [17,18], a large amount of high-temperature waste heat is not utilized at all. In order to solve this issue, researchers placed other waste heat recovery system between the ORC and exhaust gas to exploit to high-temperature waste heat. Thermoelectric generator (TEG), for

example, was introduced by Miller et al. [19] to the utilize the high temperature waste heat in exhaust gas. After the TEG process, the cooled exhaust gas could drive the ORC safely. However, because of the low energy conversion capacity of the TEG, power generated by the TEG was much smaller than the ORC in the same system [20]. Shu et al. [21] placed a steam Rankine cycle between ORC and exhaust gas for waste heat recovery from the gas engines. The steam Rankine cycle was the topping cycle to recovery heat from the high-temperature exhaust gas and organic Rankine cycle was the bottoming cycle to recovery heat from the exhaust water vapor. Large power output was provided by both the steam Rankine cycle and the ORC in the system. However, steam in the steam Rankine cycle requires a large superheated degree, or it may condense during the expansion and damage the turbine blades. As a result, structure of the steam Rankine cycle turbine is complex. Brayton cycle (BC), on the contrary, presents the advantages of simple and reliable structure. It uses gas as working fluid which does not involve phase change during the expansion [22]. Thus, Brayton-ORC systems can be used to exploit the waste heat from ICE effectively and safely.

Quite a few studies have been published to improve the waste heat recovery from exhaust gas. Jacket water, though explored by some researchers, is mainly used as the low-temperature heat source to preheat the organic working fluid in ORC. However, the mismatching mass flow rate of organic working fluid in the preheater and the evaporator causes a large amount of heat waste in jacket water. Yu et al. [23] calculated the energy recovery efficiency from an ORC- based ICE waste heat

recovery system. 75% waste heat could be recovered from exhaust gas while 9.5% waste heat was recovered from jacket water. But for most ICEs (rated power between 500 kW and 2000 kW), discharged thermal energy in jacket water is approximately the same as the energy in exhaust gas [24]. Thus, a large amount of waste heat in jacket water is potentially valuable for recovery.

Usually, traditional power plants only generate power and can't fulfill the requirements of the consumers for energy supply. Cooling capacity, for example, is needed in many places such as hospital, hotel, restaurant, etc. To satisfy the various demands of the consumers and to recover the waste heat more efficiently, cogeneration systems is introduced by many researchers. Cogeneration systems driven by waste heat in internal combustion engines were developed by a number of investigators. Chen et al. [25] designed an ammonia-water combined cooling and power system using the waste heat from the ICEs. Ammonia-water was heated by exhaust gas and jacket water. One part of the ammonia-water vapor flew into the turbine to provide power and the other part flew into the evaporator to provide refrigeration. Salek et al. [26] coupled an ammonia absorption refrigeration cycle and a bottoming Rankine cycle with internal combustion engine to produce power and cooling capacity. Absorption refrigeration cycles were considered by most of the combined cooling and power systems to convert exhaust gas waste heat to cooling capacity. However, ejector refrigeration cycle, which presents the advantages of desirable efficiency, small structure and simple layout [27,28], is always neglected.

In this study, a combined cooling and power system is developed, which comprises

a CO2 Brayton cycle, a dual-pressure ORC and an ejector refrigeration cycle. The CO2 Brayton cycle is used to recover the waste heat from high-temperature exhaust gas directly. The turbine exhaust in the CO2 Brayton cycle and the engine exhaust gas after heat transfer are respectively regarded as the heat sources for the high-pressure side and low-pressure side of the dual-pressure ORC, realizing the cascading utilization of exhaust gas waste heat. Meanwhile, organic working fluid in high-pressure side and low-pressure side are both preheated by jacket water to make full use of the waste heat. What's more, the ejector refrigeration cycle is adapted to recover the waste heat of jacket water further and produce cooling capacity simultaneously. Thermodynamic and exergoeconomic analysis is carried out to examine the effects of key parameters on system performances. Then a system optimization is conducted to obtain the minimum levelized exergy cost for the system product by means of genetic algorithm.

2. System description

2.1. CCP system

The combined cooling and power (CCP) system is shown in Fig 1. The system integrates a dual-pressure organic Rankine cycle with a CO_2 Brayton cycle and an ejector refrigeration, which can produce power and cooling capacity simultaneously. The exhaust gas from the internal consumption engine enters the gas heater to drive the CO_2 Brayton cycle. CO_2 cooled by the precooler flows through the compressor to be compressed to a supercritical state. Then the high-pressure CO_2 absorbs heat in the

gas heater, becoming high-pressure and high-temperature state, and enters BC turbine to produce power.

After expanding in the BC turbine, the high-temperature exhaust CO_2 flows into vapor generator 2 to heat the organic working fluid. High-pressure side organic working fluid heated by the CO_2 then flows into the ORC turbine to produce power. Meanwhile low-pressure side organic working fluid absorbs heat from the secondary engine exhaust gas in vapor generator 1 and then enters ORC turbine to produce power.

Exhaust vapor from the ORC turbine is cooled by condenser 1 to liquid state and pressured by pump 1. Jacket water with large mass flow rate is used to preheat the organic working fluid in the preheater. The preheated organic working fluid then separates. One part of the fluid is pumped by pump 3 to the vapor generator 1 to cycle in the low-pressure side. The other part is pumped by pump 2 to the vapor generator 2 to cycle in the high-pressure side.

The jacket water then flows into vapor generator 3 to provide heat for the ejector refrigeration cycle. After the condensation process in condenser 2, liquid working fluid is divided into two separated parts. One part of the fluid is pumped to the vapor generator 3 to absorb heat from jacket water and then becomes superheated vapor. The other part of the working fluid flows through the throttle valve to become low-pressure vapor-liquid mixture. The low-pressure mixture enters the evaporator to produce cooling capacity when absorbing heat from the environment and become low-pressure vapor. After that, the superheated vapor mixes with the low-pressure

vapor in the ejector. The mixed working fluid enters the condenser 2 to be condensed to liquid.

R245fa is selected as the working fluid for the organic Rankine cycle and the ejector refrigeration cycle because of the great thermodynamic performance and the low environment effect [29,30].

3. System model

Several assumptions are made to simplify the simulation of the system.

(1) The system keeps a steady state.

(2) The heat and friction losses in the system are not considered.

(3) The pressure losses in the vapor generator, preheater, precooler, evaporator and condenser are neglected.

(4) Considering the low gas acid dew point temperature, the gas temperature at the outlet of the vapor generator 1 is higher than 110℃[31].

(5) The working fluid out of the condensers and preheater is saturated liquid and the state at the outlet of the evaporator is saturated vapor.

(6) The process through the throttle valve is isenthalpic.

3.1. Thermodynamic model

3.1.1. Energy model

The net power of the CO_2 Brayton cycle is expressed as:

$$W_{BC} = W_{Bt} - W_{comp} \quad (1)$$

The net power of the DORC is given as:

$$W_{\mathrm{ORC}} = W_{\mathrm{Ot}} - W_{\mathrm{p1}} - W_{\mathrm{p2}} - W_{\mathrm{p3}} \tag{2}$$

The cooling capacity of the ERC is given as:

$$Q_{\mathrm{cool}} = M_{\mathrm{cool}} \cdot (h_{21} - h_{20}) \tag{3}$$

The net power output of the whole system is calculated as:

$$W_{\mathrm{net}} = W_{\mathrm{ORC}} + W_{\mathrm{BC}} - W_{\mathrm{p4}} \tag{4}$$

The thermal efficiency of the system is given as:

$$\eta_{\mathrm{th}} = \frac{W_{\mathrm{net}} + Q_{\mathrm{cool}}}{M_{\mathrm{g1}} \cdot (h_{\mathrm{g1}} - h_{\mathrm{g3}}) + M_{\mathrm{w1}} \cdot (h_{\mathrm{w1}} - h_{\mathrm{w3}})} \tag{5}$$

The detailed energy model equations of each component are list in Table 1. Note that there are two expanding processes in the ORC turbine. The high-pressure side vapor expands from high pressure (state 10) to low pressure (state 11) for the first time and then mixes with the low-pressure side vapor. After that, the mixed vapor expands from low pressure (state 11) to the back pressure of ORC turbine (state 12) for the secondary time.

3.1.2. Exergy model

In general, the energy model of a system is based on the first law of the thermodynamic which focuses the amount of the thermal energy in the system. The exergy model of the system is based on the second law of the thermodynamic which focuses on the quality of the thermal energy. The exergy analysis of the system is based on a dead state (the ambient conditions in this paper). The equation of exergy for unit working fluid is expressed as:

$$e = (h - h_0) - T_0 \cdot (s - s_0) \quad (6)$$

where h_0, T_0 and s_0 are the parameters under the ambient conditions.

The exergy flow rate in this study is given by:

$$E = M \cdot e \quad (7)$$

All the components in the system are associated directly or indirectly with fuel or other heat sources, such as exhaust gas and jacket water in this study. The heat sources provide exergy for the components to operate. For each component, there is an exergy balance equation, being expressed as [32]:

$$E_{\mathrm{F}} = E_{\mathrm{P}} + E_{\mathrm{D}} + E_{\mathrm{L}} \quad (8)$$

where E_{F} is the rate of exergy for the component fuel and E_{P} represents the rate of exergy for the component product; E_{D} denotes the rate of component exergy destruction and E_{L} expresses the rate of exergy loss for the component.

The details of the exergy balance equations for each component are listed in Table 1.

The exergy efficiency represents the degree of the utilization of the waste heat in the system, being expressed as:

$$\eta_{\mathrm{ex}} = \frac{W_{\mathrm{net}} + E_{\mathrm{cool}}}{E_{\mathrm{g1}} - E_{\mathrm{g3}} + E_{\mathrm{w1}} - E_{\mathrm{w3}}} \quad (9)$$

where E_{cool} is the exergy rate of the cooling process, being expressed as:

$$E_{\mathrm{cool}} = E_{25} - E_{24} \quad (10)$$

3.2. Capital cost and exergoeconomic model of the system

3.2.1. Capital cost calculation

In this study, a method of modeling the capital costs of the main component is employed [33]. At first, the bare module cost of the components is calculated as the basic cost. The basic cost of the components includes the direct project cost (such as equipment cost, material cost for the installation, etc.) and the indirect project cost (like the taxes, insurance engineering expenses etc.). The bare module cost of the components is calculated under basic conditions. For conditions different from the basic conditions, multiplying factors (the specific equipment type, the specific system pressure and the specific material of construction) are added in the calculation to correct the results.

Axial turbines (BC turbine and ORC turbine) are used in this study. The bare module cost equation of the turbine is:

$$\log_{10} C_{\text{turb}}^{0} = K_{1,\text{turb}} + K_{2,\text{turb}} \cdot \log_{10} W + K_{3,\text{turb}} \cdot (\log_{10} W)^2 \tag{11}$$

where K_{turb} is constant corresponding to the turbine type; W is the power output of the turbine.

Turbines used in this study are made of carbon steel (CS) and operate under high pressure. Thus, a multiplying factor is used to correct the result. The capital cost of the turbine is given as:

$$C_{\text{turb}} = F_{\text{BM,turb}} \cdot C_{\text{turb}}^{0} \tag{12}$$

where $F_{\text{BM,turb}}$ is the multiplying factor corresponding to the working conditions of the turbine.

Reciprocating pumps are used in this study. The bare module cost equation of the pumps is given as:

$$\log_{10} C_{\text{pump}}^{0} = K_{1,\text{pump}} + K_{2,\text{pump}} \cdot \log_{10} W + K_{3,\text{pump}} \cdot (\log_{10} W)^2 \quad (13)$$

where K_{pump} is constant corresponding to the pump type; W is the power input of the pump.

Pumps used in this study are made of stainless steel (SS) and work under high pressure. Thus, multiplying factors are used to correct the bare module cost. The capital cost of the pump is given as:

$$C_{\text{pump}} = \left(B_{1,\text{pump}} + B_{2,\text{pump}} \cdot F_{\text{M,pump}} \cdot F_{\text{P,pump}} \right) \cdot C_{\text{pump}}^{0} \quad (14)$$

where B_{pump} is constant corresponding to the type of the pump; $F_{\text{M,pump}}$ is the material factor of the pump and $F_{\text{P,pump}}$ is the pressure factor of the pump. The equation of the pressure factor is given as:

$$\log_{10} F_{\text{P,pump}} = C_{1,\text{pump}} + C_{2,\text{pump}} \cdot \log_{10} P_{\text{pump}} + C_{3,\text{pump}} \cdot (\log_{10} P_{\text{pump}})^2 \quad (15)$$

where C_{pump} is the constant corresponding to the type of the pump and P_{pump} is the pressure of the pump under working conditions.

Axial compressor is used in this study. The bare module cost equation of the compressor is given as:

$$\log_{10} C_{\text{comp}}^{0} = K_{1,\text{comp}} + K_{2,\text{comp}} \cdot \log_{10} W + K_{3,\text{comp}} \cdot (\log_{10} W)^2 \quad (16)$$

where K_{comp} is the constant corresponding to the type of the compressor; W is the power input of the compressor.

The compressor is made of carbon steel (CS) and works under high pressure.

Correction equation of the bare module cost is given as:

$$C_{\text{comp}} = F_{\text{BM,comp}} \cdot C^0_{\text{comp}} \tag{17}$$

where $F_{\text{BM,comp}}$ is the constant corresponding to the type of the compressor.

Tube-and-shell heat exchangers (gas heater, vapor generators, precooler, preheater, evaporator and condensers) are used in this study. The bare module cost equation of the heat exchanger is given as:

$$\log_{10} C^0_{\text{he}} = K_{1,\text{he}} + K_{2,\text{he}} \cdot \log_{10} A + K_{3,\text{he}} \cdot (\log_{10} A)^2 \tag{18}$$

where K_{he} is the constant corresponding to the type of the heat exchanger; A is the heat transfer area of the heat exchanger. The calculation of the heat exchanger areas is presented in Appendix A.

Heat exchangers used in this study are made of carbon steel (CS) and work under different pressure. Multiplying factors are needed to correct the results, the equation is given as:

$$C_{\text{he}} = \left(B_{1,\text{he}} + B_{2,\text{he}} \cdot F_{\text{M,he}} \cdot F_{\text{P,he}}\right) \cdot C^0_{\text{he}} \tag{19}$$

where B_{he} are the constants correspond to the type of the heat exchanger. $F_{\text{M,he}}$ and $F_{\text{P,he}}$ are the material factor and pressure factor, respectively. The pressure factor is obtained from the following equation:

$$\log_{10} F_{\text{P,he}} = C_{1,\text{he}} + C_{2,\text{he}} \cdot \log_{10} P_{\text{he}} + C_{3,\text{he}} \cdot (\log_{10} P_{\text{he}})^2 \tag{20}$$

where C_{he} is the constant corresponding to the type of the heat exchanger; P_{he} is the designed working pressure for the heat exchanger.

The values of the constants mentioned above for the main components are listed in Appendix B.

316 The calculation of the bare module cost depends on past records or published
317 correlations for price information. It is necessary to update the costs because of the
318 changing economic conditions (inflation). This can be achieved by the following
319 expression:

320 $$C_2 = C_1 \cdot \left(\frac{I_2}{I_1} \right) \quad (21)$$

321 where C is the purchased cost and I is the cost index. The subscript 1 refers to base
322 time when cost is known and subscript 2 refers to time when cost is desired. The
323 *CEPCI* (Chemical Engineering Plant Cost Index) is employed to calculate the
324 inflation. The values of $CEPCI_{2016}$ and $CEPCI_{\text{ref},2001}$ are 541.7 and 397, respectively
325 [34,35].

326 3.2.2. Exergoeconomic model

327 Exergoeconomic is a branch of engineering which combines the thermodynamic
328 analysis and economic principles. Thermodynamic performance and economic cost of
329 the system are all taken into consideration.

330 To find the relationship between the present value of the expenditure and the
331 equivalent annually levelized costs, the capital recovery factor (CRF) is employed,
332 being expressed as [32]:

333 $$Z_{\text{i}} = CRF \cdot C_{\text{i}} \quad (22)$$

334 $$CRF = \frac{i_{\text{eff}} \cdot (1+i_{\text{eff}})^n}{(1+i_{\text{eff}})^n - 1} \quad (23)$$

where i_{eff} is the effective discount rate with a value of 0.05 [36]; n is the lifetime of the CCP system being assumed as 30 [37].

In order to calculate the equivalent annually levelized costs, the annual working time of the system is assumed as 8000 h [38]. Then the annual exergy rates and annual power output or consumption are obtained.

In a steady system, there are a number of entering and outing working fluid steams and heat and work interactions with the surroundings. In exergoeconomic analysis, each flowing steam is associated with a levelized exergy cost. The equations to calculate the cost of the steam product are given as:

$$C_{\mathrm{in}} = c_{\mathrm{in}} \cdot E_{\mathrm{y,in}} \tag{24}$$

$$C_{\mathrm{out}} = c_{\mathrm{out}} \cdot E_{\mathrm{y,out}} \tag{25}$$

$$C_{\mathrm{work}} = c_{\mathrm{work}} \cdot W_{\mathrm{y}} \tag{26}$$

$$C_{\mathrm{heat}} = c_{\mathrm{heat}} \cdot E_{\mathrm{y,heat}} \tag{27}$$

where c denotes levelized exergy cost of the steams; $E_{\mathrm{y,in}}$ and $E_{\mathrm{y,out}}$ are the exergy transfer rate of the steam flowing in and out a component; W_{y} and $E_{\mathrm{y,heat}}$ are the power and the heat transfer rate of the components considering the annual working time.

The cost balance equation applied to the kth system component is given as:

$$\sum\nolimits_{\mathrm{out}} C_{\mathrm{out,k}} + C_{\mathrm{w,k}} = C_{\mathrm{heat,k}} + \sum\nolimits_{\mathrm{in}} C_{\mathrm{in,k}} + Z_{\mathrm{k}} \tag{28}$$

Details of the cost balance equation are listed in Table 2.

The levelized exergy cost for system product is chosen to indicate the exergoeconomic performance, being expressed as [39,40]:

$$c_{\mathrm{product}} = c_{\mathrm{capital}} + c_{\mathrm{fuel}} \tag{29}$$

where c_{capital} is the capital-cost-related part of the levelized exergy cost for the system product, being expressed as:

$$c_{\mathrm{capital}} = \frac{Z_{\mathrm{total}}}{W_{\mathrm{net}} + E_{\mathrm{cool}}} \tag{30}$$

c_{fuel} is the fuel-cost-related part of the levelized exergy cost for the system product, being expressed as:

$$c_{\mathrm{fuel}} = \frac{c_{\mathrm{Bt}} \cdot W_{\mathrm{y,comp}} + c_{\mathrm{Ot}} \cdot W_{\mathrm{y,pump1}} + c_{\mathrm{Ot}} \cdot W_{\mathrm{y,pump2}} + c_{\mathrm{Ot}} \cdot W_{\mathrm{y,pump3}} + c_{\mathrm{Ot}} \cdot W_{\mathrm{y,pump4}}}{W_{\mathrm{net}} + E_{\mathrm{cool}}} \tag{31}$$

c_{Bt} and c_{Ot} are the levelized exergy cost for the BC turbine power output and the ORC turbine power output, which are calculated in Table 3. Likewise, they can be expressed as the capital-cost-related part and the fuel-cost-related part:

$$c_{\mathrm{Bt}} = \frac{Z_{\mathrm{Bt}}}{W_{\mathrm{y,Bt}}} + \frac{c_3 \cdot \left(E_{\mathrm{y},3} - E_{\mathrm{y},4}\right)}{W_{\mathrm{y,Bt}}} \tag{32}$$

$$c_{\mathrm{Ot}} = \frac{Z_{\mathrm{Ot}}}{W_{\mathrm{y,Ot}}} + \frac{c_{10} \cdot \left(E_{\mathrm{y},10} + E_{\mathrm{y},11} - E_{\mathrm{y},12}\right)}{W_{\mathrm{y,Ot}}} \tag{33}$$

In addition, the levelized exergy cost for the condensers and the precooler is equal to zero, being given by:

$$c_{26}=c_{28}=c_{30}=0 \tag{34}$$

The levelized exergy cost for the exhaust gas as well as the jacket water is zero, being expressed as:

$$c_{\mathrm{g1}}=c_{\mathrm{w1}}=0 \tag{35}$$

4. Results and discussion

4.1.1. Simulation conditions for the system

The thermodynamic parameters of the working fluid are calculated under the environment of MATLAB with the help of REFPROP 9.1 [41]. The basic conditions of simulation for the CCP system are listed in Table 3

4.1.2. Internal combustion engine

In this study, the engine selected [8] is a 12-cylinder 4-stroke supercharged gas engine. The main designed parameters of the engine are listed in Table 4. The composition of the engine exhaust gas is presented in Table 5. The heat load capacity of the engine exhaust gas is about 1700 kW when cooled down to the acid dew temperature and the 1000 kW can be obtained from the engine jacket water.

4.2. Analysis for the thermodynamic and exergoeconimic performance

Seven key parameters (BC turbine inlet temperature, BC turbine inlet pressure, inlet temperature at the high-pressure side of ORC turbine, inlet pressure at the high-pressure side of ORC turbine, inlet temperature at the low-pressure side of ORC turbine, inlet pressure at the low-pressure side of ORC turbine and the ejector primary inlet pressure) are chosen to analyze the thermodynamic and exergoeconomic performance of the system. In the thermodynamic aspect, the net power output of the CO_2 Brayton cycle (W_{BC}), net power output of the DORC (W_{ORC}), net power of the whole system (W_{net}), cooling capacity of the system (Q_{cool}) and the exergy efficiency

of the system (η_{exergy}) are selected to reflect the system performance. Levelized exergy cost for the BC turbine power output (c_{Bt}), levelized exergy cost for the ORC turbine power output (c_{Ot}), levelized exergy cost the system product ($c_{product}$) and the system capital cost ($z_{capital}$) are chosen to represent the exergoeconomic performance.

4.2.1. Variations of thermal parameters in CBC

The influences of the BC turbine inlet temperature on the output and the exergy efficiency of the system are shown in Fig. 2. The net power output of the CO_2 Brayton cycle (CBC) increases with the rise of the BC turbine inlet temperature. That can be explained by the decrease of the compressor power consumption. With the increase of the CO_2 temperature at the BC turbine inlet, the mass flow rate of CO_2 decreases. As a result, less CO_2 working fluid is compressed by the compressor, leading to the decrease of the compressor power consumption. On the one hand, the decrease of the mass flow rate cuts down the BC turbine power output. On the other hand, the increase of inlet temperature causes the increase of enthalpy drop of CO_2 in the turbine which results in the increase of the BC turbine power output. The two effects mention above cause the slight decrease of the BC turbine power output, which is smaller than the decrease of the compressor power consumption. Thus, the large decrease of the compressor power consumption determines the increase of the CBC net power output.

It is presented that the net power output of the DORC increases with the rise of the BC turbine inlet temperature. The temperature of the exhaust CO_2 increases with the

415 increase of BC turbine inlet temperature. Since the exhaust CO_2 acts as the heat
416 source for organic working fluid in the high-pressure side of DORC, more heat is
417 provided in vapor generator 2. As a result, the mass flow rate of the organic working
418 fluid increases, leading to the rise of the power output of the ORC turbine. The
419 increase of the power consumption of the pumps in the DORC is much smaller than
420 the increase of the ORC turbine power output. Thus, the net power output of the
421 DORC increases.

422 The net power of the whole CCP system increases with the increase of the BC
423 turbine inlet temperature. That can be explained by the increase of the CO_2 Brayton
424 cycle net power output and the DORC net power output. The increase of the net
425 power output of the system causes the increase of the exergy efficiency of the system.

426 With the increase of the BC turbine inlet temperature, the cooling capacity of the
427 ejector refrigeration cycle (ERC) decreases, as shown in Fig. 2. As discussed above,
428 the increase of the exhaust CO_2 temperature causes the increase of the organic
429 working fluid mass flow rate in DORC. Thus, more heat is absorbed by the organic
430 working fluid in the preheater from the jacket water. Less heat is available for the
431 ERC working fluid in vapor generator 3. As a result, the mass flow rate of the
432 working fluid in the evaporator decreases, resulting in the decrease of the cooling
433 capacity of the CCP system.

434 The influences of the BC turbine inlet temperature on the levelized exergy cost and
435 the system capital cost of the system are shown in Fig. 3. The levelized exergy cost
436 for the BC turbine power output decreases with the increase of the BC turbine inlet

temperature. Since the decrease of the compressor power consumption, the cost of compressor decreases. According to Eq. (32), the decrease of compressor cost leads to the decrease of capital-cost-part of the levelized exergy cost for the BC turbine power output c_{Bt}. Thus, c_{Bt} decreases. The levelized exergy cost for the ORC turbine decreases with the increase of the BC turbine inlet temperature. The reason for this is the large increase of the power output of the ORC turbine. The increase of the ORC turbine power output causes the increase of both the capital-cost-related part and fuel-cost-related part of c_{Ot}.

The system capital cost increases with the increase of the BC turbine inlet temperature. Since the large increase of the ORC turbine power output, the cost of the ORC turbine increases. Meanwhile, the increase of the mass flow rate of the organic working fluid in the DORC causes the increase of the cost for the vapor generator 2 and preheater. Though the cost of the compressor decreases with the decrease of the compressor power consumption, the effect of the ORC turbine cost is more important, which determines the rise of the system capital cost.

It can be obtained in Fig. 3 that the levelized exergy cost for the system product decreases with the increase of the BC turbine inlet temperature. As mentioned above, the levelized exergy cost for the BC turbine and ORC turbine decrease. Analyzing from Eq. (31), the fuel-cost-related part of the levelized exergy cost for system product decreases. According to Eq. (30), the increase of system net power output causes the decrease of the capital-cost-related part of the levelized exergy cost for the system product. As a result, the levelized exergy cost for the system product

459 decreases.

460 The influences of the BC turbine inlet pressure on the output and the exergy
461 efficiency of the system are shown in Fig. 4. The net power output of the CBC
462 increases with the increase of the BC turbine inlet pressure. Since the increase of
463 pressure at BC turbine inlet, the enthalpy drop of the CO_2 in the BC turbine increases,
464 causing the increase of the BC turbine power output. The pressure rise also causes the
465 increase of compressor power consumption. But the increase of the BC turbine power
466 output is larger than the increase of the compressor power consumption. As a result,
467 the net power output of the CBC increases.

468 The net power output of the DORC decreases with the increase of the BC turbine
469 inlet pressure. On the one hand, the temperature of the exhaust CO_2 at the BC turbine
470 outlet decreases with the increase of the BC turbine inlet pressure. Thus, less heat is
471 provided in vapor generator 2, causing the decrease of the mass flow rate of the
472 organic working fluid in the high-pressure side DORC. As a result, the power output
473 of the high-pressure side DORC decreases. On the other hand, the increase of the BC
474 turbine inlet pressure causes the increase of the compressor power consumption which
475 results in the rise of the CO_2 temperature at the compressor outlet. Thus, less heat is
476 absorbed by CO_2 in the gas heater and more heat is transferred to the organic working
477 fluid in vapor generator 1. The mass flow rate of the organic working fluid in the
478 low-pressure side DORC increases, causing the increase of the power output in the
479 low-pressure side. The increase of the power output in low-pressure side is smaller

than the decrease of power output in the high-pressure side. Thus, the net power of the whole DORC decreases.

The cooling capacity of the system increases with the increase of the BC turbine inlet pressure. The decrease of the mass flow rate in the high-pressure side of DORC is more than the increase of the mass flow rate in the low-pressure side. As a result, the total mass flow in the DORC decreases. Thus, less heat is absorbed from the jacket water in the preheater and more heat is available in vapor generator 3 for working fluid in the ERC. The mass flow rate of the working fluid in ERC increases, causing the increase of the cooling capacity.

The net power output of the whole system increases with the increase of the BC turbine inlet pressure. Though the net power output of the DORC decreases, the increase of CBC net power output is much larger than the decrease. As a result, the net power output of the whole system increases. The increase of the net power output of the CCP system causes the increase of the exergy efficiency of the system, as shown in Fig. 4.

The influences of the BC turbine inlet pressure on the levelized exergy cost and the system capital cost of the system are presented in Fig. 5. The levelized exergy cost for the BC turbine output c_{Bt} increases with the increase of the BC turbine inlet pressure. With the increase of the BC turbine output, the cost of the turbine increases, causing the increase of the capital-cost-related part of c_{Bt}. Meanwhile, the increase of the compressor power consumption causes the increase of the levelized exergy cost for

501 the CO_2 at the turbine inlet, resulting in the increase of the fuel-cost-related part of c_{Bt}.
502 As a result, c_{Bt} increases.

503 The levelized exergy cost for the ORC turbine product c_{Ot} increases with the
504 increase of the BC turbine inlet pressure. The decrease of the mass flow rate in the
505 DORC causes that less exergy is produced by the vapor generator 2. As a result, the
506 levelized exergy cost for the vapor at the high-pressure side of ORC turbine inlet
507 increases, which determines the increase of the fuel-cost-related part of the levelized
508 exergy for the ORC turbine power output. Thus, the levelized exergy cost for the ORC
509 turbine increases.

510 The system capital cost of increases with the increase of the BC turbine inlet
511 pressure. The increase of the BC turbine power output and the compressor power
512 consumption results in the increase of the BC turbine cost and compressor cost. The
513 increase of the mass flow rate in the ERC causes the increase of capital cost for the
514 evaporator and vapor generator 3. All the cost increase mention above accounts for
515 the increase of the system capital cost.

516 The levelized exergy cost for the system product decreases with the increase of BC
517 turbine inlet pressure as shown in Fig. 5. According to Eq. (31), the increase of c_{Ot}, c_{Bt}
518 and compressor power consumption could cause the increase of the fuel-cost-related
519 part of the levelized exergy cost for the system product. However, because of the large
520 increase of the system net power output, the capital-cost-related part and the
521 fuel-cost-related part decrease actually. Thus, the levelized exergy cost for the system
522 product decreases.

523 4.2.2. Variations of thermal parameters in DORC.

524 The influences of inlet temperature at the high-pressure side of ORC turbine on the
525 output and the exergy efficiency of the system are shown in Fig. 6. The net power
526 output of the CBC remains unchanged. The reason is that the change of thermal
527 parameters in dual-pressure ORC can’t affect the thermodynamic performance of the
528 CBC.

529 The net power output of the DORC cycle decreases with the increase of inlet
530 temperature at the high-pressure side of ORC turbine. With the increase of the vapor
531 temperature at the high-pressure ORC inlet, the mass flow rate of the organic working
532 fluid in the high-pressure side of DORC decreases. The decrease of organic working
533 fluid mass flow rate causes the decrease of the power output of the ORC turbine,
534 which further causes the decrease of the net power output of the DORC.

535 The cooling capacity of the ejector refrigeration cycle increases with the rise of
536 inlet temperature at the high-pressure side of ORC turbine. The decrease of the
537 organic working fluid mass flow rate in the DORC results in the decrease of the heat
538 transfer rate in the preheater. More heat is released in vapor generator 3 from the
539 jacket water to the working fluid in the ejector refrigeration cycle, leading to the
540 increase of the working fluid mass flow rate. Consequently, the cooling capacity of
541 the ejector refrigeration cycle increases.

542 The net power output of the CCP system decreases with the increase of inlet
543 temperature at the high-pressure side of ORC turbine. The increase of the working
544 fluid mass flow rate in the ERC causes the increase of the power consumption of

pump 4. Power output of the CBC keeps unchanged and dual-pressure ORC power output decreases. According to Eq. (4), the net power output of the CCP system decreases. The decrease of the CCP system net power output causes the decrease of the exergy efficiency of the system, as shown in Fig. 6.

The influences of inlet temperature at the high-pressure side of ORC turbine on the levelized exergy cost and the system capital cost of the system are presented in Fig. 7. The levelized exergy cost for the ORC turbine (c_{Ot}) increases with the increase of inlet temperature at the high-pressure side of ORC turbine. The can be explained by the decrease of the decrease of the ORC turbine power output.

The levelized exergy cost for the BC turbine power output (c_{Bt}) increases with the increase of inlet temperature at the high-pressure side of ORC turbine. Since the decrease of the mass flow rate in the high-pressure side of ORC, the exergy of the organic working fluid vapor generated by the vapor generator 2 decreases, causing the increase of the levelized exergy cost of the vapor. The organic working fluid vapor is heat by the BC turbine exhaust CO_2. Thus, the increase of the vapor levelized exergy cost causes the increase of the levelized exergy cost for the exhaust CO_2. According to Eq. (32), the increase of the levelized exergy cost for the exhaust CO_2 causes the increase of the fuel-cost-related part of BC turbine levelized exergy cost. As a result, the levelized exergy cost for the BC turbine power output increases.

The system capital cost decreases with the increase of inlet temperature at the high-pressure side of ORC turbine. Because of the decrease of the organic working

566 fluid mass flow rate in the dual-pressure ORC, the cost of the ORC turbine and vapor
567 generator 2 decreases. Thus, the system capital cost decreases.

568 The levelized exergy cost for the system product ($c_{product}$) increases with the increase
569 of inlet temperature at the high-pressure side of ORC turbine, as shown in Fig. 7.
570 Since the increase of the levelized exergy cost for the BC turbine and ORC turbine
571 power output, the fuel-cost-related part of $c_{product}$ increases. Meanwhile, the large
572 decrease of the net power of the CCP system causes the increase of the
573 capital-cost-related part of $c_{product}$, according to Eq. (30). Thus, levelized exergy cost
574 for the system product increases.

575 The influences of inlet pressure at the high-pressure side of ORC turbine on the
576 output and the exergy efficiency of the system are presented in Fig. 8. The net power
577 output of the CBC keeps unchanged because of the unchanged thermal parameters in
578 the cycle.

579 The net power output of the DORC increase with the increase of inlet pressure at
580 the high-pressure side of ORC turbine. The increase of the evaporation pressure cuts
581 down the latent heat of the organic working fluid, which causes the increase of the
582 mass flow rate in the high-pressure side of the DORC. As a result, the net power
583 output of the ORC turbine increases, leading to the increase of the net power output of
584 the DORC.

585 Considering the increase of the DORC net power output and the unchanged CBC
586 net power output, the net power output of the whole system increases. Also, the
587 exergy efficiency of the system increases.

588 The increase of the mass flow rate in the DORC absorbs more heat from the jacket
589 water in the preheater. Thus, less heat is released in the vapor generator 3, causing the
590 decrease of the mass flow rate of the working fluid in the ERC. As a result, the
591 cooling capacity of the system decreases.

592 The influences of inlet pressure at the high-pressure side of ORC turbine on the
593 levelized exergy cost and system capital cost of the system are presented in Fig. 9.
594 The large increase of the net power output accounts for the decrease of the levelized
595 exergy cost for the ORC turbine power output. The increase of the mass flow rate of
596 the organic working fluid in the high-pressure side of the DORC means that more
597 exergy in the vapor is generated by the vapor generator 2. The levelized exergy cost
598 for the vapor at the vapor generator 2 outlet decreases. The exhaust CO_2 of the BC
599 turbine provides heat for the vapor. The decrease of the vapor levelized exergy cost
600 causes the decrease of the exhaust CO_2 levelized exergy cost. Meanwhile, the
601 decrease of the levelized exergy cost for the CO_2 causes results in the decrease of the
602 fuel-cost-related part of the levelized exergy cost for the BC turbine output. As a
603 result, the levelized exergy cost for the BC turbine power output decreases.

604 The increase of the ORC turbine power output and the increase of mass flow rate in
605 the DORC cause the increase of the turbine cost and the vapor generator 2 cost,
606 respectively. Thus, the system capital cost increases.

607 The levelized exergy cost for the system product decreases with the increase of
608 inlet pressure at the high-pressure side of ORC turbine. The decrease of the levelized
609 exergy cost for the ORC turbine power output and the BC turbine power output

accounts the decrease of the fuel-cost-related part of the levelized exergy cost for the system product. The increase of the system net power outweighs the increase of the system capital cost. Thus, the capital-cost-related part of the levelized exergy cost of the system product. As a result, the levelized exergy cost of the system product decreases.

The influences of inlet temperature at the low-pressure side of ORC turbine on the output and the exergy efficiency of the system are presented in Fig. 10. Parameters changes in the DORC can't affect the thermodynamic performance of the CBC. Thus, the net power output of the CBC remains unchanged.

The net power of the DORC decreases with the increase of inlet temperature at the low-pressure side of ORC turbine. The increase of the inlet temperature causes the decrease of the mass flow rate in the low-pressure side of DORC, leading to the decrease of the DORC net power output.

Considering the decrease of the DORC net power output and the unchanged CBC net power output, the net power output of the whole system decreases. Also, the exergy efficiency of the system decreases.

The cooling capacity of the ejector refrigeration cycle increases with the increase of inlet temperature at the low-pressure side of ORC turbine. The increase of the inlet temperature causes the decrease of the mass flow rate of the organic working fluid in the low-pressure cycle. Thus, less heat is absorbed from the jacket water in the preheater and more heat is released in vapor generator 3. The mass flow rate of the working fluid in the ERC increases, leading to the increase of the cooling capacity.

632 The influences of inlet temperature at the low-pressure side of ORC turbine on the
633 levelized exergy cost and system capital cost of the system are presented in Fig. 11.
634 The levelized exergy cost for the BC turbine power output increases with the increase
635 of inlet temperature at the low-pressure side of ORC turbine. Though the enthalpy of
636 the organic working fluid increases with the increase of the low-pressure side inlet
637 temperature, the decrease of the mass flow rate causes the decrease of the exergy
638 provided by the vapor generator 1. Thus, the levelized exergy cost of the vapor
639 generated by vapor generator 1 increases. The levelized exergy cost for vapor in vapor
640 generator 2 is the equal to the levelized exergy cost for vapor in vapor generator 1. As
641 a result, the levelized exergy cost for the vapor generator 2 vapor increases, causing
642 the increase of the levelized exergy cost of the exhaust CO_2 after the BC turbine. The
643 increase of the levelized exergy cost for the exhaust CO_2 causes the increase of the
644 levelized exergy cost of the BC turbine power output.
645 The levelized exergy cost for the ORC turbine (c_{Ot}) increases with the increase of
646 inlet temperature at the low-pressure side of ORC turbine. As mentioned above, the
647 levelized exergy cost for the vapor at the low-pressure side of ORC turbine inlet
648 increases. Thus, the fuel-cost-related part of the levelized exergy cost for the ORC
649 turbine output increases. Also, the decrease of the ORC turbine power output causes
650 the increase both the fuel-cost-related part and the capital-cost-related part. As a result,
651 the levelized exergy cost for the ORC turbine power output increases.
652 The decrease of the mass flow rate and the ORC turbine power output cause the
653 decrease of the vapor generator 1 cost and the turbine cost. Thus, the capital cost of

654 the system decreases.

655 The levelized exergy cost for the system product increases with the increase of inlet
656 temperature at the low-pressure side of ORC turbine. The increase of c_{Bt} and c_{Ot} cause
657 the increase of the fuel-cost-related part of the levelized exergy cost for the system
658 product. Though, the decrease of the system capital cost causes the decrease of the
659 capital-cost-related part, its effect is less important. Thus, the increase of the
660 fuel-cost-related part determines the increase of the levelized exergy cost for the
661 system product.

662 The influences of the inlet pressure at the low-pressure side of ORC turbine on the
663 output and the exergy efficiency of the system are shown in Fig. 12. The net power of
664 the CBC keeps unchanged with the increase of the increase of the low evaporation
665 pressure. That reason is that the thermodynamic performance of the CBC is irrelevant
666 to the thermal parameters in DORC.

667 The net power output of the DORC increases with the increase of inlet pressure at
668 the low-pressure side of ORC turbine. The increase of inlet pressure at the
669 low-pressure side of ORC turbine causes the increase of the enthalpy drop of the
670 organic working fluid in the ORC turbine. Though the mass flow rate of the working
671 fluid decreases as well, the effect of the enthalpy drop is more important. Thus, the net
672 power of the DORC increases.

673 The unchanged CBC power output and the increase of the DORC power accounts
674 for the increase of the system net power output. The exergy efficiency of the system
675 increases as a result.

The cooling capacity increases with the increase of inlet pressure at the low-pressure side of ORC turbine. Because of the decrease of the mass flow rate in the DORC, less heat is absorbed in the preheater and more heat is provided in vapor generator 3. Thus, the mass flow rate of the working fluid in the ERC increases, causing the increase of the cooling capacity.

The influences of inlet pressure at the low-pressure side of ORC turbine on the levelized exergy cost and system capital cost of the system are shown in Fig. 13. The levelized exergy cost for the ORC turbine power output decreases with the increase of inlet pressure at the low-pressure side of ORC turbine. The reason is that the decrease of the mass flow rate in the DORC cuts down the capital cost of the vapor generator 1. The power output of the DORC increases as well. Thus, both the capital-cost-related part and the fuel-cost-related part of the system decrease. Consequently, the levelized exergy cost of the ORC turbine power output decreases.

The levelized exergy cost for the BC turbine power output decreases with the increase of the inlet pressure at the low-pressure side of ORC turbine. The decrease of the levelized exergy cost causes the decrease of the levelized exergy cost for the vapor at vapor generator 2 inlet. The vapor is heated by the exhaust CO_2 in the CBC. Thus, the decrease of the vapor levelized exergy cost results in the decrease of the CO_2 levelized exergy cost which determines the fuel-cost-related part of the BC turbine power levelized exergy cost. As a result, the levelized exergy cost for the BC turbine power output decreases.

The increase of the ORC turbine power output causes the increase of the ORC

turbine cost. Meanwhile, the increase of the cooling capacity causes the increase of the heat transfer area in the evaporator which requires the rise of the evaporator cost. Thus, the capital cost of the system increases.

The levelized exergy cost for the system product decreases with the increase of inlet pressure at the low-pressure side of ORC turbine. The decrease of the levelized exergy cost of the BC turbine power output and ORC turbine power output cause the decrease of the fuel-cost-related part of the system levelized exergy cost, which determines the decrease of the levelized exergy cost for the system product.

4.2.3. Variations of thermal parameters in ERC.

The influences of the ejector primary inlet pressure on the output and the exergy efficiency of the system are shown in Fig. 14. Thermal parameters changes in the ERC can' affect the thermodynamic performance of the CBC and DORC. Thus, the net power output of the two cycles remain unchanged. With the increase of the ejector primary inlet pressure, the power consumption of pump 4 increases, leading to the slight decrease of the net power output of the whole system.

Since the entrainment ratio of the ejector increases with the increase of the ejector primary inlet pressure. More working fluid in the is entrained to the ejector from the ejector secondary inlet. Thus, the mass flow rate of the working fluid in the evaporator increases, leading to the increase of the cooling capacity.

With the increase of the ejector primary inlet pressure, the power consumption of pump 4 increase gradually. At first, the exergy loss in the pump 4 power consumption

719 is smaller than the exergy produced in the cooling capacity. Then, the power
720 consumption becomes larger. Thus, the exergy efficiency for the system increases at
721 first and then decreases with the increase of the ejector primary inlet pressure.

722 The influences of the ejector primary inlet pressure on the levelized exergy cost and
723 the system capital cost of the system are presented in Fig. 15. The increase of the
724 ejector primary inlet pressure can't affect the power output of the BC turbine and
725 ORC turbine. Thus, the levelized exergy cost for the BC turbine and ORC turbine
726 output remain unchanged.

727 The increase of the pump power consumption results in the increase of the pump 4
728 cost. The increase of the mass flow rate in the evaporator causes the increase of
729 evaporator cost. Thus, the system capital cost increases. The increase of the system
730 capital cost causes the increase of the capital-cost-related part of $c_{product}$. As a result,
731 the levelized exergy cost for the system product increases.

732 4.3. System optimization

733 The parametric analysis reveals the potential of optimization for the CCP system.
734 With the increase of the BC turbine inlet temperature, the net power output of the
735 system increases while the cooling capacity decreases. With the increase of the inlet
736 temperature at the high-pressure side of ORC turbine, the net power output of the
737 system decreases while the cooling capacity increases. In this study, seven key
738 parameters (BC turbine inlet temperature, BC turbine inlet pressure, inlet temperature
739 at the high-pressure side of ORC turbine, inlet pressure at the high-pressure side of

ORC turbine, inlet temperature at the low-pressure side of ORC turbine, inlet pressure at the low-pressure side of ORC turbine and the ejector primary inlet pressure) are chosen as the variables to optimize the system. The ranges of these parameters are listed in Table 6.

Considering that the levelized exergy cost reflects the thermodynamic and the exergoeconomic aspect of the system, the levelized exergy cost for the system product is selected as the objective function and genetic algorithm is selected to conduct the single-objective optimization.

Genetic algorithm (GA) is an optimization method based on the natural biological evaluation. [42] It simulates the natural genetic rules and searches the optimization result in all the generation. The control parameters of the GA are listed in Table 7.

The optimization results of GA are listed in Table 8. It can be obtained that the minimum levelized exergy cost for the system product $c_{product}$ is 53.25 \$ $(MWh)^{-1}$. The exergy efficiency of the CCP system is 37.31% which is also desirable.

5. Conclusion

In this paper, a combined cooling and power system is developed. Seven parameters (temperature and pressure at the inlet of BC turbine, temperature at the high-pressure inlet and the low-pressure inlet of the ORC turbine, high-pressure side and low-pressure side evaporation pressure in DORC and the ejector primary inlet pressure) are selected to analyze the thermodynamic and exergoeconomic

performance of the system. Single-objective optimization is carried out with the help of GA. The conclusions of this study are presented as follows:

(1) Both the increase of the BC turbine inlet temperature and pressure contribute to the increase of the exergy efficiency and the decrease of the levelized exergy cost for the system product.

(2) For both the high-pressure side and the low-pressure side of the DORC, the increase of the ORC turbine inlet temperature causes the decrease of exergy efficiency and the increase of the levelized exergy cost for the system product while the increase of the ORC turbine inlet pressure results in the increase of exergy efficiency and the decrease of the levelized exergy cost.

(3) The ERC performance analysis shows that the increase of the ejector primary inlet pressure causes the increase of the cooling capacity and the decrease of system net power output. Levelized exergy cost for the system product increases with the increase of ejector primary inlet pressure.

(4) Single-objective optimization results show that the minimum levelized exergy cost for the system product is obtained as 53.25 $(MWh)^{-1}$ with net power output of 374.37 kW, cooling capacity of 188.63 kW and system exergy efficiency of 37.31%.

Acknowledgement

The authors gratefully acknowledge the financial support by the National Natural Science Foundation of China (Grant No. 51476121)

Appendix A

This section shows the calculation of the heat transfer area in the heat exchangers used in this study.

All the heat exchangers used in this study are tube-and-shell heat exchanger. The thermodynamic properties of the working fluid vary with the heat transfer process. Thus, to calculate the heat transfer area actually, the heat transfer processes are discretized into a lot of small sections. In each section, the heat transfer area is small and the thermodynamic properties are assumed to be constant.

For each section the heat transfer area is calculated as:

$$A_{\mathrm{i}} = Q_{\mathrm{i}} \Big/ \left(\Delta T_{\mathrm{i}} \cdot U_{\mathrm{i}}\right) \tag{B1}$$

where ΔT_{i} is the log-mean temperature difference (LMTD) and U_{i} is the overall heat transfer coefficient.

$$\frac{1}{U_{\mathrm{i}}} = \frac{1}{\alpha_{\mathrm{t,i}}} + \frac{\delta}{\lambda} + \frac{1}{\alpha_{\mathrm{s,i}}} \tag{B2}$$

In Eq. (B2) δ and λ represent the thickness of the tube and the thermal conductivity of the tube wall, respectively. $\alpha_{\mathrm{t,i}}$ is the convection heat transfer coefficient in the tube side and $\alpha_{\mathrm{s,i}}$ is the convection heat transfer coefficient in the shell side.

For different heat transfer process, the convection heat transfer coefficient has different format. We classify the heat transfer processes into single-phase heat transfer process and two-phase heat transfer process. In gas heater, precooler and the preheater, single-phase heat transfer process happens. In evaporator, two-phase heat transfer process occurs. In vapor generators and the condensers, both the single-phase and the

two-phase heat transfer process happen.

In the single-phase heat transfer process, the convection heat transfer coefficient in the tube side and the shell side are expressed as [43]:

$$\alpha_{\mathrm{t,i}} = \frac{\lambda \cdot Nu}{D_{\mathrm{i}}} \tag{B3}$$

$$\alpha_{\mathrm{s,i}} = 0.36\left(\frac{\lambda}{D_{\mathrm{es}}}\right)\cdot\left(\frac{D_{\mathrm{es}}\cdot G_{\mathrm{s}}}{\mu}\right)^{0.55}\cdot \mathrm{Pr}^{\frac{1}{3}}\cdot\left(\frac{\mu}{\mu_{\mathrm{w}}}\right)^{0.14} \tag{B4}$$

In Eq. (B3), the Nusselt number is calculated as [44,45]:

$$Nu = \left[\frac{(f/8)\cdot \mathrm{Re}\cdot \mathrm{Pr}}{12.7(f/8)^{0.5}\cdot\left(\mathrm{Pr}^{2/3}-1\right)+1.07}\right],\ for\ \mathrm{Re}<10^4 \tag{B5}$$

$$Nu = \left[\frac{(f/8)\cdot(\mathrm{Re}-1000)\cdot \mathrm{Pr}}{12.7(f/8)^{0.5}\cdot\left(\mathrm{Pr}^{2/3}-1\right)+1.07}\right],\ for\ 10^4<\mathrm{Re}<5\times10^6 \tag{B6}$$

where f is the Darcy frication factor, Re is the Reynolds and Pr is the Prandtl number.

In Eq. (B4), D_{es} is the equivalent diameter of the shell, being expressed as:

$$D_{\mathrm{es}} = \frac{1.10\mathrm{Pt}^2}{D_{\mathrm{out,i}}} - D_{\mathrm{out,i}} \tag{B7}$$

where Pt is the center distance between the tubes.

Evaporation and condensation are two different two-phase heat transfer processes. In this study, the cold organic working fluid flows in the tubes of the heat exchangers. The convection heat transfer coefficient of evaporation and condensation are expressed as [46,47]:

$$\alpha_{\mathrm{ev,i}} = 0.023\left[\frac{G(1-x)}{\mu_{\mathrm{l}}}\right]^{0.8}\cdot \mathrm{Pr}_{\mathrm{l}}^{0.4}\cdot\frac{\lambda_{\mathrm{l}}}{d}\cdot\left[1+3000Bo^{0.86}+1.12\left(\frac{x}{1-x}\right)^{0.75}\cdot\left(\frac{\rho_{\mathrm{l}}}{\rho_{\mathrm{v}}}\right)^{0.41}\right] \tag{B8}$$

$$\alpha_{\mathrm{cond,i}} = 0.023\left[\frac{G(1-x)}{\mu_{\mathrm{l}}}\right]^{0.8}\cdot \mathrm{Pr}_{\mathrm{l}}^{0.4}\cdot\frac{\lambda_{\mathrm{l}}}{d}\cdot\left[(1-x)^{0.8}+\frac{3.8x^{0.76}(1-x)0.04}{P_r^{0.38}}\right] \tag{B9}$$

In Eq. (B9), P_r is the reduced pressure. In Eq. (B8) Bo is the boiling number, being expressed as:

$$Bo = \frac{q_{\mathrm{m}}}{G \cdot r_{\mathrm{f}}} \tag{B10}$$

Appendix B

The constants for component capital cost calculation are list in Table B1.

Reference

[1] Heywood J. B. Internal combustion engine fundamentals. New York: McGraw-Hill; 1988.

[2] Chao H, Chao L, Hong G, Hui X, You L, Shuang W. The optimal evaporation temperature and working fluids for subcritical Organic Rankine Cycle. Energy 2012; 38: 136-143.

[3] Bombarda P, Invernizzi C, Pietra C. Heat recovery from Diesel engines: A thermodynamic comparison between Kalina and ORC cycles. Applied Thermal Engineering 2010; 30: 212-219.

[4] Kalyan K, Pedro J, Sundar R. Analysis of exhaust waste heat recovery from a dual fuel low temperature combustion engine using an Organic Rankine Cycle. Energy 2010; 35: 2387-2399.

[5] Wei M, Fang J, Ma C, Danish S. Waste heat recovery from heavy-duty diesel engine exhaust gases by medium temperature ORC system. Science China Technological Sciences 2011; 54: 2746-2753.

840 [6] Srinivasan K, Mago P, Zdaniuk G, Chamra L, Midkiff K. Improving the Efficiency
841 of the Advanced Injection Low Pilot Ignited Natural Gas Engine Using Organic
842 Rankine Cycles. 2008; 130: 022201.
843 [7] Tian H, Shu G, Wei H, Liang X, Liu L. Fluids and parameters optimization for the
844 organic Rankine cycles (ORCs) used in exhaust heat recovery of Internal Combustion
845 Engine (ICE). Energy 2012; 47: 125-136.
846 [8] Vaja I, Gambarotta A. Internal Combustion Engine (ICE) bottoming with Organic
847 Rankine Cycles (ORCs). Energy 2010; 35(2): 1084-1093.
848 [9] Rosset K, Mounier V, Guenat E, Schiffmann J. Multi-objective optimization of
849 turbo-ORC systems for waste heat recovery on passenger car engines. Energy 2018;
850 159: 751-765.
851 [10] Zhang H G, Wang E H, Fan B Y. A performance analysis of a novel system of a
852 dual loop bottoming organic Rankine cycle (ORC) with a light-duty diesel engine.
853 Applied Energy 2013;102: 1504-1513.
854 [11] Yang F, Cho H, Zhang H, Zhang J. Thermoeconomic multi-objective
855 optimization of a dual loop organic Rankine cycle (ORC) for CNG engine waste heat
856 recovery. Applied Energy 2017; 205: 1100-1118.
857 [12] Ge Z, Li J, Liu Q, Duan Y, Yang Z. Thermodynamic analysis of dual-loop
858 organic Rankine cycle using zeotropic mixtures for internal combustion engine waste
859 heat recovery. Energy Conversion and Management 2018; 166: 201-214.

860 [13] Chen T, Zhuge W, Zhang Y, Zhang L. A novel cascade organic Rankine cycle
861 (ORC) system for waste heat recovery of truck diesel engines. Energy Conversion and
862 Management 2017;138: 210-223.
863 [14] Mansoury M, Jafarmadar S, Khalilarya S. Energetic and exergetic assessment of
864 a two-stage Organic Rankine Cycle with reactivity-controlled compression ignition
865 engine as a low temperature heat source. Energy Conversion and Management 2018;
866 166: 201-214.
867 [15] Seyedkavoosi S, Javan S, Kota K. Exergy-based optimization of an organic
868 Rankine cycle (ORC) for waste heat recovery from an internal combustion engine
869 (ICE). Applied Thermal Engineering 2017; 126: 447-457.
870 [16] Rajabloo T, Davide B, Paolo lora. Effect of a partial thermal decomposition of
871 the working fluid on the performances of ORC power plants. Energy 2017;
872 133:1013-1026.
873 [17] Shu G, Zhao M, Tian H, Wei H, Liang X, Huo Y, et al. Experimental
874 investigation on thermal OS/ORC (Oil Storage/Organic Rankine Cycle) system for
875 waste heat recovery from diesel engine. Energy 2016; 107: 693-706.
876 [18] Wang X, Tian H, Shu G. Part-load performance prediction and operation strategy
877 design of organic Rankine cycles with a medium cycle used for recovering waste heat
878 from gaseous fuel engines. Energies 2016; 9: 527.
879 [19] Miller E, Hendricks T, Peterson R. Modeling Energy Recovery Using
880 Thermo-electric Conversion Integrated with an Organic Rankine Bottoming Cycle.
881 Journal of Electron Mater 2009; 38: 1206-1213.

882 [20] Miller E, Hendricks T, Wang H, Peterson R. Integrated dual-cycle energy
883 recovery using thermoelectric conversion and an organic Rankine bottoming cycle.
884 Proceedings of the Institution of Mechanical Engineers, Part A: Journal of Power and
885 Energy 2011; 225: 33-43.
886 [21] Shu G, Wang X, Tian H. Theoretical analysis and comparison of Rankine cycle
887 and different organic Rankine cycles as waste heat recovery system for a large
888 gaseous fuel internal combustion engine. Applied Thermal Engineering 2016; 108:
889 525-537.
890 [22] Galindo J, Guardiola C, Dolz V, Kleut P. Further analysis of a
891 compression-expansion machine for a Brayton Waste Heat Recovery cycle on an IC
892 engine. Applied Thermal Engineering 2018; 128: 345-356.
893 [23] Yu G, Shu G, Tian Hua, Wei H, Liu L. Simulation and thermodynamic analysis
894 of a bottoming Organic Rankine Cycle (ORC) of diesel engine (DE). Energy 2013; 51:
895 281-290.
896 [24] Ma J, Liu L, Zhu T, Zhang T. Cascade utilization of exhaust gas and jacket water
897 waste heat from an Internal Combustion Engine by a single loop Organic Rankine
898 Cycle system. Applied Thermal Engineering 2016; 107: 218-226.
899 [25] Chen Y, Han W, Jin H. Investigation of an ammonia-water combined power and
900 cooling system driven by the jacket water and exhaust gas heat of an internal
901 combustion engine. International Journal of Refrigeration 2017; 82: 174-188.

902 [26] Salek F, Moghaddam A, Naserian M. Thermodynamic analysis of diesel engine
903 coupled with ORC and absorption refrigeration cycle. Energy Conversion and
904 Management 2017; 140: 240-246.
905 [27] Wang J, Dai Y, Sun Z, A theoretical study on a novel combined power and ejector
906 refrigeration cycle. International Journal of Refrigeration 2009; 32: 1186-1194.
907 [28] Ahmadi P, Dincer I, Rosen M. Performance assessment and optimization of a
908 novel integrated multigeneration system for residential buildings. Energy and
909 Buildings 2013; 67: 568-578.
910 [29] Dai Y, Wang J, Gao L. Parametric optimization and comparative study of organic
911 Rankine cycle (ORC) for low grade waste heat recovery. Energy Conversion
912 Management 2009; 50: 576-582.
913 [30] Shu G, Zhao M, Tian H, Huo Y, Zhu W. Experimental comparison of R123 and
914 R245fa as working fluids for waste heat recovery from heavy-duty diesel engine.
915 Energy 2016; 115: 756-769.
916 [31] Zhang J, Zhang H, Yang K, Yang F, Wang Z, Zhao G, et al. Performance analysis
917 of regenerative organic Rankine cycle (RORC) using the pure working fluid and the
918 zeotropic mixture over the whole operating range of a diesel engine. Energy
919 Conversion Management 2014; 84: 282-294.
920 [32] Adrian Bejan GT, Moran Michael. Thermal design and optimization. New York:
921 Jogn Wiley & Sons; 1996.
922 [33] Turton R. Analysis, synthesis, and design of chemical processes. 3rd ed. Upper
923 Saddle River, N.J: Prentice Hall; 2009.

924 [34] Li J, Ge Z, Liu Q, Duan Y, Yang Z. Thermo-economic performance analyses and
925 comparison of two turbine layouts for organic Rankine cycles with dual-pressure
926 evaporation. Energy Conversion and Management, 2018; 164: 603-614.
927 [35] http://www.chemengonline.com/pci-home
928 [36] Sheng Z, Huai W, Tao G. Performance comparison and parametric optimization
929 of subcritical organic Rankine cycle (ORC) and transcritical power cycle system for
930 low-temperature geothermal power generation. Applied Energy
931 2011;88(8):2740-2754.
932 [37] Tempesti D, Fiaschi D. Thermo-economic assessment of a micro CHP system
933 fueled by geothermal and solar energy. Energy 2013; 58: 45-51.
934 [38] Velez F, Segovia JJ, Martin MC, Antonlin G, Chejne F, Quijano A. A technical,
935 economical and market review of organic Rankine cycles for the conversion of
936 low-grade heat for power generation. Renewable and Sustainable Energy Reviews,
937 2012; 16:4175-4189.
938 [39] Akbari D, Mahmoudi M. Thermoeconomic analysis & optimization of the
939 combined supercritical CO2 (carbon dioxide) recompression Brayton/ organic
940 Rankine cycle. Energy 2014; 78:501-512.
941 [40] Zare V, Mahmoudi M, Yari M. An exergoeconomic investigation of waste heat
942 recovery from the Gas Turbine-Modular Helium Reactor (GT-MHR) employing an
943 ammonia–water power/cooling cycle. Energy 2013;61. 397-409.

944 [41] Lemmon EW, Huber ML, McLinden MO. NIST standard reference database 23,
945 reference fluid thermodynamic and transport properties (REFPROP). Version 9.1.
946 National Institute of Standards and Technology; 2010
947 [42] Wang J, Dai Y, Gao L. Parametric analysis and optimization for a combined
948 power and refrigeration cycle. Applied Energy 2008;85(11):1071-1085
949 [43] Kern DQ. Process heat transfer. New York: McGraw-Hill; 1950
950 [44] Kandylas IP, Stamatelos AM. Engine exhaust system design based on heat
951 transfer computation. Energy Conversion Management 1999; 40:1057-1072.
952 [45] Incropera FP, DeWitt DP. Fundamentals of heat and mass transfer. New York:
953 Wiley; 2002
954 [46] Gungor KE, Winterton RHS. Simplified general correlation for saturated flow
955 boiling and comparisons of correlations with data. Chemical Engineering Research
956 and Design, 1987; 65:148-156.
957 [47] Shah MM. A general correlation for heat transfer during film condensation inside
958 pipes. International Journal of Heat and Mass Transfer 1979; 22:547-556.
959

Figure captions

Fig. 1. Schematic diagram of the CCP system

Fig. 2. Influences of BC turbine inlet temperature on the output and the exergy efficiency of the system.

Fig. 3. Influences of BC turbine inlet temperature on the levelized exergy cost and the system capital cost of the system.

Fig. 4. Influences of BC turbine inlet pressure on the output and the exergy efficiency of the system.

Fig. 5. Influences of BC turbine inlet pressure on the levelized exergy cost and the system capital cost of the system.

Fig. 6. Influences of inlet temperature at the high-pressure side of ORC turbine on the output and the exergy efficiency of the system.

Fig. 7. Influences of inlet temperature at the high-pressure side of ORC turbine on the levelized exergy cost and the system capital cost of the system.

Fig. 8. Influences of inlet pressure at the high-pressure side of ORC turbine on the output and the exergy efficiency of the system.

Fig. 9. Influences of inlet pressure at the high-pressure side of ORC turbine on the levelized exergy cost and the system capital cost of the system.

Fig. 10. Influences of inlet temperature at the low-pressure side of ORC turbine on the output and the exergy efficiency of the system.

Fig. 11. Influences of inlet temperature at the low-pressure side of ORC turbine on the levelized exergy cost and system capital cost of the system.

Fig. 12. Influences of inlet pressure at the low-pressure side of ORC turbine on the output and the exergy efficiency of the system.

Fig. 13. Influences of inlet pressure at the low-pressure side of ORC turbine on the levelized exergy cost and system capital cost of the system.

Fig. 14. Influences of ejector primary inlet pressure on the output and the exergy efficiency of the system.

Fig. 15. Influences of ejector primary inlet pressure on the levelized exergy cost and the system capital cost of the system.

991 **Table 1** Energy and exergy models for each component in CCP system

Component	Energy equation	E_F	E_P	E_D	E_L
Gas heater	$M_{g1}\cdot(h_{g1}-h_{g2})=M_2\cdot(h_3-h_2)$	$E_{g1}-E_{g2}$	E_3-E_2	$E_{g1}+E_2-E_3-E_{g2}$	/
BC turbine	$W_{Bt}=M_3\cdot(h_3-h_4)=M_3\cdot(h_3-h_{4s})\cdot\eta_{Bt}$	E_3-E_4	W_{Bt}	$E_3-E_4-W_{Bt}$	/
Vapor generator 2	$M_4\cdot(h_4-h_5)=M_9\cdot(h_{10}-h_9)$	E_4-E_5	$E_{10}-E_9$	$E_4+E_9-E_5-E_{10}$	/
Precooler	$M_1\cdot(h_5-h_1)=M_{26}\cdot(h_{27}-h_{26})$	/	/	$E_5+E_{26}-E_1-E_{27}$	$E_{27}-E_{26}$
Compressor	$W_{comp}=M_1\cdot(h_2-h_1)=M_1\cdot(h_{2s}-h_1)/\eta_{comp}$	W_{comp}	E_2-E_1	$E_1-E_2+W_{comp}$	/
Vapor generator 1	$M_{g2}\cdot(h_{g2}-h_{g3})=M_8\cdot(h_{11}-h_8)$	$E_{g2}-E_{g1}$	$E_{11}-E_8$	$E_{g2}+E_8-E_{11}-E_{g3}$	/
ORC turbine	$W_{Ot}=M_{10}\cdot(h_{10}-h_{12})+M_{11}\cdot(h_{11}-h_{12})$	$E_{10}+E_{11}-E_{12}$	W_{Ot}	$E_{10}+E_{11}-E_{12}+W_{Ot}$	/
Condenser 1	$M_{12}\cdot(h_{12}-h_{13})=M_{28}\cdot(h_{29}-h_{28})$	/	/	$E_{12}+E_{28}-E_{13}-E_{29}$	$E_{29}-E_{28}$
Pump 1	$W_{p1}=M_{13}\cdot(h_{14}-h_{13})=M_{13}\cdot(h_{14s}-h_{13})/\eta_{p1}$	W_{p1}	$E_{14}-E_{13}$	$E_{13}-E_{14}+W_{p1}$	/
Preheater	$M_{15}\cdot(h_{15}-h_{14})=M_{w1}\cdot(h_{w1}-h_{w2})$	$E_{w1}-E_{w2}$	$E_{15}-E_{14}$	$E_{w1}+E_{14}-E_{15}-E_{w2}$	/
Pump 2	$W_{p2}=M_7\cdot(h_9-h_7)=M_7\cdot(h_{9s}-h_7)/\eta_{p2}$	W_{p2}	E_9-E_7	$E_7-E_9+W_{p2}$	/
Pump 3	$W_{p3}=M_6\cdot(h_8-h_6)=M_6\cdot(h_{8s}-h_6)/\eta_{p3}$	W_{p3}	E_8-E_6	$E_6-E_8+W_{p3}$	/
Vapor generator 3	$M_{23}\cdot(h_{23}-h_{22})=M_{w2}\cdot(h_{w2}-h_{w3})$	$E_{w2}-E_{w3}$	$E_{23}-E_{22}$	$E_{w2}+E_{22}-E_{23}-E_{w3}$	/
Condenser 2	$M_{16}\cdot(h_{16}-h_{17})=M_{30}\cdot(h_{31}-h_{30})$	/	/	$E_{16}+E_{30}-E_{17}-E_{31}$	$E_{31}-E_{30}$
Valve	$h_{19}=h_{20}$	/	/	$E_{19}-E_{20}$	/
Pump 4	$W_{p4}=M_{22}\cdot(h_{22}-h_{18})=M_{22}\cdot(h_{22s}-h_{18})/\eta_{p4}$	W_{p4}	$E_{22}-E_{18}$	$E_{18}-E_{22}+W_{p4}$	/
Ejector	$M_{16}\cdot h_{16}=M_{23}\cdot h_{23}+M_{21}\cdot h_{21}$	$E_{23}+E_{21}$	E_{16}	$E_{23}+E_{21}-E_{16}$	/
Evaporator	$M_{20}\cdot(h_{21}-h_{20})=M_{24}\cdot(h_{24}-h_{25})$	$E_{20}-E_{21}$	$E_{25}-E_{24}$	$E_{20}+E_{24}-E_{21}-E_{25}$	/

992 **Table 2** Cost balance and auxiliary relation [32] for each component of CCP system

Component	Cost balance	Auxiliary relation

Gas heater	$c_{g2} \cdot E_{y,g2} + c_3 \cdot E_{y,3} = c_{g1} \cdot E_{y,g1} + c_2 \cdot E_{y,2} + Z_{gh}$	c_{g1}=c_{g2}=0
Vapor generator 2	$c_5 \cdot E_{y,5} + c_{10} \cdot E_{y,10} = c_4 \cdot E_{y,4} + c_9 \cdot E_{y,9} + Z_{vg,2}$	c_4=c_5
BC turbine	$c_4 \cdot E_{y,4} + c_{Bt} \cdot W_{y,Bt} = c_3 \cdot E_{y,3} + Z_{Bt}$	c_4=c_3
Precooler	$c_1 \cdot E_{y,1} + c_{26} \cdot E_{y,26} = c_5 \cdot E_{y,5} + c_{27} \cdot E_{y,27} + Z_{prec}$	c_1=c_5
Compressor	$c_2 \cdot E_{y,2} = c_1 \cdot E_{y,1} + c_{elec,1} \cdot W_{y,comp} + Z_{comp}$	$c_{elec,1}$=c_{Bt}
Vapor generator 1	$c_{g3} \cdot E_{y,g3} + c_{11} \cdot E_{y,11} = c_{g2} \cdot E_{y,g2} + c_8 \cdot E_{y,8} + Z_{vg,1}$	c_{g2}=c_{g3}
ORC turbine	$c_{12} \cdot E_{y,12} + c_{Ot} \cdot W_{y,Ot} = c_{11} \cdot E_{y,11} + c_{10} \cdot E_{y,10} + Z_{Ot}$	c_{10}=c_{11}=c_{12}
Pump 1	$c_{14} \cdot E_{y,14} = c_{13} \cdot E_{y,13} + c_{elec,3} \cdot W_{y,pump1} + Z_{pump1}$	$c_{elec,3}$=c_{Ot}
Condenser 1	$c_{13} \cdot E_{y,13} + c_{29} \cdot E_{y,29} = c_{28} \cdot E_{y,28} + c_{12} \cdot E_{y,12} + Z_{cond1}$	c_{13}=c_{12}
Preheater	$c_{w2} \cdot E_{y,w2} + c_{15} \cdot E_{y,15} = c_{w1} \cdot E_{y,w1} + c_{14} \cdot E_{y,14} + Z_{preh}$	c_{w1}=c_{w2}=0
Pump 2	$c_9 \cdot E_{y,9} = c_7 \cdot E_{y,7} + c_{elec,2} \cdot W_{y,pump2} + Z_{pump2}$	$c_{elec,2}$=c_{Ot}
Pump 3	$c_8 \cdot E_{y,8} = c_6 \cdot E_{y,6} + c_{elec,3} \cdot W_{y,pump3} + Z_{pump3}$	$c_{elec,3}$=c_{Ot}
Vapor generator 3	$c_{w3} \cdot E_{y,w3} + c_{23} \cdot E_{y,23} = c_{w2} \cdot E_{y,w2} + c_{22} \cdot E_{y,22} + Z_{vg,3}$	c_{w3}=c_{w2}
Valve	/	c_{19}=c_{20}
Pump 4	$c_{22} \cdot E_{y,22} = c_{18} \cdot E_{y,18} + c_{elec,3} \cdot W_{y,pump4} + Z_{pump4}$	$c_{elec,4}$=c_{Ot}
Condenser 2	$c_{17} \cdot E_{y,17} + c_{31} \cdot E_{y,31} = c_{30} \cdot E_{y,30} + c_{16} \cdot E_{y,16} + Z_{cond2}$	c_{16}=c_{17}
Ejector	$c_{16} \cdot E_{y,16} = c_{23} \cdot E_{y,23} + c_{21} \cdot E_{y,21}$	/
Evaporator	$c_{21} \cdot E_{y,21} + c_{25} \cdot E_{y,25} = c_{20} \cdot E_{y,20} + c_{24} \cdot E_{y,24} + Z_{ev}$	c_{20}=c_{21}

993 **Table 3** Condition of simulation for the CCP system

Term	Value
Ambient temperature (℃)	20
Ambient pressure (MPa)	0.101

Compressor inlet temperature (℃)	35
BC turbine inlet temperature (℃)	400
BC turbine inlet pressure (MPa)	18
BC turbine outlet pressure (MPa)	8
Inlet temperature at the high-pressure side of ORC turbine (℃)	150
Inlet pressure at the high-pressure side of ORC turbine (MPa)	1.6
Inlet temperature at the low-pressure side of ORC turbine (℃)	100
Inlet pressure at the low-pressure side of ORC turbine (MPa)	1.0
Outlet pressure of pump 1 (MPa)	0.9
Ejector primary inlet pressure (MPa)	0.4
Terminal temperature difference at gas heater outlet (℃)	100
Pinch point temperature difference in vapor generator 1 (℃)	30
Pinch point temperature difference in vapor generator 2 (℃)	30
Pinch point temperature difference in vapor generator 3 (℃)	25
Condensation temperature of condenser 1 (℃)	30
Condensation temperature of condenser 2 (℃)	30
Evaporation temperature of evaporator (℃)	5
Isentropic efficiency of BC turbine (%)	80
Isentropic efficiency of ORC turbine (%)	80
Isentropic efficiency of compressor (%)	80
Isentropic efficiency of pump 1 (%)	75
Isentropic efficiency of pump 2 (%)	75

Isentropic efficiency of pump 3 (%)	75
Inlet temperature of cooling water (℃)	20

994 **Table 4** Main parameters of the engine [8]

Parameters	Value
Power output (kW)	2928
Rotation ($r(min)^{-1}$)	1000
Exhaust gas temperature (℃)	470
Exhaust gas mass flow rate ($kg\ s^{-1}$)	4.35
Temperature of jacket water (℃)	90/79
Mass flow rate of jacket water ($kg\ s^{-1}$)	25

995 **Table 5** Composition of the exhaust gas [8]

Composition	Molecular ($g(mol)^{-1}$)	Fraction (%)
O_2	32.00	9.3
CO_2	44.00	9.1
H_2O	18.01	7.4
N_2	28.01	74.2

996 **Table 6** Parameters for GA

Ranges of the decision variables	Range
BC turbine inlet temperature (℃)	330-440
BC turbine inlet pressure (MPa)	15-20
Inlet temperature at the high-pressure side of ORC turbine (℃)	130-180
Inlet pressure at the high-pressure side of ORC turbine (MPa)	1.4-2

Inlet temperature at the low-pressure side of ORC turbine (℃)	90-150
Inlet pressure at the low-pressure side of ORC turbine (MPa)	0.9-1.3
Ejector primary inlet pressure (MPa)	0.3-1

997 **Table 7** Control parameters of GA

Tuning parameters	Value
Population size	20
Mutation probability	0.01
Crossover probability	0.8
Stop generation	200

998 **Table 8** Single-objective optimization results

Term	Value
BC turbine inlet temperature (℃)	425.457
BC turbine inlet pressure (MPa)	20
Inlet temperature at the high-pressure side of ORC turbine (℃)	144.315
Inlet pressure at the high-pressure side of ORC turbine (MPa)	1.847
Inlet temperature at the low-pressure side of ORC turbine (℃)	100.032
Inlet pressure at the low-pressure side of ORC turbine (MPa)	1.264
Ejector primary inlet pressure (MPa)	0.537
Net power output (kW)	374.37
Cooling capacity (kW)	188.63
Exergy efficiency (%)	37.31
Levelized exergy cost ($ $(MWh)^{-1}$)	53.25

Table B1 Constants for component costs [32]

Constant	Value	Constant	Value	Constant	Value
$B_{1,he}$	1.63	$K_{3,pump}$	0.1538	$C_{3,he}$	0.08183
$B_{2,he}$	1.66	$K_{1,turb}$	2.7051	$C_{1,pump}$	-0.3635
$B_{1,pump}$	1.89	$K_{2,turb}$	1.4398	$C_{2,pump}$	0.3957
$B_{2,pump}$	1.35	$K_{3,turb}$	-0.1776	$C_{3,pump}$	-0.0026
$K_{1,he}$	4.3247	$K_{1,comp}$	2.2897	$F_{M,he}$	1.0
$K_{2,he}$	-0.3030	$K_{2,comp}$	1.3604	$F_{BM,turb}$	3.5
$K_{3,he}$	0.1634	$K_{3,comp}$	-0.1027	$F_{BM,comp}$	2.7
$K_{1,pump}$	3.3892	$C_{1,he}$	0.03881	$F_{M,pump}$	2.2
$K_{2,pump}$	0.0536	$C_{2,he}$	-0.11272		

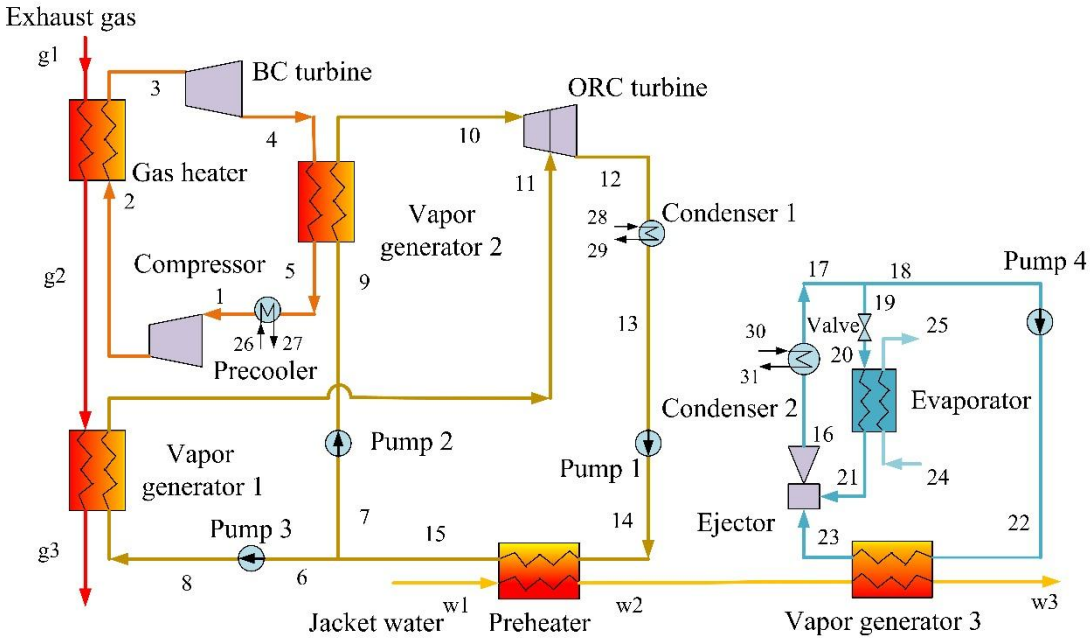

Fig. 1. Schematic diagram of the CCP system

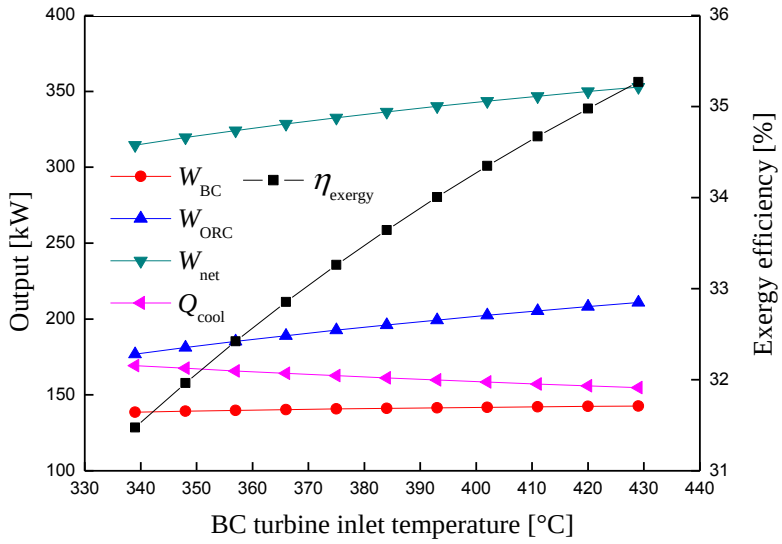

Fig. 2. Influences of BC turbine inlet temperature on the output and the exergy efficiency of the system.

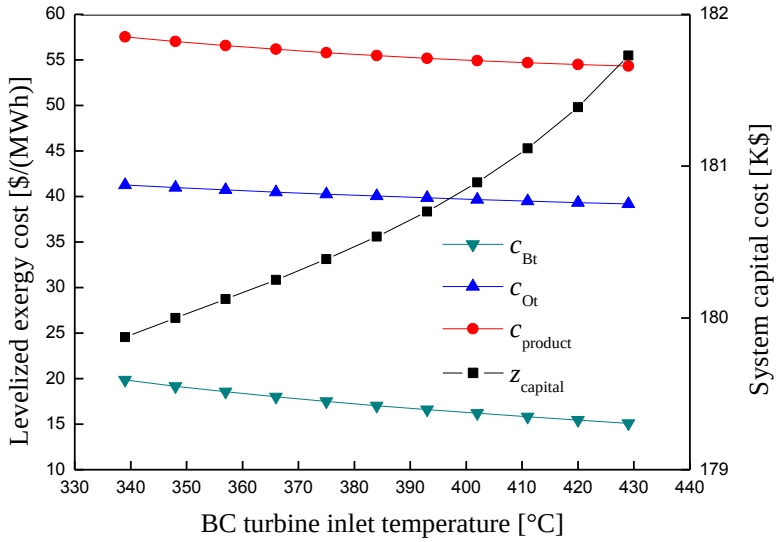

1006

1007 **Fig. 3.** Influences of BC turbine inlet temperature on the levelized exergy cost and the

1008 system capital cost of the system.

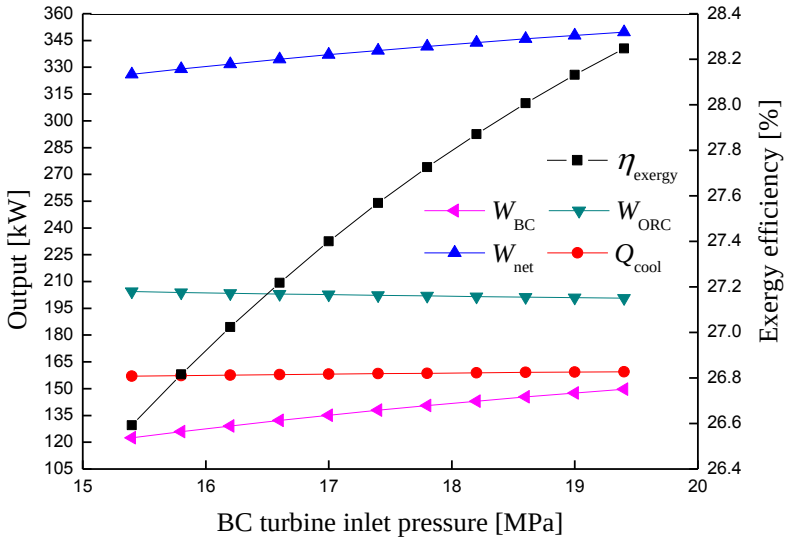

1009

1010 **Fig. 4.** Influences of BC turbine inlet pressure on the output and the exergy efficiency

1011 of the system.

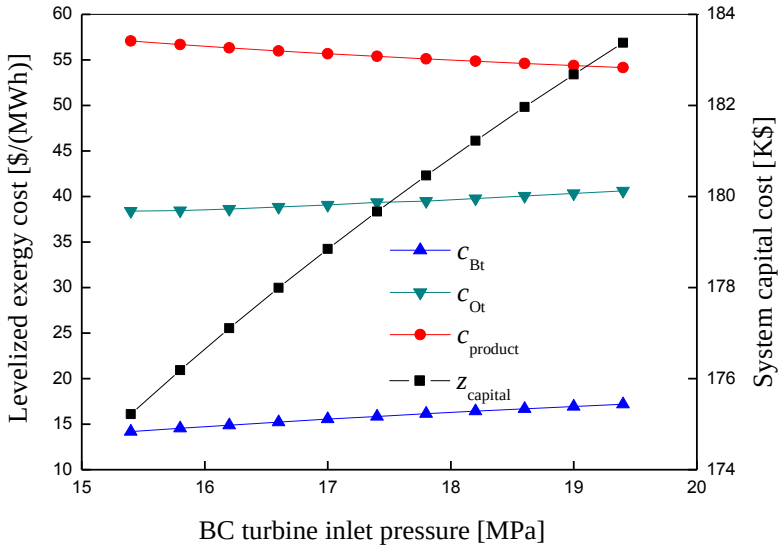

1012

1013 **Fig. 5.** Influences of BC turbine inlet pressure on the levelized exergy cost and the

1014 system capital cost of the system.

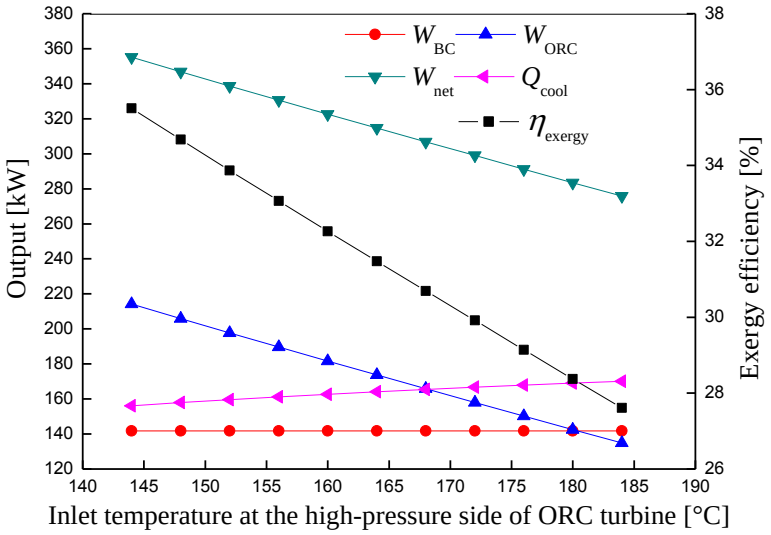

1015

1016 **Fig. 6.** Influences of inlet temperature at the high-pressure side of ORC turbine on the

1017 output and the exergy efficiency of the system.

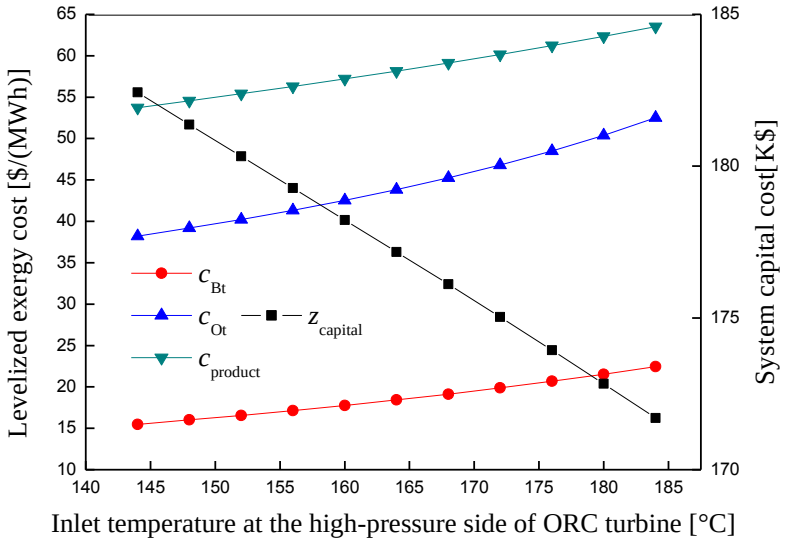

1018

1019 **Fig. 7.** Influences of inlet temperature at the high-pressure side of ORC turbine on the

1020 levelized exergy cost and the system capital cost of the system.

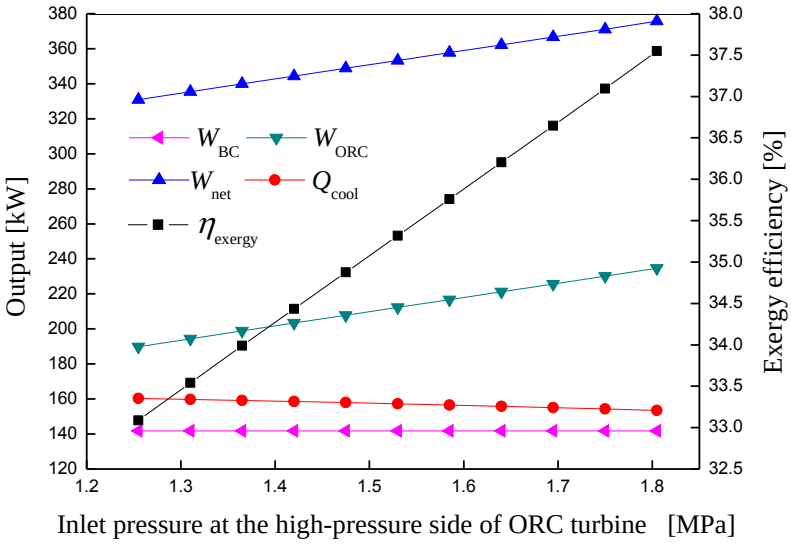

1021

1022 **Fig. 8.** Influences of inlet pressure at the high-pressure side of ORC turbine on the

1023 output and the exergy efficiency of the system.

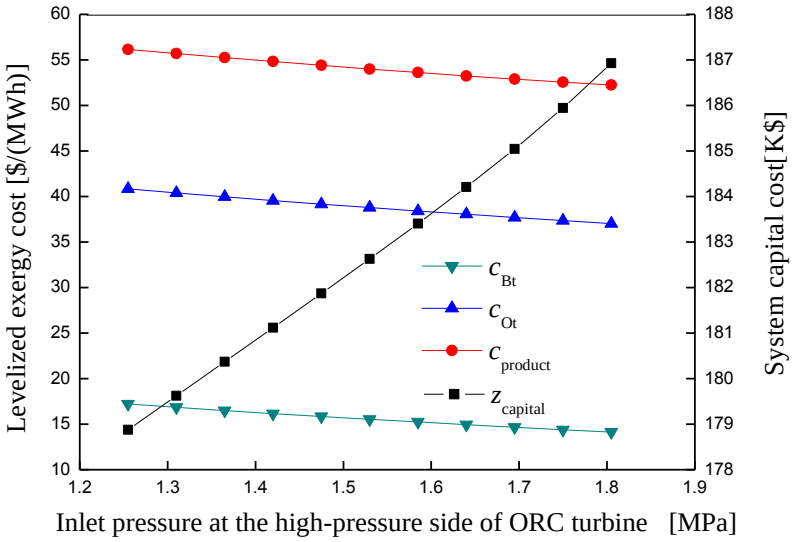

1024

1025 **Fig. 9.** Influences of inlet pressure at the high-pressure side of ORC turbine on the

1026 levelized exergy cost and the system capital cost of the system.

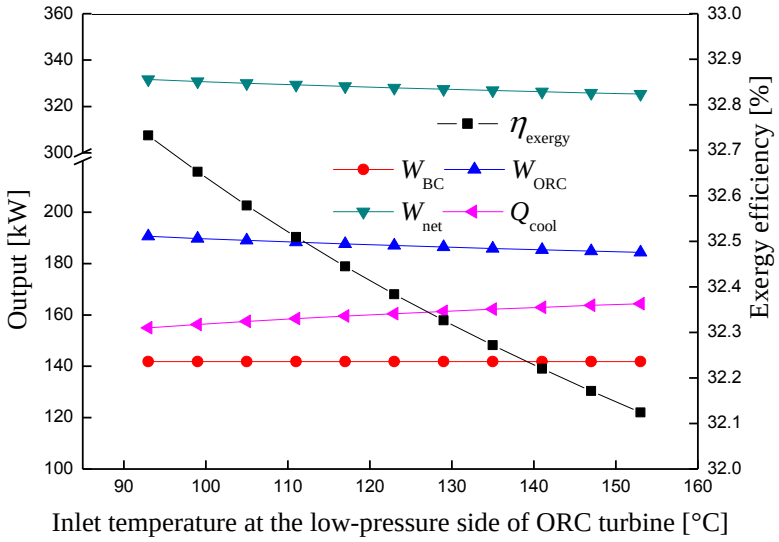

1027

1028 **Fig. 10.** Influences of inlet temperature at the low-pressure side of ORC turbine on the

1029 output and the exergy efficiency of the system.

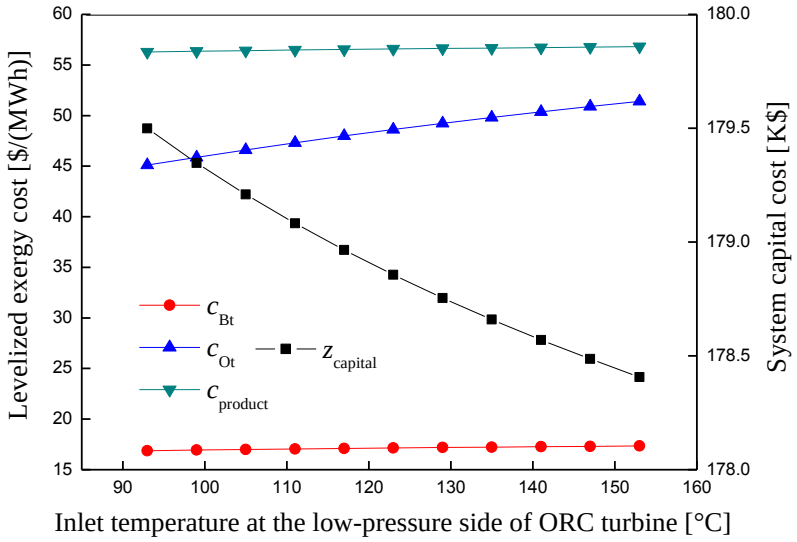

1030

1031 **Fig. 11.** Influences of inlet temperature at the low-pressure side of ORC turbine on

1032 the levelized exergy cost and system capital cost of the system.

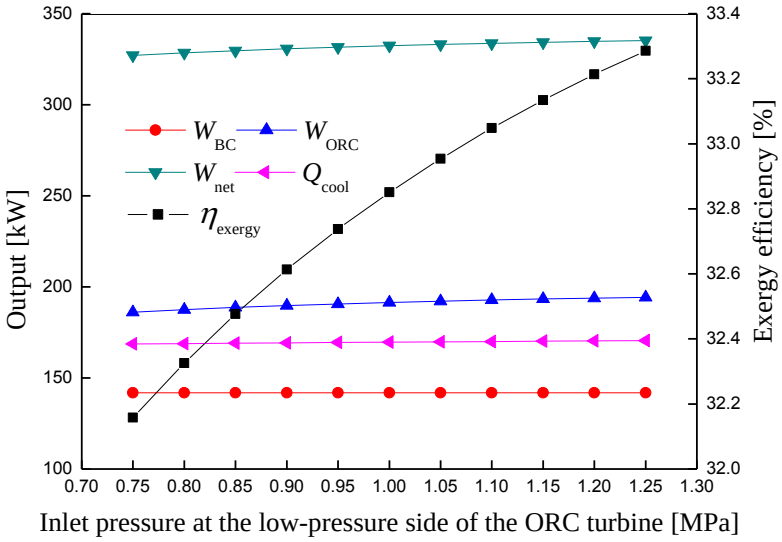

1033

1034 **Fig. 12.** Influences of inlet pressure at the low-pressure side of ORC turbine on the

1035 output and the exergy efficiency of the system.

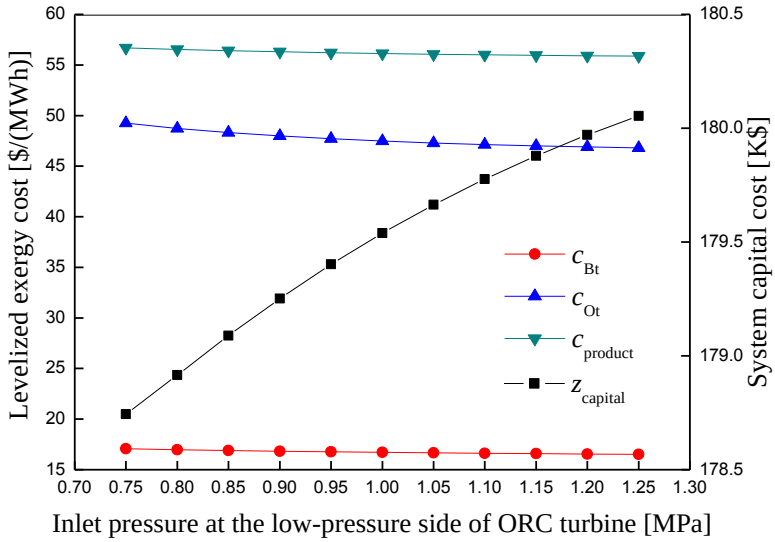

1036

1037 **Fig. 13.** Influences of the inlet pressure at the low-pressure side of ORC turbine on

1038 the levelized exergy cost and system capital cost of the system.

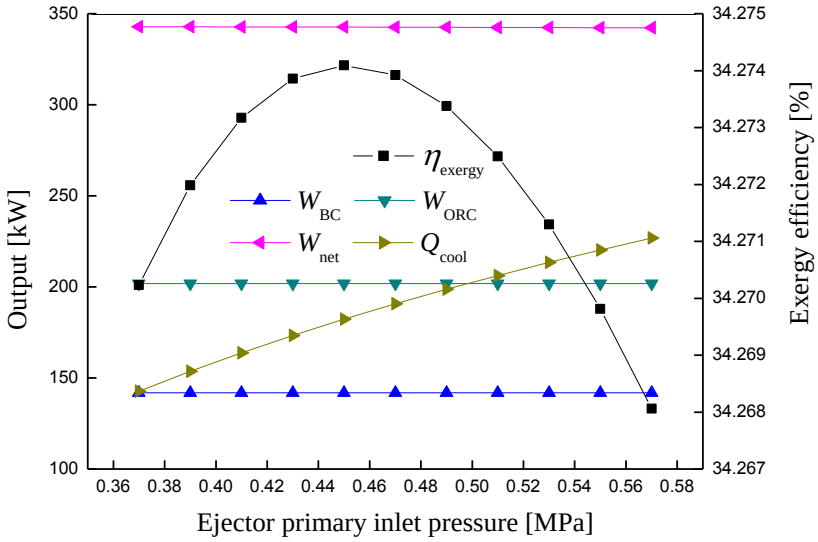

1039

1040 **Fig. 14.** Influences of ejector primary inlet pressure on the output and the exergy

1041 efficiency of the system.

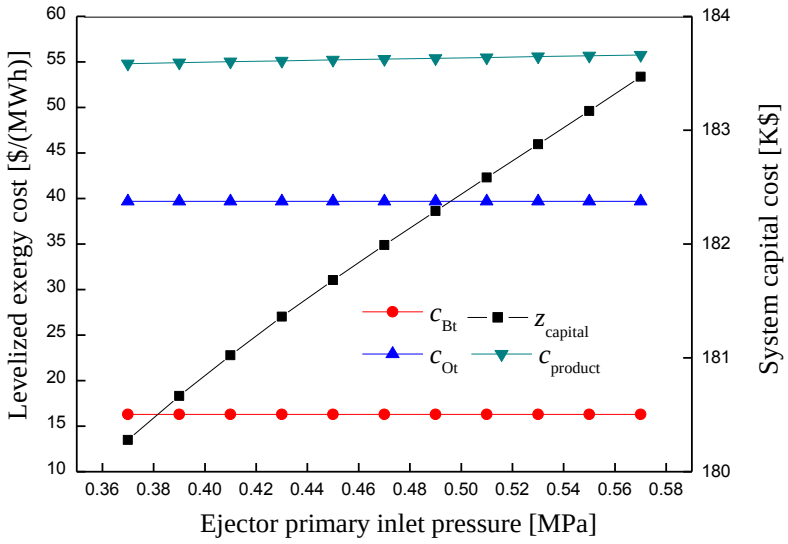

1042

1043 **Fig. 15.** Influences of ejector primary inlet pressure on the levelized exergy cost and

1044 the system capital cost of the system.

Performance analysis and optimization of a combined cooling and power system using low boiling point working fluid driven by engine waste heat

Wenge Huang, Jiangfeng Wang*, Jiaxi Xia, Pan Zhao, Yiping Dai

Institute of Turbomachinery, Shaanxi Engineering Laboratory of Turbomachinery and Power Equipment, State Key Laboratory of Multiphase Flow in Power Engineering, School of Energy and Power Engineering, Xi'an Jiaotong University, Xi'an 710049, China

Corresponding author: Jiangfeng Wang

Mailing address:

Institute of Turbomachinery, Shaanxi Engineering Laboratory of Turbomachinery and Power Equipment, State Key Laboratory of Multiphase Flow in Power Engineering, School of Energy and Power Engineering

Xi'an Jiaotong University, Xi'an 710049, China

E-mail address: jfwang@mail.xjtu.edu.cn (JF Wang).

Performance analysis and optimization of a combined cooling and power system using low boiling point working fluid driven by engine waste heat

Wenge Huang, Jiangfeng Wang*, Jiaxi Xia, Pan Zhao, Yiping Dai

Institute of Turbomachinery, Shaanxi Engineering Laboratory of Turbomachinery and Power Equipment, State Key Laboratory of Multiphase Flow in Power Engineering, School of Energy and Power Engineering, Xi'an Jiaotong University, Xi'an 710049, China

Abstract

This paper develops a combined cooling and power system, which consists of a carbon dioxide Brayton cycle, a dual-pressure organic Rankine cycle and an ejector refrigeration cycle, to recover waste heat from exhaust gas and jacket water in internal combustion engines. Thermodynamic models of the system are performed and exergoeconomic methods are used to calculate the levelized exergy cost of the component products. Effects of seven parameters, including temperature and pressure at the Brayton cycle turbine inlet, temperature and pressure at the high-pressure and low-pressure side of the organic Rankine cycle turbine inlet and pressure at the ejector primary inlet, are evaluated. Single-objective optimization is carried out by means of genetic algorithm to obtain the minimum levelized exergy cost of system product. Results show that the increase of pressure at Brayton cycle turbine inlet and high-pressure and low-pressure side of the organic Rankine cycle turbine inlet

contributes to the decrease of levelized exergy cost of the system product. Optimization results show that minimum levelized exergy cost for system product is 53.25 \$ $(MWh)^{-1}$. When system product levelized exergy cost is minimum, system net power output, cooling capacity and exergy efficiency are 374.37 kW, 188.63 kW and 37.31%, respectively.

Nomenclature

Latin symbols		ρ	density, kg m^{-3}
A	area, m^2	μ	dynamic viscosity, m^2 s^{-1}
B_o	boiling number	η	efficiency, %
c	levelized average cost, \$ $(MWh)^{-1}$	δ	thickness, m
c_p	specific heat, kJ kg^{-1} K^{-1}	*Subscribes*	
C	cost rate, \$ $year^{-1}$	1-31	state points
D	diameter, m	g1-g3	state points
e	exergy, kJ kg^{-1}	w1-w3	state points
E	exergy flow rate, kJ s^{-1}	Bt	Brayton cycle turbine
E_y	exergy flow rate per year, kJ $year^{-1}$	BM	bare module
F	multiplying factor	cond	condenser
f	friction factor	comp	compressor
G	mass flow rate, kg s^{-1}	D	destruction
h	enthalpy, kJ kg^{-1}	elec	electricity
H	depth, m	es	equivalent diameter
i_{eff}	interest rate	ev	evaporation/evaporator

l	length, m	ex	exergy
M	mass flow rate, kg s^{-1}	F	fuel
n	lifetime, year	g	exhaust gas
Nu	Nusselt number	gh	gas heater
P	pressure, MPa	he	heat exchanger
Pr	Prandtl number	L	loss
Pt	center distance between tubes, m	l	liquid
P_r	reduced pressure	M	material
Q	heat transfer rate, kW	Ot	ORC turbine
Q_{cool}	cooling capacity, kW	P	product
q_m	average imposed wall heat flux, W m^{-2}	p1	pump 1
r_f	enthalpy of vaporization, kJ kg^{-1}	p2	pump 2
T	temperature, K	p3	pump 3
U	overall heat transfer coefficient, W m^{-2} K^{-1}	p4	pump 4
W	power, kW	pf	primary flow
W_y	annually power, MWh $year^{-1}$	prec	precooler
x	vapor quality	preh	preheater
Z	annually levelized cost value, \$ $year^{-1}$	s	shell
z	capital cost, k\$	t	tube
Acronyms		th	thermal
BC	Brayton cycle	turb	turbine
CBC	CO_2 Brayton cycle	vg	vapor generator

CCP	combined cooling and power	w	tube wall
CRF	capital recovery factor		
CEPCI	chemical engineering plant cost index		
DORC	dual-pressure organic Rankine cycle		
ERC	ejector refrigeration cycle		
GA	genetic algorithm		
TEG	thermoelectric generator		
AARC	ammonia absorption refrigeration cycle		
Greek symbols			
α	convection heat transfer coefficient, W m^{-2} K^{-1}		
λ	heat conductivity, W m^{-1} K^{-1}		

1. Introduction

Nowadays, internal combustion engine (ICE) is the major motive power source in energy field, which are widely used in transport, construction, agriculture, etc. Over 50 % of the total transportation fuel is consumed by ICEs [1]. However, only 30-45% of the fuel energy is converted into effective power output, while the remaining energy is discharged to the environment via exhaust gas, jacket water and charge air, causing a large amount of waste fuel energy [2]. Thus, technology for waste heat recovery from ICEs has drawn much interest of researchers in the last decade. Much effort has been devoted to the study of organic Rankine cycle (ORC) based ICE waste heat recovery system for its advantages of high efficiency and simple structure [3].

There are two important pathways that will lead to the improvement of the ORC system for ICE waste heat recovery. One will be selecting organic working fluids which are suitable for the system under certain conditions. Another is to optimize the system configuration to make full use of the waste heat.

The work of selecting suitable organic working fluids for ORC was carried out by many researchers to improve the efficiency of the ICE waste heat recovery. Tian et al. [4] evaluated the performance of 20 different working fluids in an ORC system for ICE waste heat recovery. Rijpkema et al. [5] compared the performance of twelve working fluids in an ORC-based ICE waste heat recovery system to find the suitable candidate. Su et al. [6] developed a theoretical efficiency model about working fluids selecting for ORC-based ICE waste heat recovery system via strict mathematical derivation.

Configuration optimization in ORC-based ICE waste heat recovery system mainly focuses on reducing the system irreversible rate to fully utilize the engine waste heat. Vaja and Gambarotta [7] added a preheater and a recuperator separately to a simple ORC system to improve the performance for the ICE waste heat recovery. Kim et al. [8] proposed a novel single-loop ORC system to recovery engine waste heat. They employed two recuperators in series to heat the working fluid. Comparison showed that the net power output of the system was 35.6% more than simple ORC system. Because that the maximum power output of single-loop ORC is lower than that of the dual-loop ORC system [9], more attention has been focused on dual-loop ORC based ICE waste heat recovery system in recent years. Wang et al. [10] modeled a dual-loop

ORC system for engine waste heat recovery. The high-temperature loop absorbed heat from exhaust gas and its residual heat acted as heat source for the low-temperature loop. Wang et al. [11] investigated a dual-loop ORC system for ICE waste heat recovery. The high-temperature loop absorbed heat from exhaust gas for the first time. Then the low-temperature loop absorbed heat from the residual heat of the exhaust gas to realize the cascading utilization of the waste heat. Huang et al. [12] proposed a complex dual-loop ORC system for engine waste heat recovery. The high-temperature loop absorbed heat from the exhaust gas and residual heat from both the exhaust gas and the high-temperature loop provided heat for the low-temperature loop.

When referring to heat transfer in the high-temperature loop, thermal stability of organic working fluid is necessary to be considered. In previous studies, refrigerants were most selected as working fluids. The decomposition temperatures of refrigerants are relatively low (200-300 ℃) [13], while the temperature of exhaust gas is above 450 ℃[14]. Direct heat transfer between high-temperature exhaust gas and refrigerant caused the risk of working fluid decomposition. Though high decomposition temperature working fluids such as siloxanes and alkanes were adopted by some researchers, their flammability hindered their further applications [15]. Though placing a heat transfer oil intermediate loop between the exhaust gas and the ORC system could address this issue [16], it would cause a large amount of the high-temperature waste heat unharnessed. Therefore, some other high-temperature loops for waste heat recovery were employed by researchers to couple with the ORC. Miller et al. [17] introduced thermoelectric generator (TEG) technology.

98 High-temperature exhaust gas was first exploited by the TEG, then the cooled exhaust
99 gas could drive the ORC safely. But the energy conversion capacity of TEG is low
100 because of the material limitation. Steam Rankine for its high efficiency and stable
101 operation attracted much attention of researchers. Shu et al. [18] placed a steam
102 Rankine cycle between the ORC and the exhaust gas. Yu et al. [19] coupled a steam
103 Rankine cycle with an ORC for the ICE waste heat recovery. However, the large bulk
104 of the components in steam Rankine cycle limits further applications (such as
105 application in vehicles) [20]. Considering the requirement of high thermal efficiency
106 and compact configuration, Brayton cycle could be a compromise solution. Brayton
107 cycle with CO_2 (carbon dioxide) as working fluid has the advantage of low
108 environmental impact and good thermodynamic performance [21]. Few studies about
109 ORC system coupled with CO_2 Brayton cycle (CBC) for ICE waste heat recovery
110 have been published. Though Zhang et al. [20] carried out some relevant studies, their
111 attention was focused on comparing the performance of CBC, TEG and steam
112 Rankine cycle when coupled with the same bottom ORC. Detailed analysis of the
113 CBC was not given and the energy in jacket water was not harnessed.

114 Jacket water, though containing large amounts of energy [22], obtained little
115 attention in the previous studies. For its relatively low temperature, jacket water was
116 mainly used to preheat the organic working fluid in the ORC system. In the
117 ORC-based ICE waste heat recovery system designed by Zhang et al. [23] jacket
118 water was used to preheat the organic working fluid. Then the organic working fluid
119 was heat by the high-temperature exhaust gas to vapor state and expanded in the ORC

turbine. In Yang's [24] ICE waste heat recovery system, jacket water and secondary exhaust gas were used to preheat the organic working fluids in ORC. In the dual-loop ORC based ICE waste heat recovery system investigated by Song et al. [25], jacket water was used to preheat the low-temperature-loop. Yu et al. [26] calculated the energy recovery efficiency from an ORC-based ICE waste heat recovery system. 75% waste heat could be recovered from the exhaust gas, while only 9.5% waste heat was recovery from jacket water. The relatively low utilization rate of jacket water in the ORC system is caused by the mismatch of working fluid mass flow rate in the preheater and the evaporator. Thus, the utilization of energy in jacket water could be further explored.

Multigeneration system driven by waste heat has drawn increasing interest of researchers in light of the trend towards reducing emissions, increasing the efficiency of energy use and providing variable energy. Li et al. [27] modeled a combined cooling, heating and power system to highly utilize the waste heat. Yari et al. [28] proposed a waste heat recovery system to provide power, distilled water and heat. Bai et al. [29] investigated a cooling, heating and power system driven by exhaust gas to recovery the waste heat. Combined cooling and power (CCP) systems driven by ICE waste heat were also investigated by some researchers. Chen et al. [30] designed an ammonia-water combined cooling and power system using the waste heat from the ICEs. Ammonia-water was heated by exhaust gas and jacket water. One part of the ammonia-water vapor flew into the turbine to provide power and the other part flew into the evaporator to provide refrigeration. Salek et al. [31] coupled an ammonia

absorption refrigeration cycle and a bottoming Rankine cycle with internal combustion engine to produce power and cooling capacity.

Ammonia absorption refrigeration cycle (AARC) were widely used in the combined cooing and power system for its large refrigeration output. However, the complex cycle structure and high driven temperature requirement of AARC might sometimes limit its applications. On the contrary, ejector refrigeration cycle (ERC) exhibits the advantages of easy maintenance and high reliability [32] and it can be driven by low-temperature heat source such as the jacket water. Thus, ICE waste heat recovery system with ERC driven by jacket water not only simultaneously generate power and refrigeration but also fully utilized the jacket water waste heat.

In this study, a combined cooling and power system is developed, which comprises a CO_2 Brayton cycle, a dual-pressure organic Rankine (DORC) cycle and an ejector refrigeration cycle. The CO_2 Brayton cycle absorbs heat from the high-temperature exhaust gas directly to prevent the decomposition risk. The turbine exhaust in the CO_2 Brayton cycle and the engine exhaust gas after heat transfer are respectively regarded as the heat sources for the high-pressure side and low-pressure side of the dual-pressure ORC, realizing the cascading utilization of exhaust gas. Meanwhile, organic working fluids in high-pressure side and low-pressure side are both preheated by jacket water which increases the mass flow rate of the organic working fluid preheated by jacket water. What's more, the ejector refrigeration cycle is adopted to produce refrigeration and fully utilize waste heat in jacket water. Thermodynamic and exergoeconomic analysis is carried out to examine the effects of key parameters on

system performance. Then a system optimization is conducted to obtain the minimum levelized exergy cost for the system product by means of genetic algorithm (GA).

The innovative features of this paper are as follow:

- A CO_2 Brayton cycle is investigated to prevent the risk of decomposition of organic working fluid and provide power.
- A novel dual-pressure ORC system is developed to cascading utilize the waste heat in exhaust gas and jacket water and provide large amounts of power output.
- An ejector refrigeration cycle driven by jacket water is designed to provide refrigeration and fully utilize the jacket water waste heat.

2. System description

The combined cooling and power system is shown in Fig. 1. The system integrates a dual-pressure organic Rankine cycle with a CO_2 Brayton cycle and an ejector refrigeration, which can produce power and refrigeration simultaneously. High-temperature gas heat from the ICE enters the gas heater to provide heat for the CBC. In the CBC, compressor compresses the CO_2 to a supercritical state. The high-pressure CO_2 flows into the gas heater to absorb heat. Then CO_2 with high temperature and high pressure expands through the BC turbine to produce power.

After expanding in the BC turbine, the high-temperature exhaust CO2 flows into vapor generator 2 to heat the organic working fluid. High-pressure side organic working fluid heated by the CO2 then flows into the ORC turbine to produce power. Meanwhile low-pressure side organic working fluid absorbs heat from the secondary

185 engine exhaust gas in vapor generator 1 and then enters ORC turbine to produce
186 power.

187 Exhaust vapor from the ORC turbine is cooled by condenser 1 to liquid state and
188 pressured by pump 1. Jacket water with large mass flow rate is used to preheat the
189 organic working fluid in the preheater. The preheated organic working fluid then
190 separates. One part of the fluid is pumped by pump 3 to the vapor generator 1 to cycle
191 in the low-pressure side. The other part is pumped by pump 2 to the vapor generator 2
192 to cycle in the high-pressure side.

193 The jacket water then flows into vapor generator 3 to provide heat for the ejector
194 refrigeration cycle. After the condensation process in condenser 2, liquid working
195 fluid is divided into two separated parts. One part of the fluid is pumped to the vapor
196 generator 3 to absorb heat from jacket water and then becomes superheated vapor.
197 The other part of the working fluid flows through the throttle valve to become
198 low-pressure vapor-liquid mixture. The low-pressure mixture enters the evaporator to
199 produce cooling capacity when absorbing heat from the environment and become
200 low-pressure vapor. After that, the superheated vapor mixes with the low-pressure
201 vapor in the ejector. The mixed working fluid enters the condenser 2 to be condensed
202 to liquid.

203 R245fa is selected as the working fluid for the organic Rankine cycle and the
204 ejector refrigeration cycle because of the great thermodynamic performance [33] and
205 the low environment effects [34].

3. System model

Several assumptions are made to simplify the simulation of the system, which are: (1) the system keeps a steady state; (2) the heat and frication in the system are not considered; (3) the pressure losses in the vapor generators, preheater, evaporator, condensers and pipes are neglected; (4) the gas temperature at the outlet of the vapor generator 1 is higher than 110 ℃ [35], considering the low gas dew point temperature; (5) the working fluids at the outlet of the condensers and the preheater are saturated liquids, and the evaporator outlet state is saturated vapor; (6) the process through the throttle valve is isenthalpic.

3.1.Energy model

The net power of the CO_2 Brayton cycle is expressed as:

$$W_{BC} = W_{Bt} - W_{comp} \tag{1}$$

The net power of the DORC is given as:

$$W_{ORC} = W_{Ot} - W_{p1} - W_{p2} - W_{p3} \tag{2}$$

The cooling capacity of the ERC is given as:

$$Q_{cool} = M_{cool} \cdot (h_{21} - h_{20}) \tag{3}$$

The net power output of the whole system is calculated as:

$$W_{net} = W_{ORC} + W_{BC} - W_{p4} \tag{4}$$

The thermal efficiency of the system is given as:

$$\eta_{th} = \frac{W_{net} + Q_{cool}}{M_{g1} \cdot (h_{g1} - h_{g3}) + M_{w1} \cdot (h_{w1} - h_{w3})} \tag{5}$$

The detailed energy model equations of each component are list in Table 1. Note

227 that there are two expanding processes in the ORC turbine. The high-pressure vapor
228 expands in the turbine and then mixes with the vapor from vapor generator 1. After
229 that, the mixed vapor expands in the turbine for the second time.

230 3.2.Exergy model

231 The energy model of the system is based on the first law of thermodynamics. From
232 the viewpoint of the first law, it is equivalent for work and heat. Nevertheless,
233 according to the second law of the thermodynamics, the irreversibility of work and
234 heat is different. The exergy is used to quantifies the difference between them. The
235 exergy model of the system is based on a dead state (the ambient condition in this
236 study). Definition of exergy is given as:

237 $$e = (h - h_0) - T_0 \cdot (s - s_0) \quad (6)$$

238 where h_0, T_0 and s_0 are the parameters under the ambient conditions.

239 The exergy flow rate in this study is given by:

240 $$E = M \cdot e \quad (7)$$

241 In this study, all the components in the system are associated directly or indirectly
242 with fuel of other heat sources, such as exhaust as and jacket water. The heat sources
243 provide exergy for the components to operate. For each component, there is an exergy
244 balance equation, being expressed as [36]:

245 $$E_F = E_P + E_D + E_L \quad (8)$$

where E_F, E_P, E_D, E_L donate the rate of exergy for the component fuel, the rate of exergy for component product, the rate of component exergy destruction and the rate of component exergy loss, respectively.

The details of the exergy balance equations for each component are listed in Table 1.

The exergy efficiency represents the degree of the utilization of the waste heat in the system, being expressed as:

$$\eta_{ex} = \frac{W_{net} + E_{cool}}{E_{g1} - E_{g3} + E_{w1} - E_{w3}} \tag{9}$$

where E_{cool} is the exergy rate of the cooling process, being expressed as:

$$E_{cool} = E_{25} - E_{24} \tag{10}$$

3.3.Capital cost calculation

A method of modeling the capital costs of main components is used in this study. According to Ref. [37], the bare module cost of the components is calculated as the basic cost. The basic cost of the components includes the direct project cost (such as component cost, material cost of the installation, etc.) and the indirect project cost (like the taxes, insurance engineering expenses, etc.). The bare module cost of the components is calculated under basic conditions. For deviations from the based conditions, multiplying factors (the specific component type, the specific system pressure and the specific material of construction) are added in the calculation to correct the results. In the following text, equations from Eq. (11) to Eq. (21) are proposed in Ref. [37].

Axial turbines (BC turbine and ORC turbine) are used in this study. The bare module cost equation of the turbine is:

$$\log_{10} C_{\text{turb}}^{0} = K_{1,\text{turb}} + K_{2,\text{turb}} \cdot \log_{10} W + K_{3,\text{turb}} \cdot (\log_{10} W)^2 \quad (11)$$

where $K_{\text{i, turb}}$ are constants corresponding to the turbine type; and W is the power output of the turbine.

Turbines used in this study are made of carbon steel (CS) and operate under high pressure. Thus, a multiplying factor is used to correct the result. The capital cost of the turbine is given as:

$$C_{\text{turb}} = F_{\text{BM,turb}} \cdot C_{\text{turb}}^{0} \quad (12)$$

where $F_{\text{BM,turb}}$ is the multiplying factor corresponding to the working conditions of the turbine.

Reciprocating pumps are used in this study. The bare module cost equation of the pumps is given as:

$$\log_{10} C_{\text{pump}}^{0} = K_{1,\text{pump}} + K_{2,\text{pump}} \cdot \log_{10} W + K_{3,\text{pump}} \cdot (\log_{10} W)^2 \quad (13)$$

where $K_{\text{i, pump}}$ are the constants corresponding to the pump type; and W is the power input of the pump.

Pumps used in this study are made of stainless steel (SS) and work under high pressure. Thus, multiplying factors are used to correct the bare module cost. The capital cost of the pump is given as:

$$C_{\text{pump}} = \left(B_{1,\text{pump}} + B_{2,\text{pump}} \cdot F_{\text{M,pump}} \cdot F_{\text{P,pump}} \right) \cdot C_{\text{pump}}^{0} \quad (14)$$

where $B_{\text{i, pump}}$ are the constants corresponding to the type of the pump; $F_{\text{M,pump}}$ is the material factor of the pump and $F_{\text{P,pump}}$ is the pressure factor of the pump. The equation of the pressure factor is given as:

$$\log_{10} F_{\text{P,pump}} = C_{1,\text{pump}} + C_{2,\text{pump}} \cdot \log_{10} P_{\text{pump}} + C_{3,\text{pump}} \cdot (\log_{10} P_{\text{pump}})^2 \quad (15)$$

where $C_{\text{i, pump}}$ are the constants corresponding to the type of the pump; and P_{pump} is the pressure of the pump under working conditions.

Axial compressor is used in this study. The bare module cost equation of the compressor is given as:

$$\log_{10} C^0_{\text{comp}} = K_{1,\text{comp}} + K_{2,\text{comp}} \cdot \log_{10} W + K_{3,\text{comp}} \cdot (\log_{10} W)^2 \quad (16)$$

where $K_{\text{i,comp}}$ are the constants corresponding to the type of the compressor; W is the power input of the compressor.

The compressor is made of carbon steel (CS) and works under high pressure. Correction equation of the bare module cost is given as:

$$C_{\text{comp}} = F_{\text{BM,comp}} \cdot C^0_{\text{comp}} \quad (17)$$

where $F_{\text{BM,comp}}$ is the constant corresponding to the type of the compressor.

Shell-and-tube heat exchangers (gas heater, vapor generators, precooler, preheater, evaporator and condensers) are used in this study. The bare module cost equation of the heat exchanger is given as:

$$\log_{10} C^0_{\text{he}} = K_{1,\text{he}} + K_{2,\text{he}} \cdot \log_{10} A + K_{3,\text{he}} \cdot (\log_{10} A)^2 \quad (18)$$

where $K_{\text{i,he}}$ are the constants corresponding to the type of the heat exchanger; A is the heat transfer area of the heat exchanger. The calculation of the heat exchanger areas is presented in Appendix A.

Heat exchangers used in this study are made of carbon steel (CS) and work under different pressure. Multiplying factors are needed to correct the results, the equation is given as:

$$C_{\mathrm{he}} = \left(B_{1,\mathrm{he}} + B_{2,\mathrm{he}} \cdot F_{\mathrm{M,he}} \cdot F_{\mathrm{P,he}}\right) \cdot C_{\mathrm{he}}^{0} \quad (19)$$

where $B_{\mathrm{i,he}}$ are the constants corresponding to the type of the heat exchanger. $F_{\mathrm{M,he}}$ and $F_{\mathrm{P,he}}$ are the material factor and pressure factor, respectively. The pressure factor is obtained from the following equation:

$$\log_{10} F_{\mathrm{P,he}} = C_{1,\mathrm{he}} + C_{2,\mathrm{he}} \cdot \log_{10} P_{\mathrm{he}} + C_{3,\mathrm{he}} \cdot (\log_{10} P_{\mathrm{he}})^{2} \quad (20)$$

where $C_{\mathrm{i,he}}$ are the constants corresponding to the type of the heat exchanger; P_{he} is the designed working pressure for the heat exchanger.

The values of the constants mentioned above for the main components are listed in Appendix B.

The calculation of the bare module cost depends on past records or published correlations for price information. It is necessary to update the costs because of the inflation. This can be achieved by the following equation:

$$C_2 = C_1 \cdot \left(\frac{I_2}{I_1}\right) \quad (21)$$

where C is the purchased cost and I is the cost index. The subscript 1 refers to base time when cost is known and subscript 2 refers to time when cost is desired. The *CEPCI* (Chemical Engineering Plant Cost Index) is employed to calculate the inflation. The values of $CEPCI_{2016}$ and $CEPCI_{\mathrm{ref,2001}}$ are 541.7 and 397, respectively [38].

3.4.Exergoeconomic model

Exergoeconomic is a branch of engineering which combines the thermodynamic analysis and economic principles. Thermodynamic performance and economic cost of the system are all taken into consideration.

To find the relationship between the present value of the expenditure and the equivalent annually levelized costs, the capital recovery factor (CRF) is employed, being expressed as [36]:

$$Z_{\mathrm{i}} = CRF \cdot C_{\mathrm{i}} \tag{22}$$

$$CRF = \frac{i_{\mathrm{eff}} \cdot (1+i_{\mathrm{eff}})^{n}}{(1+i_{\mathrm{eff}})^{n}-1} \tag{23}$$

where i_{eff} is the effective discount rate with a value of 0.05 [39]; and n is the lifetime of the CCP system, being assumed as 30 years [40].

In order to calculate the equivalent annually levelized costs, the annual working time of the system is assumed as 8000 h [41]. Then the annual exergy rates and annual power output or consumption are obtained.

In a steady system, there are a number of entering and outing working fluid streams and heat and work interactions with the surroundings. In exergoeconomic analysis, each flowing stream is associated with a levelized exergy cost. The equations to calculate the cost of the stream product are given as:

$$C_{\mathrm{in}} = c_{\mathrm{in}} \cdot E_{\mathrm{y,in}} \tag{24}$$

$$C_{\mathrm{out}} = c_{\mathrm{out}} \cdot E_{\mathrm{y,out}} \tag{25}$$

$$C_{\mathrm{work}} = c_{\mathrm{work}} \cdot W_{\mathrm{y}} \tag{26}$$

$$C_{\text{heat}} = c_{\text{heat}} \cdot E_{\text{y,heat}} \tag{27}$$

where c denotes levelized exergy cost of the streams; $E_{y,in}$ and $E_{y,out}$ are the exergy transfer rate of the stream flowing in and out of a component; W_y and $E_{y,heat}$ are the power and the heat transfer rate of the components considering the annual working time.

The cost balance equation applied to the kth system component is given as:

$$\sum_{\text{out}} C_{\text{out,k}} + C_{\text{w,k}} = C_{\text{heat,k}} + \sum_{\text{in}} C_{\text{in,k}} + Z_{\text{k}} \tag{28}$$

Details of the cost balance equation are listed in Table 2.

The levelized exergy cost for system product is chosen to indicate the exergoeconomic performance, being expressed as [42,43]:

$$c_{\text{product}} = c_{\text{capital}} + c_{\text{fuel}} \tag{29}$$

where $c_{capital}$ is the capital-cost-related part of the levelized exergy cost for the system product, being expressed as:

$$c_{\text{capital}} = \frac{Z_{\text{total}}}{W_{\text{net}} + E_{\text{cool}}} \tag{30}$$

where c_{fuel} is the fuel-cost-related part of the levelized exergy cost for the system product, being expressed as:

$$c_{\text{fuel}} = \frac{c_{\text{Bt}} \cdot W_{\text{y,comp}} + c_{\text{Ot}} \cdot W_{\text{y,pump1}} + c_{\text{Ot}} \cdot W_{\text{y,pump2}} + c_{\text{Ot}} \cdot W_{\text{y,pump3}} + c_{\text{Ot}} \cdot W_{\text{y,pump4}}}{W_{\text{net}} + E_{\text{cool}}} \tag{31}$$

where c_{Bt} and c_{Ot} are the levelized exergy cost for the BC turbine power output and the ORC turbine power output, which are calculated in Table 3. Likewise, they can be expressed as the capital-cost-related part and the fuel-cost-related part, given by Eq. (32) and Eq. (33).

373 $$c_{\mathrm{Bt}}=\frac{Z_{\mathrm{Bt}}}{W_{\mathrm{y,Bt}}}+\frac{c_3\cdot\left(E_{\mathrm{y},3}-E_{\mathrm{y},4}\right)}{W_{\mathrm{y,Bt}}} \quad (32)$$

374 $$c_{\mathrm{Ot}}=\frac{Z_{\mathrm{Ot}}}{W_{\mathrm{y,Ot}}}+\frac{c_{10}\cdot\left(E_{\mathrm{y},10}+E_{\mathrm{y},11}-E_{\mathrm{y},12}\right)}{W_{\mathrm{y,Ot}}} \quad (33)$$

375 In addition, the levelized exergy cost for the condensers and the precooler is equal
376 to zero, being given by:

377 $c_{26}=c_{28}=c_{30}=0$ (34)

378 The levelized exergy cost for the exhaust gas as well as the jacket water is zero,
379 being expressed as:

380 $c_{g1}=c_{w1}=0$ (35)

381 3.5.Internal combustion engine

382 In this study, the engine selected [7] is a 12-cylinder 4-stroke supercharged engine.
383 The main designed parameters of the engine are listed in Table 3. The composition of
384 the engine exhaust gas is presented in Table 4. The thermal load of the engine exhaust
385 gas is about 1700 kW and 1000 kW can be obtained from the engine jacket water.

386 3.6.Simulation conditions for the system

387 The thermodynamic parameters of the working fluid are calculated under the
388 environment of MATLAB with the help of REFPROP 9.1 [44]. The basic conditions
389 of simulation for the CCP system are listed in Table 5.

390 Seven key parameters : BC turbine inlet temperature ($T_{\mathrm{Bt,in}}$), BC turbine inlet
391 pressure ($P_{\mathrm{Bt,\,in}}$), inlet temperature at the high-pressure side of ORC turbine ($T_{\mathrm{Ot,\,in,\,h}}$),
392 inlet pressure at the high-pressure side of ORC turbine ($P_{\mathrm{Ot,\,in,\,h}}$), inlet temperature at

393 the low-pressure side of ORC turbine ($T_{Ot,\,in,\,l}$), inlet pressure at the low-pressure side
394 of ORC turbine ($P_{Ot,\,in,\,l}$) and the ejector primary inlet pressure ($P_{ej,\,in}$), are chosen to
395 analyze the thermodynamic and exergoeconomic performance of the system. When
396 one parameter is investigated to analyze the system performance, other parameters are
397 maintained constants based on the conditions in Table 5.

398 In the thermodynamic aspect, the net power output of the CO_2 Brayton cycle (W
399 $_{BC}$), net power output of the DORC (W_{ORC}), net power of the whole system (W_{net}),
400 cooling capacity of the system (Q_{cool}) and the exergy efficiency of the system (η_{exergy})
401 are selected to reflect the system performance. Levelized exergy cost for the BC
402 turbine power output (c_{Bt}), levelized exergy cost for the ORC turbine power output
403 (c_{Ot}), levelized exergy cost the system product ($c_{product}$) and the system capital cost
404 ($z_{capital}$) are chosen to represent the exergoeconomic performance.

405 **4. Results and discussion**

406 The influence of the BC turbine inlet temperature ($T_{Bt,in}$) on the output and the
407 exergy efficiency of the system are shown in Fig. 2. The net power output of the CBC
408 increases with the rise of $T_{Bt,in}$. That can be explained by the large decrease of the
409 compressor power consumption. With the increase of the CO_2 temperature at the BC
410 turbine inlet, the mass flow rate of CO_2 decreases, leading to the decrease of the
411 compressor power consumption. Although the drop of CO_2 mass flow rate would cut
412 down the BC turbine power output, the decrease quantity of compressor power
413 consumption is larger than the decrease of the BC turbine power output. Thus, the

large decrease of the compressor power consumption determines the increase trend of the CBC net power output.

It is presented that the net power output of the DORC increases with the rise of the BC turbine inlet temperature. Since the residual heat in exhaust CO_2 acts as the heat source for the high-pressure side of DORC, the temperature rise of the exhaust CO_2, caused by the rise of $T_{Bt,in}$, would offer more heat for the bottom cycle, which causes the increase of the mass flow rate of the organic working fluid in the high-pressure side of DORC . Hence, the power output of the ORC turbine increases, leading to the increase of the net power output of the DORC.

With the increase of $T_{Bt,in}$, the cooling capacity of the ERC decreases, as shown in Fig. 2. The increase of the organic working fluid mass flow rate in DORC would absorb more heat from jacket water, resulting in the decrease of energy available for the ERC. As a result, less secondary flow working fluid from the evaporator is entrained to the ejector, resulting the decrease of the cooling capacity of the CCP system.

The increase of the CBC net power output and the DORC net power output account for the increase of the net power output of the whole CCP system. Though the cooling capacity of the ERC is large, it produces only a small amount of exergy. The decrease of the exergy output caused by the refrigeration capacity decrease can be made up by the increase of the power exergy output. Thus, the exergy efficiency of the system increases.

The influences of the BC turbine inlet temperature on the levelized exergy cost and

436 the system capital cost of the system are shown in Fig. 3. The levelized exergy cost
437 for the BC turbine power output (c_{Bt}) drops with the rise of the BC turbine inlet
438 temperature ($T_{Bt,in}$). That can be explained by the decrease of the capital-cost-related
439 part of c_{Bt}. The capital-cost-related part of c_{Bt} decreases with the decrease of cost of
440 compressor, which is cut down by the drop of the compressor power consumption.
441 The increase of the ORC turbine power output causes the decrease of both the
442 capital-cost related part and the fuel-cost-related part of c_{Ot}, resulting in the decrease
443 of c_{Ot}.

444 The system capital cost ($z_{capital}$) rises with the rise of $T_{Bt,in}$. The large increase of the
445 ORC turbine power output increases the cost of the ORC turbine. Moreover, the
446 increase of the mass flow rate of the organic working fluid in the DORC causes the
447 increase of cost for the vapor generator 2 and the preheater. Though the cost of
448 compressor decreases, it can't change the ascending trend of the total system capital.

449 It can be obtained in Fig. 3 that the levelized exergy cost for the system product
450 ($c_{product}$) decreases with the rise of $T_{Bt,in}$. The decline in levelized exergy cost for the
451 BC turbine and ORC turbine power output, according to Eq. (31), would cause the
452 decrease of the fuel-cost related part of $c_{product}$. Though the increase of $z_{capital}$ would cut
453 down the capital-cost-related part of $c_{product}$, the impact of levelized exergy cost for the
454 BC turbine and ORC turbine is greater, which leads to the descending trend of $c_{product}$.

455 The influence of the BC turbine inlet pressure ($P_{Bt,\,in}$) on the output and the exergy
456 efficiency of the system are shown in Fig. 4. The net power output of the CBC
457 increases with the increase of $P_{Bt,\,in}$, which can be explained by the rise of enthalpy

458 drop of the CO_2 in the BC turbine. Though the rise of $P_{Bt,\ in}$ requires more compressor
459 power consumption, the increase of the BC turbine power output is larger in quantity
460 than the consumption, which leads to the increase of the CBC net power output.

461 The net power output of the DORC decreases with the rise of $P_{Bt,\ in}$. On the one
462 hand, the temperature of the exhaust CO_2 at the BC turbine outlet decreases with the
463 increase of $P_{Bt,\ in}$. Thus, less heat is offered to the high-pressure cycle of DORC,
464 resulting in the decrease of the high-pressure cycle power output. On the other hand,
465 the increase of $P_{Bt,\ in}$ causes the increase of the compressor power consumption, which
466 results in the rise of the CO_2 temperature at the compressor outlet. Thus, less heat is
467 released in the gas heater and more heat is provided to the low-pressure cycle of
468 DORC, which leads to the increase of the low-pressure cycle power output. However,
469 the increase of the power output in low-pressure side is smaller than the decrease of
470 the power output in the high-pressure side. Thus, the net power of the DORC
471 decreases slightly.

472 The cooling capacity of the system increases with the increase of $P_{Bt,\ in}$. Just like the
473 variation of the power output, the decrease of the mass flow rate in the high-pressure
474 side of DORC is larger than the increase of mass flow rate in the low-pressure side.
475 Therefore, the total mass flow rate in the DORC decreases, resulting in the reduction
476 of heat provided for the ejector refrigeration cycle. Thus, the cooling capacity of the
477 ERC decreases.

478 The net power output of the whole system increases with the increase of the BC
479 turbine inlet pressure. Though the net power output of the DORC decreases, the

480 increase of CBC net power output is much larger. Thus, the net power output of the
481 CCP system increases with the increase of $P_{\mathrm{Bt,\,in}}$. The exergy efficiency of the system
482 likewise has the same rising trend.

483 The influences of the BC turbine inlet pressure ($P_{\mathrm{Bt,\,in}}$) on the levelized exergy cost
484 and the system capital cost of the system are depicted in Fig. 5. The levelized exergy
485 cost for the BC turbine output c_{Bt} increases with the rise of the $P_{\mathrm{Bt,\,in}}$, which can be
486 explained by the variations of the capital-cost-related part and the fuel-cost-related
487 part. The increase of $P_{\mathrm{Bt,\,in}}$ causes the increase of cost for both the BC turbine and the
488 compressor, which lead to the rise of the two related parts.

489 The levelized exergy cost for the ORC turbine product (c_{Ot}) increases with the rise
490 of $P_{\mathrm{Bt,in}}$. The decrease of the mass flow rate in the DORC causes that less exergy is
491 produced in vapor generator 2, causing the increase of the fuel-related part of c_{Ot}.
492 Therefore, the levelized exergy cost for the ORC turbine (c_{Ot}) increases.

493 The system capital cost (z_{capital}) increases with the rise of ($P_{\mathrm{Bt,\,in}}$). The increase of the
494 mass flow rate in the ERC causes the rise of capital cost for the evaporator and vapor
495 generator 3, which combined with the rise of the BC turbine cost and compressor cost
496 accounts for the system capital cost rise.

497 The levelized exergy cost for the system product decreases with the rise of $P_{\mathrm{Bt,\,in}}$ as
498 presented in Fig. 5. According to Eq. (31), the rise of the c_{Ot}, c_{Bt} would cause the rise
499 of the fuel-cost-related part of c_{product}. However, because of the large increase of the
500 system net power output, the capital-cost-related part and the fuel-cost-related part
501 decrease actually, which determines the decrease of c_{product}.

The influence of inlet temperature at the high-pressure side of ORC turbine ($T_{\mathrm{Ot,\,in,\,h}}$) on the output and the exergy efficiency of the system are shown in Fig. 6. The net power output of the CBC remains unchanged since thermal parameters in dual-pressure ORC are irrelevant to the thermodynamic performance of the CBC.

The net power output of the DORC decreases with the increase of $T_{\mathrm{Ot,\,in,\,h}}$. Though the increase of the vapor temperature could lead to the rise of the enthalpy drop in the ORC turbine, it would also cause the decrease of the mass flow rate in the high-pressure side, whose impact is greater than that of the enthalpy drop. Therefore, the power output of the DORC decreases.

The cooling capacity of the ejector refrigeration cycle increases with the rise of $T_{\mathrm{Ot,\,in,\,h}}$. More heat is provided for the ERC because of the decrease of the mass flow rate in the DORC, leading to the increase of the mass flow rate in vapor generator 3. Thus, more secondary flow from the evaporator is entrained into the ejector, resulting in the increase of the cooling capacity.

The net power output of the CCP system decreases with the rise of $T_{\mathrm{Ot,\,in,\,h}}$. The unchanged CBC power output and the drop of the DORC power output determine the decrease of the net power output of the CCP system. The exergy efficiency of the system as well drops with the increase of the increase of $T_{\mathrm{Ot,\,in,\,h}}$.

The influences of inlet temperature at the high-pressure side of ORC turbine on the levelized exergy cost and the system capital cost of the system are presented in Fig. 7. The levelized exergy cost for the ORC turbine output (c_{Ot}) increases with the increase of $T_{\mathrm{Ot,\,in,\,h}}$. The reason is that the two related parts of c_{Ot} increase with the drop of the

524 ORC turbine power output.

525 The levelized exergy cost for the BC turbine power output (c_{Bt}) increases with the
526 rise the $T_{Ot,\,in,\,h}$. Since the decrease of the mass flow rate in the high-pressure side of
527 DORC, the exergy generated in the vapor generator 2 decreases, causing the increase
528 of the levelized exergy cost of the vapor. Thus, the increase levelized exergy cost of
529 the vapor, which is heated by the BC turbine residual heat, causes the increase of the
530 levelized exergy cost for the exhaust CO_2. According to Eq. (32), the fuel-cost-related
531 part of c_{Bt} increases, leading to the increase of c_{Bt}.

532 The system capital cost ($z_{capital}$) decreases with the increase of $T_{Ot,\,in,\,h}$. The
533 decrease of the DORC power output causes the drop of the ORC turbine cost, which
534 leads to the descending trend of $z_{capital}$.

535 The levelized exergy cost for the system product ($c_{product}$) increases with the rise of
536 $T_{Ot,\,in,\,h}$, as shown in Fig. 7. The increase of the levelized exergy cost for the BC
537 turbine and ORC turbine power output cause the rise of fuel-cost-related part of $c_{product}$.
538 Meanwhile, the large decrease of the net power of the CCP system causes the increase
539 of the capital-cost-related part. The two increase parts determine the rise of $c_{product}$.
540 The influences of the inlet pressure at the high-pressure side of ORC turbine ($P_{Ot,\,in,\,h}$)
541 on the output and exergy efficiency of the system are presented in Fig. 8. The net
542 power of the CBC keeps unchanged because of the unchanged thermal parameters in
543 the cycle.

544 The net power output of the DORC increase with the rise of $P_{Ot,\,in,\,h}$. The increase
545 of the evaporation pressure cuts down the latent heat of the organic working fluid,

546 which causes the increase of the mass flow rate in the high-pressure side of DORC.
547 As a result, the net power output of the ORC turbine increases, leading to the increase
548 of the net power output of the DORC.

549 Considering the increase of the DORC net power output and the unchanged CBC
550 net power output, the net power output of the whole system increases. Also, the
551 exergy efficiency of the system increases.

552 The increase of the mass flow rate in the DORC absorbs more heat from the jacket
553 water in the preheater. Thus, less heat is released in the vapor generator 3, causing the
554 decrease of the mass flow rate of the working fluid in the ERC. As a result, the
555 cooling capacity of the system decreases.

556 The influence of the inlet pressure at the high-pressure side of the ORC turbine ($P_{\mathrm{Ot,}}$
557 $_{\mathrm{in,\,h}}$) on the levelized exergy cost and system capital cost of the system are presented
558 in Fig. 9. The large increase of the ORC turbine power output accounts for the
559 decrease of the levelized exergy cost for the ORC turbine power output (c_{Ot}). The
560 increase of the mass flow rate in the high-pressure side of DORC means that more
561 exergy in the vapor is generated by the vapor generator 2, which leads to the decrease
562 of its levelized exergy cost. Thus, the levelized exergy cost for the BC turbine exhaust
563 CO_2, which provides heat for the vapor, decreases with the vapor levelized exergy
564 cost. Moreover, the drop of the CO_2 levelized exergy cost causes the decrease of the
565 fuel-cost-related part of c_{Bt}, which further results in the decrease of c_{Bt}.

566 The increase of the ORC turbine power output and the increase of mass flow rate in
567 the DORC cause the increase of cost for the turbine and the vapor generator 2, leading

568 to the rise of the system capital cost.

569 The levelized exergy cost for the system product (c_{product}) decreases with the
570 increase of $P_{\text{Ot, in, h}}$. The decrease of c_{Ot} and c_{Bt} account for the decrease of the
571 fuel-cost-related part of the levelized exergy for the system product. The impact of c_{Ot}
572 and c_{Bt} is greater than that of the system capital cost whose rise would result in the
573 increase of the capital-cost-related part of c_{product}. Thus, the levelized exergy cost of the
574 system product (c_{product}) shows a descending trend.

575 The influences of the inlet temperature at the low-pressure side of ORC turbine ($T_{\text{Ot,}}$
576 $_{\text{in, l}}$) on the output and the exergy efficiency of the system are presented in Fig. 10.
577 Parameters changes in the DORC are irrelevant to the thermodynamic performance of
578 the CBC. Thus, the net power of the CBC remains unchanged.

579 The net power output of the DORC decreases with the increase of $T_{\text{Ot, in, l}}$. The
580 increase of the inlet temperature causes the decrease of the mass flow rate in the
581 low-pressure side of the DORC, leading to the decrease of the DORC net power
582 output.

583 Considering the decrease of the DORC net power output and the unchanged CBC
584 net power output, the net power output of the whole system deceases. Likewise, the
585 exergy efficiency of the system decreases.

586 The cooling capacity of the ejector refrigeration cycle increases with the increase of
587 $T_{\text{Ot, in, l}}$. The decrease of the mass flow rate in the low-pressure side means that more
588 heat is offered to the ERC. Thus, the mass flow rate of the working fluid in the vapor
589 generator 3 increases and more working fluid is entrained to the ejector from the

590 evaporator, which leads to the increase of the refrigeration cycle.

591 The influence of inlet temperature at the low-pressure side of the ORC turbine ($T_{Ot,}$
592 $_{in,\ l}$) on the levelized exergy cost and system capital cost of the system are presented in
593 Fig. 11. The levelized cost for the BC turbine power output increase with the increase
594 of $T_{Ot,\ in,\ l}$. The decrease of the mass flow rate in the vapor generator 1 leads to the
595 drop of the vapor exergy output, which results in the increase of the levelized exergy
596 cost for the vapor. The levelized exergy cost for vapor in vapor generator 2, which is
597 the equal to that of the vapor in vapor generator 1, increases as a result, causing the
598 increase of the levelized exergy cost of the exhaust CO_2 after the BC turbine. Thus,
599 the fuel-cost-related part of c_{Bt} increases, resulting in the rise of c_{Bt}.

600 The levelized exergy cost for the ORC turbine (c_{Ot}) increases with the increase of
601 $T_{Ot,\ in,\ l}$. That can be explained by the increase of the levelized exergy cost of the ORC
602 low-pressure inlet vapor and the decrease of the power output of the ORC turbine
603 power output. Both the fuel-cost-related part and the capital-cost-related part of c_{Ot}
604 increases.

605 The decrease of the mass flow rate and the ORC turbine power output cause the
606 decrease of the vapor generator 1 cost and the turbine cost. Thus, the capital cost of
607 the system decreases.

608 The levelized exergy cost for the system product increases with the increase of $T_{Ot,}$
609 $_{in,\ l}$. The increase of c_{Bt} and c_{Ot} cause the increase of the fuel-cost-related part of the
610 levelized exergy cost for the system product. Though, the decease of the system
611 capital cost causes the decrease of the capital-cost-related part, its effect is less

612 important. Thus, the increase of the fuel-cost-related part determines the increase of
613 the levelized exergy cost for the system product.

614 The influences of the inlet temperature of the low-pressure side of the ORC turbine
615 ($P_{\mathrm{Ot,\ in,\ l}}$) on the output of the exergy efficiency of the system are shown in Fig. 12.
616 The net power of the CBC keeps unchanged with the increase of the increase of the
617 low evaporation pressure. The reason is that the thermodynamic of the CBC is
618 irrelevant to the thermal parameters in DORC.

619 The net power output of the DORC increases with the rise of $P_{\mathrm{Ot,\ in,\ l}}$. The increase
620 of enthalpy drop of the organic working fluid in the low-pressure side, which is
621 caused by the rise of $P_{\mathrm{Ot,\ in,\ l}}$, results in the increase of the power output of the
622 low-pressure side. Though mass flow rate in the low-pressure side would decrease, its
623 impact is less important than that of the enthalpy drop. Thus, the net power output of
624 DORC increases.

625 The unchanged CBC power output and the increase of the DORC power accounts
626 for the increase of the system net power output and exergy efficiency of the system.

627 The cooling capacity increases slightly with the increase of $P_{\mathrm{Ot,\ in,\ l}}$. Because of the
628 decrease of the mass flow rate in DORC, less heat is released in the preheater and
629 more heat is provided in vapor generator 3. Thus, the mass flow rate of the working
630 fluid in the ERC increases, resulting in the slight increase of the cooling capacity.

631 The influences of inlet pressure at the low-pressure side of the ORC turbine ($P_{\mathrm{Ot,\ in,\ l}}$)
632 on the levelized exergy cost and system capital cost of the system are shown in Fig.
633 13. The levelized exergy cost for the ORC turbine power output decreases with the

increase of $P_{Ot,\,in,\,l}$. That can be explained by the decrease of the vapor generator 1 cost, caused by the decrease of the mass flow rate in DORC, and the increase of the DORC power output. Both the capital-cost-related part and the fuel-cost-related part of c_{Ot} decrease.

The levelized exergy cost for the BC turbine power output decreases with of $P_{Ot,\,in,\,l}$.

The decrease of the c_{Ot} causes the drop of levelized exergy cost for the vapor in vapor generator 2, which is heated by the residual heat in the BC turbine exhaust CO_2. Thus, the levelized exergy cost of the exhaust CO_2 decreases, which further leads to the drop of the fuel-cost-related part of c_{Bt}. Therefore, the levelized exergy cost for the BC turbine power output (c_{Bt}) decreases, as shown in Fig. 13.

The increase of the ORC turbine power output causes the increase of the ORC turbine cost. Meanwhile, the increase of the cooling capacity causes the increase of the heat transfer area in the evaporator which requires the rise of the evaporator cost. Thus, the capacity cost of the system increases.

The levelized exergy cost for the system product decreases with the increase of $P_{Ot,\,in,\,l}$. The decrease of the levelized exergy cost for the BC turbine power output and ORC turbine power cause the decrease of the fuel-cost-related part of the system levelized exergy cost, which determined the decrease of the levelized exergy cost for the system product.

The influence of ejector primary inlet pressure ($P_{ej,\,in}$) on the output and the exergy efficiency of the system are shown in Fig. 14. Thermal parameter changes in the ERC

656 can’t affect the thermodynamic performance of the CBC and DORC. Thus, the net
657 power output of the two cycles remain unchanged. With the increase of the ejector
658 primary inlet pressure, the power consumption of pump 4 increases, leading to the
659 slight decrease of the power output of the whole system.

660 The increase of the ejector primary inlet pressure causes the increase of the
661 entrainment ratio of the ejector. Thus, more secondary flow is entrained to the ejector
662 from the evaporation, leading to the increase of the cooling capacity.

663 With the increase of the ejector primary inlet pressure, the power consumption of
664 pump 4 increases gradually. At first, the exergy loss in pump 4 is smaller than the
665 exergy produced by the cooling capacity. Then, with the increase of the pump power
666 consumption, the exergy loss in pump 4 becomes larger than the cooling exergy
667 increase. Thus, the exergy efficiency for the system increases at first and then
668 decreases with the increase of the ejector primary inlet pressure.

669 The influence of the ejector primary inlet pressure on the levelized exergy cost and
670 the system capital cost of the system are presented in Fig. 15. The increase of the
671 ejector primary inlet pressure can’t affect the power output of the BC turbine and the
672 ORC turbine. Thus, the levelized exergy cost for the BC turbine and the ORC power
673 output remain unchanged.

674 The increase of the pump power consumption results in the increase of the pump 4
675 cost. The increase of the mass flow rate in the evaporator causes the increase of the
676 evaporator cost. Thus, the system capital cost increases, which leads to the increase of
677 the capital-cost-related part of c_{product}. As a result, the levelized exergy cost for the

system increases.

The parametric analysis reveals the potential of optimization for the CCP system. With the increase of the BC turbine inlet temperature, the net power output of the system increases while the cooling capacity decreases. With the increase of the inlet temperature at the high-pressure side of ORC turbine, the net power output of the system decreases while the cooling capacity increases. In this study, seven key parameters (BC turbine inlet temperature, BC turbine inlet pressure, inlet temperature at the high-pressure side of ORC turbine, inlet pressure at the high-pressure side of ORC turbine, inlet temperature at the low-pressure side of ORC turbine, inlet pressure at the low-pressure side of ORC turbine and the ejector primary inlet pressure) are chosen as the variables to optimize the system. The ranges of these parameters are listed in Table 6.

Considering that the levelized exergy cost reflects the thermodynamic and the exergoeconomic aspect of the system, the levelized exergy cost for the system product is selected as the objective function and genetic algorithm is selected to conduct the single-objective optimization.

Genetic algorithm (GA) is an optimization method based on the natural biological evaluation. [45] It simulates the natural genetic rules and searches the optimization result in all the generation. The control parameters of the GA are listed in Table 7.

The optimization results of GA are listed in Table 8. It can be obtained that the minimum levelized exergy cost for the system product $c_{product}$ is 53.25 \$(MWh)$^{-1}$. The net power output, exergy efficiency of the CCP system are 374.37 kW, 37.31%

700 respectively. The inlet pressure at the high-pressure side of ORC turbine is 1.85 MPa.
701 Meanwhile, it can be evidenced from Fig. 8 and 9 that the highest output power
702 (about 374.37 kW), exergy efficiency (about 37.31%) and the lowest levelized exergy
703 cost (about 53.25 $(MWh)^{-1}$) at the highest inlet pressure at the high-pressure side
704 ORC turbine (about 1.85 MPa). The results shown in Fig. 8 and 9 are close to the
705 optimization results. The inlet pressure at the high-pressure side ORC turbine is
706 varied while other six parameters are kept as constants in Fig. 8 and 9. Thus, inlet
707 pressure at the high-pressure side ORC turbine plays a more important role than other
708 six parameters when determining the performance of the system. When the inlet
709 pressure at the high-pressure side ORC turbine is close to the highest permitted
710 pressure, the system performance is close to the optimization performance.

711 Fig. 16 shows the exergy destruction of different components of the system
712 under the optimization conditions. The largest exergy destruction takes place in the
713 ORC turbine (41.26%), which is mainly caused by the mixing of the high-pressure
714 vapor and the low-pressure vapor. Gas heater contributes 13.44% of the total exergy
715 destruction. Three vapor generators take up 4.13%, 11.67% and 3.73% of the exergy
716 destruction, respectively. The exergy destruction for the ejector is 5.61%, which is
717 also caused by the working fluid mixing. For BC turbine, condenser 1, precooler and
718 preheater, the exergy destruction are 3.31%, 4.64%, 3.69% and 3.65%, respectively.
719 Other components contribute to the rest 4.87% of the exergy destruction.

5. Conclusion

In this paper, a combined cooling and power system is developed. Seven parameters are selected to analyze the thermodynamic and exergoeconomic performance of the system. Single-objective optimization is carried out with the help of GA. The conclusions of the study are presented as follows:

(1) In the CBC, the increase of $T_{Bt,in}$ and $P_{Bt,\,in}$ contribute to the increase of the system exergy efficiency and the decrease of the levelized exergy cost for the system product.

(2) In the DORC, the increase of $T_{Ot,\,in}$ and $T_{Ot,\,in,\,l}$ would cause the decrease of the system exergy efficiency and the increase of the levelized exergy cost for the system product. Meanwhile, the increase of $P_{Ot,\,in,\,h}$ and $P_{Ot,\,in,\,l}$ would result in the increase of the exergy efficiency and the decrease of the levelized exergy cost.

(3) In the ERC, the increase of $P_{ej,\,in}$ would cause the increase of the refrigeration capacity and the decrease of the system net power output.

(4) Single -objective optimization results show that the minimum levelized exergy cost for the system product is obtain as 53.25 $\$(MWh)^{-1}$ with net power output of 374.37 kW, cooling capacity of 188.63 kW and system exergy efficiency of 37.31%.

Acknowledgement

The authors gratefully acknowledge the financial support by the National Natural Science Foundation of China (Grant No. 51476121)

Appendix A

This section shows the calculation of the heat transfer area in the heat exchangers used in this study.

All the heat exchangers used in this study are shell-and-tube heat exchanger. The thermodynamic properties of the working fluid vary with the heat transfer process. Thus, to calculate the heat transfer area actually, the heat transfer processes are discretized into a lot of small sections. In each section, the heat transfer area is small and the thermodynamic properties are assumed to be constant.

For each section the heat transfer area is calculated as:

$$A_{\mathrm{i}} = Q_{\mathrm{i}} \Big/ \left(\Delta T_{\mathrm{i}} \cdot U_{\mathrm{i}}\right) \tag{B1}$$

where ΔT_{i} is the log-mean temperature difference (LMTD) and U_{i} is the overall heat transfer coefficient.

$$\frac{1}{U_{\mathrm{i}}} = \frac{1}{\alpha_{\mathrm{t,i}}} + \frac{\delta}{\lambda} + \frac{1}{\alpha_{\mathrm{s,i}}} \tag{B2}$$

In Eq. (B2) δ and λ represent the thickness of the tube and the thermal conductivity of the tube wall, respectively. $\alpha_{\mathrm{t,i}}$ is the convection heat transfer coefficient in the tube side and $\alpha_{\mathrm{s,i}}$ is the convection heat transfer coefficient in the shell side.

For different heat transfer process, the convection heat transfer coefficient has different format. We classify the heat transfer processes into single-phase heat transfer process and two-phase heat transfer process. In gas heater, precooler and the preheater, single-phase heat transfer process happens. In evaporator, two-phase heat transfer process occurs. In vapor generators and the condensers, both the single-phase and the

two-phase heat transfer process happen.

In the single-phase heat transfer process, the convection heat transfer coefficient in the tube side and the shell side are expressed as [46]:

$$\alpha_{t,i} = \frac{\lambda \cdot Nu}{D_i} \tag{B3}$$

$$\alpha_{s,i} = 0.36\left(\frac{\lambda}{D_{es}}\right)\cdot\left(\frac{D_{es}\cdot G_s}{\mu}\right)^{0.55}\cdot \mathrm{Pr}^{\frac{1}{3}}\cdot\left(\frac{\mu}{\mu_w}\right)^{0.14} \tag{B4}$$

In Eq. (B3), the Nusselt number is calculated as [47,48]:

$$Nu = \left[\frac{(f/8)\cdot \mathrm{Re}\cdot \mathrm{Pr}}{12.7(f/8)^{0.5}\cdot\left(\mathrm{Pr}^{2/3}-1\right)+1.07}\right],\ for\ \mathrm{Re}<10^4 \tag{B5}$$

$$Nu = \left[\frac{(f/8)\cdot(\mathrm{Re}-1000)\cdot \mathrm{Pr}}{12.7(f/8)^{0.5}\cdot\left(\mathrm{Pr}^{2/3}-1\right)+1.07}\right],\ for\ 10^4<\mathrm{Re}<5\times10^6 \tag{B6}$$

where f is the Darcy friction factor, Re is the Reynolds and Pr is the Prandtl number.

In Eq. (B4), D_{es} is the equivalent diameter of the shell, being expressed as:

$$D_{es} = \frac{1.10\mathrm{Pt}^2}{D_{out,i}} - D_{out,i} \tag{B7}$$

where Pt is the center distance between the tubes.

Evaporation and condensation are two different two-phase heat transfer processes. In this study, the cold organic working fluid flows in the tubes of the heat exchangers. The convection heat transfer coefficient of evaporation and condensation are expressed as [49,50]:

$$\alpha_{ev,i} = 0.023\left[\frac{G(1-x)}{\mu_l}\right]^{0.8}\cdot \mathrm{Pr}_l^{0.4}\cdot\frac{\lambda_l}{d}\cdot\left[1+3000Bo^{0.86}+1.12\left(\frac{x}{1-x}\right)^{0.75}\cdot\left(\frac{\rho_l}{\rho_v}\right)^{0.41}\right] \tag{B8}$$

$$\alpha_{cond,i} = 0.023\left[\frac{G(1-x)}{\mu_l}\right]^{0.8}\cdot \mathrm{Pr}_l^{0.4}\cdot\frac{\lambda_l}{d}\cdot\left[(1-x)^{0.8}+\frac{3.8x^{0.76}(1-x)0.04}{P_r^{0.38}}\right] \tag{B9}$$

In Eq. (B9), P_r is the reduced pressure. In Eq. (B8) Bo is the boiling number, being expressed as:

$$Bo = \frac{q_{\mathrm{m}}}{G \cdot r_{\mathrm{f}}} \tag{B10}$$

Appendix B

The constants for component capital cost calculation are list in Table B1.

Reference

[1] Abdul-Wahhab H, Al-Kayiem H, Aziz A, Nasif M. Survey of invest fuel magnetization in developing internal combustion engine characteristics. Renew Sustain Energy Rev 2017; 79:1392-99.

[2] Heywood J. B. Internal combustion engine fundamentals. New York: McGraw-Hill; 1988.

[3] Chao H, Chao L, Hong G, Hui X, You L, Shuang W. The optimal evaporation temperature and working fluids for subcritical Organic Rankine Cycle. Energy 2012; 38: 136-143.

[4] Tian H, Shu G, Wei H, Liang X, Liu L. Fluids and parameters optimization for the organic Rankine cycles (ORCs) used in exhaust heat recovery of Internal Combustion Engine (ICE). Energy 2012; 47: 125-136.

[5] Rijpkema J, Munch K, Andersson S. Thermodynamic potential of twelve working fluids in Rankine and flash cycles for waste heat recovery in heavy duty diesel engines. Energy 2018; 160:996-1007.

800 [6] Su X, Shedd T A. Towards working fluid properties and selection of Rankine cycle
801 based waste heat recovery (WHR) systems for internal combustion engines – A
802 fundamental analysis. Appl Therm Eng 2018; 142:502-10.
803 [7] Vaja I, Gambarotta A. Internal Combustion Engine (ICE) bottoming with Organic
804 Rankine Cycles (ORCs). Energy 2010; 35(2):1084-93.
805 [8] Kim M, Shin G, Kim G, Cho B. Single-loop organic Rankine cycle for engine
806 waste heat recovery using both low-and high-temperature heat sources. Energy 2016;
807 96:482-94.
808 [9] Ringer J, Seifert M, Guyotot V, Hübner W. Rankine cycle for waste heat recovery
809 of IC engines. SAE. 2009. 2009-01-0174.
810 [10] Wang X, Shu G, Tian H, Liu P, Jing D, Li X. Dynamic analysis of the dual-loop
811 Organic Rankine Cycle for waste heat recovery of a natural gas engine. Energy
812 Convers Manage 2017; 148:724-736.
813 [11] Wang E, Yu Z, Zhang H, Yang F. A regenerative supercritical dual-loop organic
814 Rankine cycle system for energy recovery from the waste heat of internal combustion
815 engines. Appl Energy 2017; 190:574-90.
816 [12] Huang H, Zhu J, Deng W, Ouyang T, Yan B, Yang X. Influence of exhaust heat
817 distribution on the performance of dual-loop organic Rankine Cycle (DORC) for
818 waste heat recovery. Energy 2018; 151:54-65.
819 [13] Rajabloo T, Bonalumi D, Lora P. Effect of a partial thermal decomposition of the
820 working fluid on the performances of ORC power plants. Energy 2017; 133:1013-26.
821 [14] Shi L, Shu G, Tian H, Deng S. A review of modified Organic Rankine cycles

822 (ORCs) for internal combustion engine waste heat recovery (ICE-WHR). Renew
823 Sustain Energy Rev 2018; 92:95-110.
824 [15] EI-Harbawi M, Shaaran S, Ahmad F, Wahi M, Abdul A, Larid D, Yin C.
825 Estimating the flammability of vapours above refinery wasterwater laden with
826 hydrocarbon mixtures. Fire Safety J 2012; 51:61-67.
827 [16] Wang X, Tian H, Shu G. Part-load performance prediction and operation strategy
828 design of organic Rankine cycles with a medium cycle used for recovering waste heat
829 from gaseous fuel engines. Energies 2016; 9: 527.
830 [17] Miller E, Hendricks T, Wang H, Peterson R. Integrated dual-cycle energy
831 recovery using thermoelectric conversion and an organic Rankine bottoming cycle.
832 Proceedings of the Institution of Mechanical Engineers, Part A: J Power Energy 2011;
833 225:33-43.
834 [18] Shu G, Wang X, Tian H. Theoretical analysis and comparison of Rankine cycle
835 and different organic Rankine cycles as waste heat recovery system for a large
836 gaseous fuel internal combustion engine. Appl Therm Eng 2016; 108:525-37.
837 [19] Yu G, Shu G, Tian H, Huo Y, Zhu W. Experimental investigations on a cascaded
838 steam-/organic-Rankine-cycle (RC/ORC) system for waste heat recovery (WHR)
839 from diesel engine. Energy Convers Manage 2016; 129:43-51.
840 [20] Zhang C, Shu G, Tian H, Wei H, Liang X. Comparative study of alternative
841 ORC-based combined power systems to exploit high temperature waste heat. Energy
842 Convers Manage 2015; 89:541-54.
843 [21] Galindo J, Guardiola C, Dolz V, Kleut P. Further analysis of a

844 compression-expansion machine for a Brayton Waste Heat Recovery cycle on an IC
845 engine. Applied Thermal Engineering 2018; 128: 345-356.
846 [22] Ma J, Liu L, Zhu T, Zhang T. Cascade utilization of exhaust gas and jacket water
847 waste heat from an Internal Combustion Engine by a single loop Organic Rankine
848 Cycle system. Appl Therm Eng 2016; 107:218-26.
849 [23] Zhang H G, Wang E H, Fan B Y. A performance analysis of a novel system of a
850 dual loop bottoming organic Rankine cycle (ORC) with a light-duty diesel engine.
851 Applied Energy 2013;102: 1504-1513.
852 [24] Yang F, Cho H, Zhang H, Zhang J. Thermoeconomic multi-objective
853 optimization of a dual loop organic Rankine cycle (ORC) for CNG engine waste heat
854 recovery. Applied Energy 2017; 205: 1100-1118.
855 [25] Song J, Gu C. Parametric analysis of a dual loop Organic Rankine cycle (ORC)
856 system for engine waste heat recovery. 2015; 105:995-1005.
857 [26] Yu G, Shu G, Tian H, Wei H, Liu L. Simulation and thermodynamic analysis of a
858 bottoming Organic Rankine Cycle (ORC) of diesel engine (DE). Energy 2013;
859 51:281-90.
860 [27] Li Fan, Sun Bo, Zhang C, Zhang L. Operation optimization for combined cooling,
861 heating, and power system with condensation heat recovery. Appl Energy 2018;
862 230:305-16.
863 [28] Yari Mortaza, Ariyanfar Leyli, Aghdam EA. Analysis and performance
864 assessment of a novel ORC based multigeneration system for power, distilled water
865 and heat. Renew Energy 2018; 119:262-81.

866 [29] Bai Z, Liu T, Liu Q, Lei J, Gong L, Jin H. Performance investigation of a new
867 cooling, heating and power system with methanol decomposition based chemical
868 recuperation process. Appl Energy 2018; 229: 1152-63.
869 [30] Chen Y, Han W, Jin H. Investigation of an ammonia-water combined power and
870 cooling system driven by the jacket water and exhaust gas heat of an internal
871 combustion engine. International Journal of Refrigeration 2017; 82: 174-188.
872 [31] Salek F, Moghaddam A, Naserian M. Thermodynamic analysis of diesel engine
873 coupled with ORC and absorption refrigeration cycle. Energy Conversion and
874 Management 2017; 140: 240-246.
875 [32] Wang J, Dai Y, Sun Z. A theoretical study on a novel combined power and ejector
876 refrigeration cycle. Int J Refrig 2009; 32(6):1186-94.
877 [33] Dai Y, Wang J, Gao L. Parametric optimization and comparative study of organic
878 Rankine cycle (ORC) for low grade waste heat recovery. Energy Convers Manage
879 2009; 50:576-82.
880 [34] Shu G, Zhao M, Tian H, Huo Y, Zhu W. Experimental comparison of R123 and
881 R245fa as working fluids for waste heat recovery from heavy-duty diesel engine.
882 Energy 2016; 115:756-69.
883 [35] Zhang J, Zhang H, Yang K, Yang F, Wang Z, Zhao G, Liu H, Wang E, Yao B.
884 Performance analysis of regenerative organic Rankine cycle (RORC) using the pure
885 working fluid and the zeotropic mixture over the whole operating range of a diesel
886 engine. Energy Convers Manage 2014; 84:282-94.
887 [36] ~~Adrian Bejan GT, Moran Michael~~ Bejan A, Tsatsaronis G, Moran M. Thermal

888 design and optimization. New York: John Wiley & Sons; 1996.
889 [37] Turton R, Bailie RC, Whiting WB, Shaeiwitz JA. Analysis, synthesis, and design
890 of chemical processes. 3rd ed. Upper Saddle River, N.J: Prentice Hall; 2009.
891 [38] Li J, Ge Z, Liu Q, Duan Y, Yang Z. Thermo-economic performance analyses and
892 comparison of two turbine layouts for organic Rankine cycles with dual-pressure
893 evaporation. Energy Conversion and Management, 2018; 164: 603-614.
894 [39] Sheng Z, Huai W, Tao G. Performance comparison and parametric optimization
895 of subcritical organic Rankine cycle (ORC) and transcritical power cycle system for
896 low-temperature geothermal power generation. Appl Energy 2011;88(8):2740-54.
897 [40] Tempesti D, Fiaschi D. Thermo-economic assessment of a micro CHP system
898 fueled by geothermal and solar energy. Energy 2013; 58: 45-51.
899 [41] Velez F, Segovia JJ, Martin MC, Antonlin G, Chejne F, Quijano A. A technical,
900 economical and market review of organic Rankine cycles for the conversion of
901 low-grade heat for power generation. Renew Sustain Energy Rev 2012; 16:4175-89.
902 [42] Akbari D, Mahmoudi M. Thermoeconomic analysis & optimization of the
903 combined supercritical CO2 (carbon dioxide) recompression Brayton/ organic
904 Rankine cycle. Energy 2014; 78:501-12.
905 [43] Zare V, Mahmoudi M, Yari M. An exergoeconomic investigation of waste heat
906 recovery from the Gas Turbine-Modular Helium Reactor (GT-MHR) employing an
907 ammonia–water power/cooling cycle. Energy 2013;61. 397-409.
908 [44] Lemmon EW, Huber ML, McLinden MO. NIST standard reference database 23,
909 reference fluid thermodynamic and transport properties (REFPROP). Version 9.1.

National Institute of Standards and Technology; 2010

[45] Wang J, Dai Y, Gao L. Parametric analysis and optimization for a combined power and refrigeration cycle. Appl Energy 2008;85(11):1071-85.

[46] Kern DQ. Process heat transfer. New York: McGraw-Hill; 1950

[47] Kandylas IP, Stamatelos AM. Engine exhaust system design based on heat transfer computation. Energy Convers Manage 1999; 40:1057-72.

[48] Incropera FP, DeWitt DP. Fundamentals of heat and mass transfer. New York: Wiley; 2002

[49] Gungor KE, Winterton RHS. Simplified general correlation for saturated flow boiling and comparisons of correlations with data. Chem Eng Res and Des, 1987; 65:148-56.

[50] Shah MM. A general correlation for heat transfer during film condensation inside pipes. Int J Heat Mass Transf 1979; 22:547-56.

Figure captions

Fig. 1. Schematic diagram of the CCP system

Fig. 2. Influences of BC turbine inlet temperature on the output and the exergy efficiency of the system.

Fig. 3. Influences of BC turbine inlet temperature on the levelized exergy cost and the system capital cost of the system.

Fig. 4. Influences of BC turbine inlet pressure on the output and the exergy efficiency of the system.

Fig. 5. Influences of BC turbine inlet pressure on the levelized exergy cost and the system capital cost of the system.

Fig. 6. Influences of inlet temperature at the high-pressure side of ORC turbine on the output and the exergy efficiency of the system.

Fig. 7. Influences of inlet temperature at the high-pressure side of ORC turbine on the levelized exergy cost and the system capital cost of the system.

Fig. 8. Influences of inlet pressure at the high-pressure side of ORC turbine on the output and the exergy efficiency of the system.

Fig. 9. Influences of inlet pressure at the high-pressure side of ORC turbine on the levelized exergy cost and the system capital cost of the system.

Fig. 10. Influences of inlet temperature at the low-pressure side of ORC turbine on the output and the exergy efficiency of the system.

Fig. 11. Influences of inlet temperature at the low-pressure side of ORC turbine on the levelized exergy cost and system capital cost of the system.

946 **Fig. 12.** Influences of inlet pressure at the low-pressure side of ORC turbine on the
947 output and the exergy efficiency of the system.
948 **Fig. 13.** Influences of inlet pressure at the low-pressure side of ORC turbine on the
949 levelized exergy cost and system capital cost of the system.
950 **Fig. 14.** Influences of ejector primary inlet pressure on the output and the exergy
951 efficiency of the system.
952 **Fig. 15.** Influences of ejector primary inlet pressure on the levelized exergy cost and
953 the system capital cost of the system.
954 **Fig. 16.** Exergy destruction of different components
955

956 **Table 1** Energy and exergy models for each component in CCP system

Component	Energy equation	E_F	E_P	E_D	E_L
Gas heater	$M_{g1}\cdot(h_{g1}-h_{g2})=M_2\cdot(h_3-h_2)$	$E_{g1}-E_{g2}$	E_3-E_2	$E_{g1}+E_2-E_3-E_{g2}$	/
BC turbine	$W_{Bt}=M_3\cdot(h_3-h_4)=M_3\cdot(h_3-h_{4s})\cdot\eta_{Bt}$	E_3-E_4	W_{Bt}	$E_3-E_4-W_{Bt}$	/
Vapor generator 2	$M_4\cdot(h_4-h_5)=M_9\cdot(h_{10}-h_9)$	E_4-E_5	$E_{10}-E_9$	$E_4+E_9-E_5-E_{10}$	/
Precooler	$M_1\cdot(h_5-h_1)=M_{26}\cdot(h_{27}-h_{26})$	/	/	$E_5+E_{26}-E_1-E_{27}$	$E_{27}-E_{26}$
Compressor	$W_{comp}=M_1\cdot(h_2-h_1)=M_1\cdot(h_{2s}-h_1)/\eta_{comp}$	W_{comp}	E_2-E_1	$E_1-E_2+W_{comp}$	/
Vapor generator 1	$M_{g2}\cdot(h_{g2}-h_{g3})=M_8\cdot(h_{11}-h_8)$	$E_{g2}-E_{g1}$	$E_{11}-E_8$	$E_{g2}+E_8-E_{11}-E_{g3}$	/
ORC turbine	$W_{Ot}=M_{10}\cdot(h_{10}-h_{12})+M_{11}\cdot(h_{11}-h_{12})$	$E_{10}+E_{11}-E_{12}$	W_{Ot}	$E_{10}+E_{11}-E_{12}-W_{Ot}$	/
Condenser 1	$M_{12}\cdot(h_{12}-h_{13})=M_{28}\cdot(h_{29}-h_{28})$	/	/	$E_{12}+E_{28}-E_{13}-E_{29}$	$E_{29}-E_{28}$
Pump 1	$W_{p1}=M_{13}\cdot(h_{14}-h_{13})=M_{13}\cdot(h_{14s}-h_{13})/\eta_{p1}$	W_{p1}	$E_{14}-E_{13}$	$E_{13}-E_{14}+W_{p1}$	/
Preheater	$M_{15}\cdot(h_{15}-h_{14})=M_{w1}\cdot(h_{w1}-h_{w2})$	$E_{w1}-E_{w2}$	$E_{15}-E_{14}$	$E_{w1}+E_{14}-E_{15}-E_{w2}$	/
Pump 2	$W_{p2}=M_7\cdot(h_9-h_7)=M_7\cdot(h_{9s}-h_7)/\eta_{p2}$	W_{p2}	E_9-E_7	$E_7-E_9+W_{p2}$	/
Pump 3	$W_{p3}=M_6\cdot(h_8-h_6)=M_6\cdot(h_{8s}-h_6)/\eta_{p3}$	W_{p3}	E_8-E_6	$E_6-E_8+W_{p3}$	/
Vapor generator 3	$M_{23}\cdot(h_{23}-h_{22})=M_{w2}\cdot(h_{w2}-h_{w3})$	$E_{w2}-E_{w3}$	$E_{23}-E_{22}$	$E_{w2}+E_{22}-E_{23}-E_{w3}$	/
Condenser 2	$M_{16}\cdot(h_{16}-h_{17})=M_{30}\cdot(h_{31}-h_{30})$	/	/	$E_{16}+E_{30}-E_{17}-E_{31}$	$E_{31}-E_{30}$
Valve	$h_{19}=h_{20}$	/	/	$E_{19}-E_{20}$	/
Pump 4	$W_{p4}=M_{22}\cdot(h_{22}-h_{18})=M_{22}\cdot(h_{22s}-h_{18})/\eta_{p4}$	W_{p4}	$E_{22}-E_{18}$	$E_{18}-E_{22}+W_{p4}$	/
Ejector	$M_{16}\cdot h_{16}=M_{23}\cdot h_{23}+M_{21}\cdot h_{21}$	$E_{23}+E_{21}$	E_{16}	$E_{23}+E_{21}-E_{16}$	/
Evaporator	$M_{20}\cdot(h_{21}-h_{20})=M_{24}\cdot(h_{24}-h_{25})$	$E_{20}-E_{21}$	$E_{25}-E_{24}$	$E_{20}+E_{24}-E_{21}-E_{25}$	/

957 **Table 2** Cost balance and auxiliary relation [30] for each component of CCP system

Component	Cost balance	Auxiliary relation

Gas heater	$c_{g2} \cdot E_{y,g2} + c_3 \cdot E_{y,3} = c_{g1} \cdot E_{y,g1} + c_2 \cdot E_{y,2} + Z_{gh}$	c_{g1}=c_{g2}=0
Vapor generator 2	$c_5 \cdot E_{y,5} + c_{10} \cdot E_{y,10} = c_4 \cdot E_{y,4} + c_9 \cdot E_{y,9} + Z_{vg,2}$	c_4=c_5
BC turbine	$c_4 \cdot E_{y,4} + c_{Bt} \cdot W_{y,Bt} = c_3 \cdot E_{y,3} + Z_{Bt}$	c_4=c_3
Precooler	$c_1 \cdot E_{y,1} + c_{26} \cdot E_{y,26} = c_5 \cdot E_{y,5} + c_{27} \cdot E_{y,27} + Z_{prec}$	c_1=c_5
Compressor	$c_2 \cdot E_{y,2} = c_1 \cdot E_{y,1} + c_{elec,1} \cdot W_{y,comp} + Z_{comp}$	$c_{elec,1}$=c_{Bt}
Vapor generator 1	$c_{g3} \cdot E_{y,g3} + c_{11} \cdot E_{y,11} = c_{g2} \cdot E_{y,g2} + c_8 \cdot E_{y,8} + Z_{vg,1}$	c_{g2}=c_{g3}
ORC turbine	$c_{12} \cdot E_{y,12} + c_{Ot} \cdot W_{y,Ot} = c_{11} \cdot E_{y,11} + c_{10} \cdot E_{y,10} + Z_{Ot}$	c_{10}=c_{11}=c_{12}
Pump 1	$c_{14} \cdot E_{y,14} = c_{13} \cdot E_{y,13} + c_{elec,3} \cdot W_{y,pump1} + Z_{pump1}$	$c_{elec,3}$=c_{Ot}
Condenser 1	$c_{13} \cdot E_{y,13} + c_{29} \cdot E_{y,29} = c_{28} \cdot E_{y,28} + c_{12} \cdot E_{y,12} + Z_{cond1}$	c_{13}=c_{12}
Preheater	$c_{w2} \cdot E_{y,w2} + c_{15} \cdot E_{y,15} = c_{w1} \cdot E_{y,w1} + c_{14} \cdot E_{y,14} + Z_{preh}$	c_{w1}=c_{w2}=0
Pump 2	$c_9 \cdot E_{y,9} = c_7 \cdot E_{y,7} + c_{elec,2} \cdot W_{y,pump2} + Z_{pump2}$	$c_{elec,2}$=c_{Ot}
Pump 3	$c_8 \cdot E_{y,8} = c_6 \cdot E_{y,6} + c_{elec,3} \cdot W_{y,pump3} + Z_{pump3}$	$c_{elec,3}$=c_{Ot}
Vapor generator 3	$c_{w3} \cdot E_{y,w3} + c_{23} \cdot E_{y,23} = c_{w2} \cdot E_{y,w2} + c_{22} \cdot E_{y,22} + Z_{vg,3}$	c_{w3}=c_{w2}
Valve	/	c_{19}=c_{20}
Pump 4	$c_{22} \cdot E_{y,22} = c_{18} \cdot E_{y,18} + c_{elec,3} \cdot W_{y,pump4} + Z_{pump4}$	$c_{elec,4}$=c_{Ot}
Condenser 2	$c_{17} \cdot E_{y,17} + c_{31} \cdot E_{y,31} = c_{30} \cdot E_{y,30} + c_{16} \cdot E_{y,16} + Z_{cond2}$	c_{16}=c_{17}
Ejector	$c_{16} \cdot E_{y,16} = c_{23} \cdot E_{y,23} + c_{21} \cdot E_{y,21}$	/
Evaporator	$c_{21} \cdot E_{y,21} + c_{25} \cdot E_{y,25} = c_{20} \cdot E_{y,20} + c_{24} \cdot E_{y,24} + Z_{ev}$	c_{20}=c_{21}

958 **Table 3** Main parameters of the engine [7]

Parameters	Value
Power output (kW)	2928
Rotation (r(min)$^{-1}$)	1000

Exhaust gas temperature (℃)	470
Exhaust gas mass flow rate (kg s^{-1})	4.35
Temperature of jacket water (℃)	90/79
Mass flow rate of jacket water (kg s^{-1})	25

959 **Table 4** Composition of the exhaust gas [7]

Composition	Molecular ($g(mol)^{-1}$)	Fraction (%)
O_2	32.00	9.3
CO_2	44.00	9.1
H_2O	18.01	7.4
N_2	28.01	74.2

960 **Table 5** Condition of simulation for the CCP system

Parameter	Value
Ambient temperature (℃)	20
Ambient pressure (MPa)	0.101
Compressor inlet temperature (℃)	35
BC turbine inlet temperature (℃)	400
BC turbine inlet pressure (MPa)	18
BC turbine outlet pressure (MPa)	8
Inlet temperature at the high-pressure side of ORC turbine (℃)	150
Inlet pressure at the high-pressure side of ORC turbine (MPa)	1.6
Inlet temperature at the low-pressure side of ORC turbine (℃)	100
Inlet pressure at the low-pressure side of ORC turbine (MPa)	1.0

Outlet pressure of pump 1 (MPa)	0.9
Ejector primary inlet pressure (MPa)	0.4
Terminal temperature difference at gas heater outlet (℃)	100
Pinch point temperature difference in vapor generator 1 (℃)	30
Pinch point temperature difference in vapor generator 2 (℃)	30
Pinch point temperature difference in vapor generator 3 (℃)	25
Condensation temperature of condenser 1 (℃)	30
Condensation temperature of condenser 2 (℃)	30
Evaporation temperature of evaporator (℃)	5
Isentropic efficiency of BC turbine (%)	80
Isentropic efficiency of ORC turbine (%)	80
Isentropic efficiency of compressor (%)	80
Isentropic efficiency of pump 1 (%)	75
Isentropic efficiency of pump 2 (%)	75
Isentropic efficiency of pump 3 (%)	75
Inlet temperature of cooling water (℃)	20

961 **Table 6** Parameters for GA

Parameter	Operation range
BC turbine inlet temperature (℃)	330-440
BC turbine inlet pressure (MPa)	15-20
Inlet temperature at the high-pressure side of ORC turbine (℃)	130-180
Inlet pressure at the high-pressure side of ORC turbine (MPa)	1.4-2

Inlet temperature at the low-pressure side of ORC turbine (℃)	90-150
Inlet pressure at the low-pressure side of ORC turbine (MPa)	0.9-1.3
Ejector primary inlet pressure (MPa)	0.3-1

962 **Table 7** Control parameters of GA

Tuning parameters	Value
Population size	20
Mutation probability	0.01
Crossover probability	0.8
Stop generation	200

963 **Table 8** Single-objective optimization results

Parameter	Value
BC turbine inlet temperature (℃)	425.46
BC turbine inlet pressure (MPa)	20.00
Inlet temperature at the high-pressure side of ORC turbine (℃)	144.32
Inlet pressure at the high-pressure side of ORC turbine (MPa)	1.85
Inlet temperature at the low-pressure side of ORC turbine (℃)	100.03
Inlet pressure at the low-pressure side of ORC turbine (MPa)	1.26
Ejector primary inlet pressure (MPa)	0.54
Net power output (kW)	374.37
Cooling capacity (kW)	188.63
Exergy efficiency (%)	37.31
Levelized exergy cost ($ $(MWh)^{-1}$)	53.25

964 **Table B1** Constants for component costs [37]

Constant	Value	Constant	Value	Constant	Value
$B_{1,he}$	1.63	$K_{3,pump}$	0.1538	$C_{3,he}$	0.08183
$B_{2,he}$	1.66	$K_{1,turb}$	2.7051	$C_{1,pump}$	-0.3635
$B_{1,pump}$	1.89	$K_{2,turb}$	1.4398	$C_{2,pump}$	0.3957
$B_{2,pump}$	1.35	$K_{3,turb}$	-0.1776	$C_{3,pump}$	-0.0026
$K_{1,he}$	4.3247	$K_{1,comp}$	2.2897	$F_{M,he}$	1.0
$K_{2,he}$	-0.3030	$K_{2,comp}$	1.3604	$F_{BM,turb}$	3.5
$K_{3,he}$	0.1634	$K_{3,comp}$	-0.1027	$F_{BM,comp}$	2.7
$K_{1,pump}$	3.3892	$C_{1,he}$	0.03881	$F_{M,pump}$	2.2
$K_{2,pump}$	0.0536	$C_{2,he}$	-0.11272		

965
966

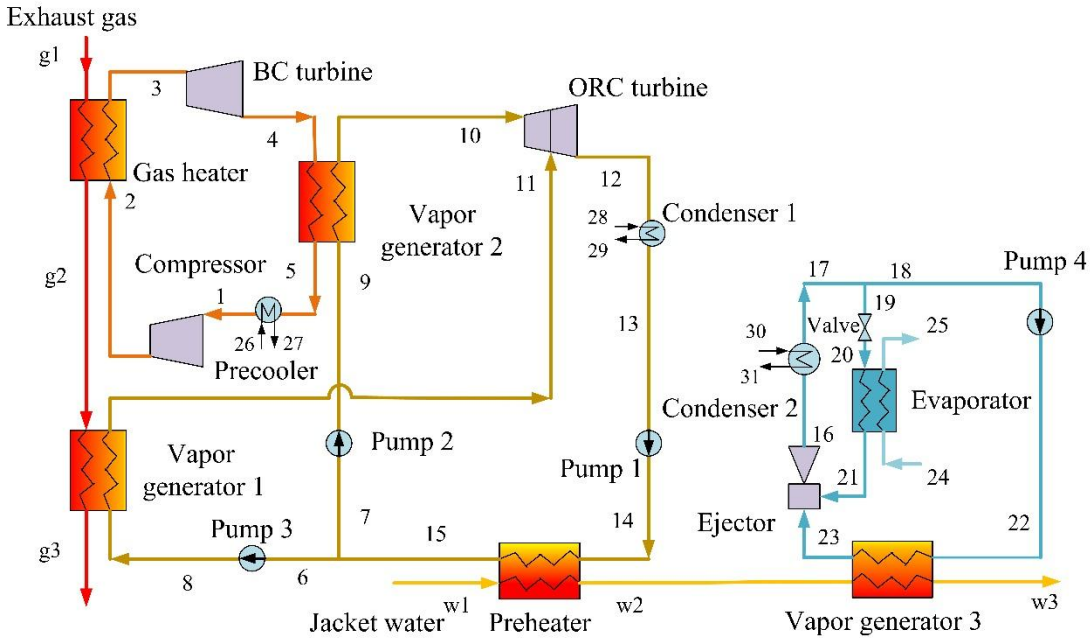

967

968 **Fig. 1.** Schematic diagram of the CCP system

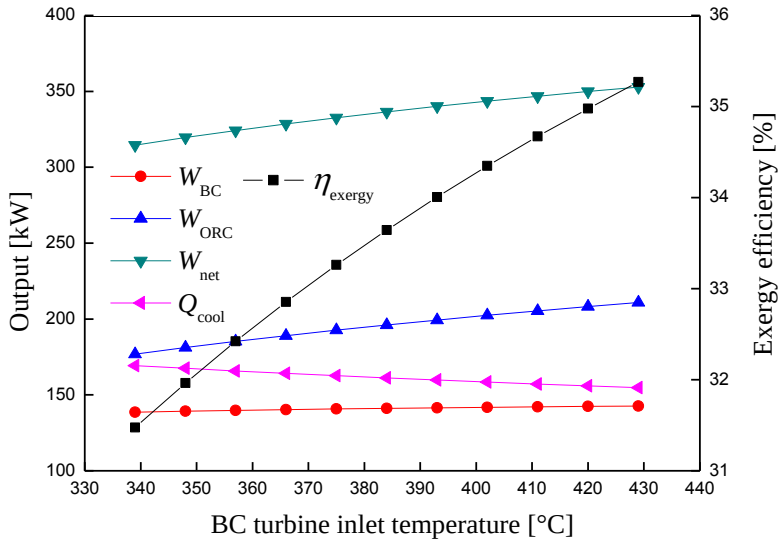

969

970 **Fig. 2.** Influences of BC turbine inlet temperature on the output and the exergy

971 efficiency of the system.

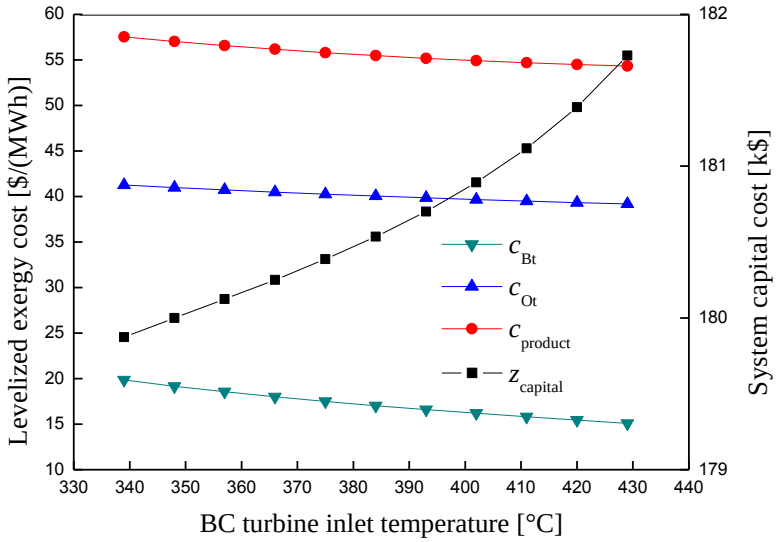

Fig. 3. Influences of BC turbine inlet temperature on the levelized exergy cost and the system capital cost of the system.

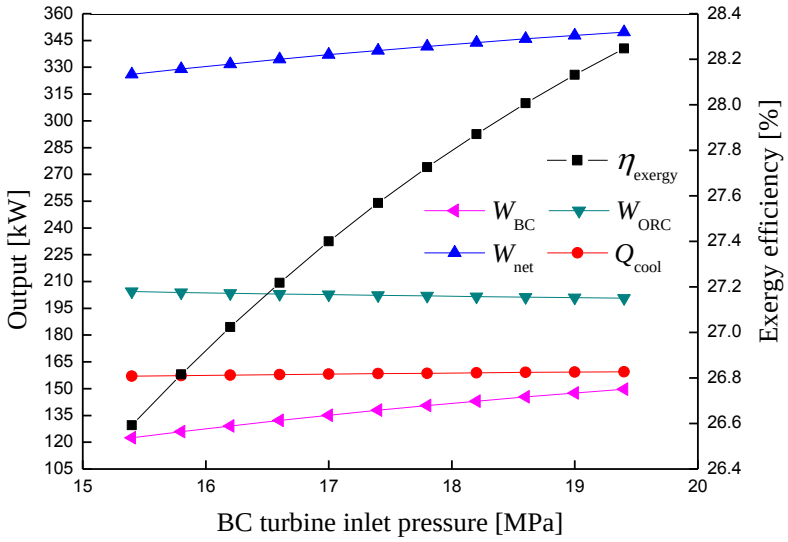

Fig. 4. Influences of BC turbine inlet pressure on the output and the exergy efficiency of the system.

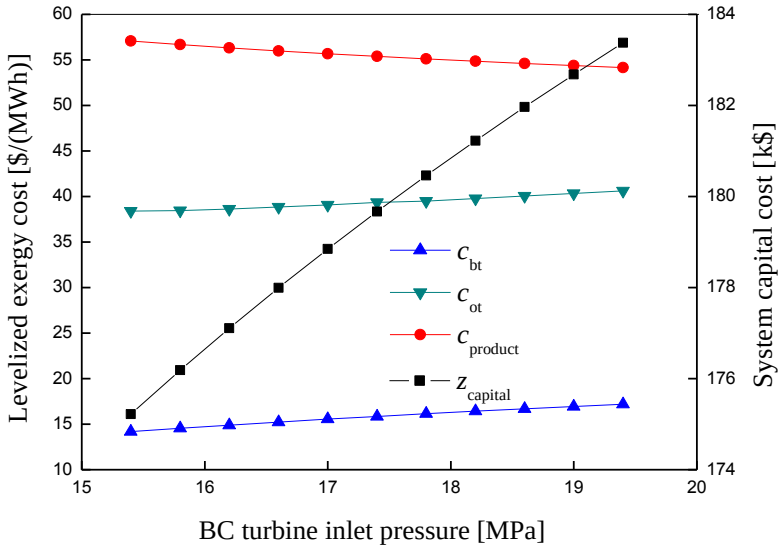

978

979 **Fig. 5.** Influences of BC turbine inlet pressure on the levelized exergy cost and the

980 system capital cost of the system.

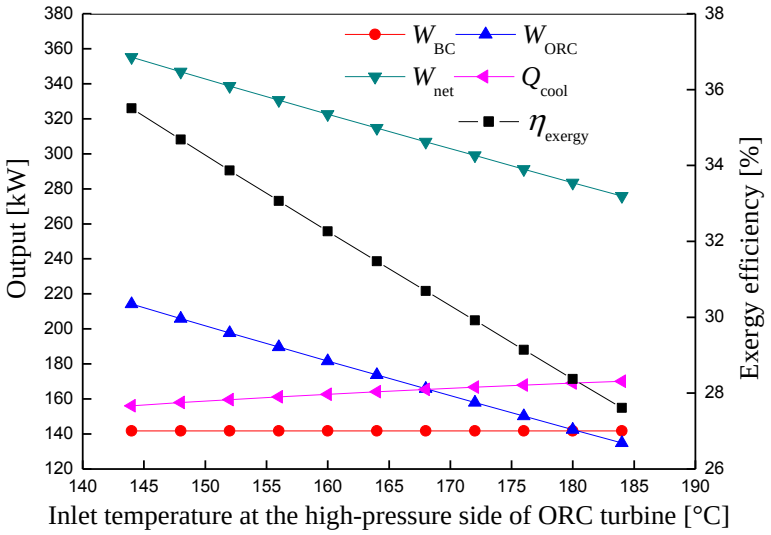

981

982 **Fig. 6.** Influences of inlet temperature at the high-pressure side of ORC turbine on the

983 output and the exergy efficiency of the system.

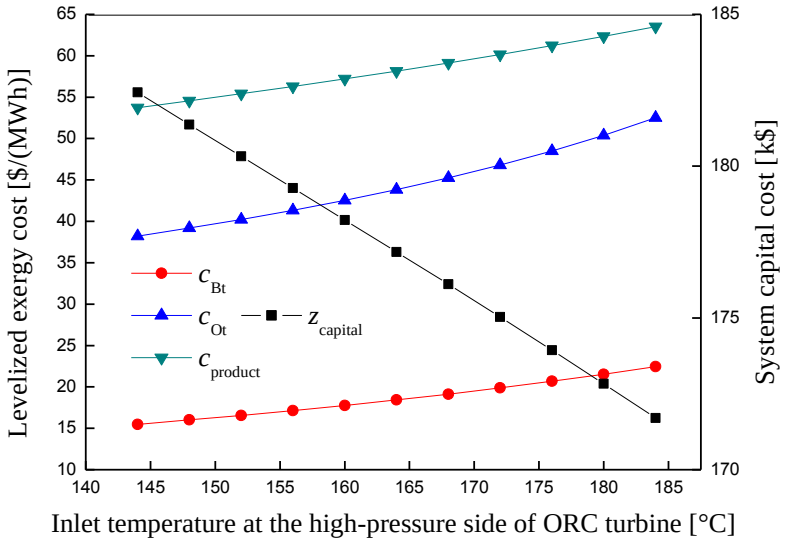

984

985 **Fig. 7.** Influences of inlet temperature at the high-pressure side of ORC turbine on the

986 levelized exergy cost and the system capital cost of the system.

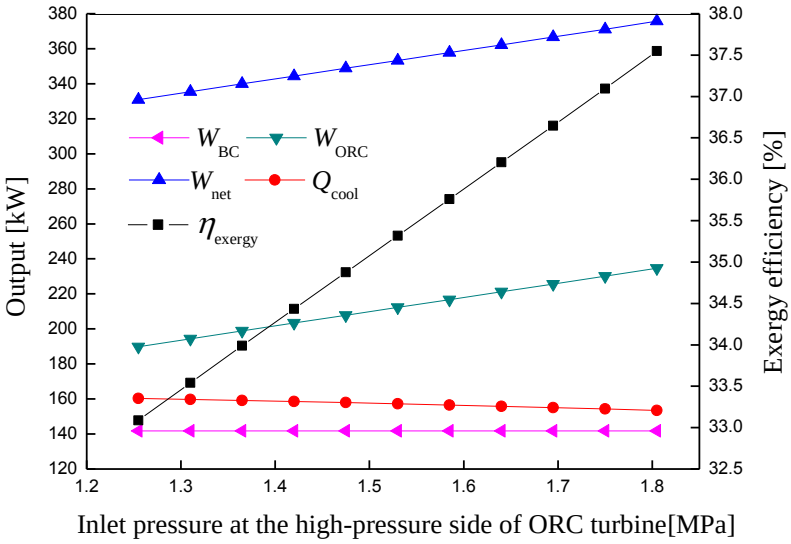

987

988 **Fig. 8.** Influences of inlet pressure at the high-pressure side of ORC turbine on the

989 output and the exergy efficiency of the system.

990

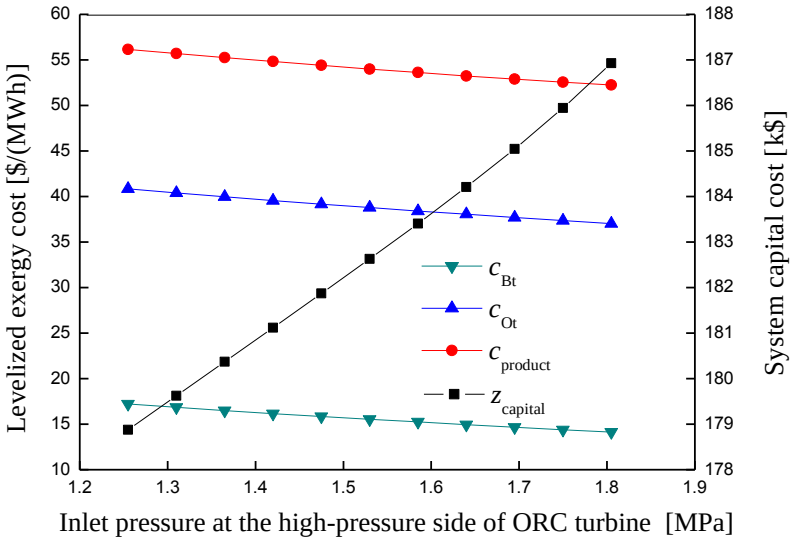

991

992 **Fig. 9.** Influences of inlet pressure at the high-pressure side of ORC turbine on the

993 levelized exergy cost and the system capital cost of the system.

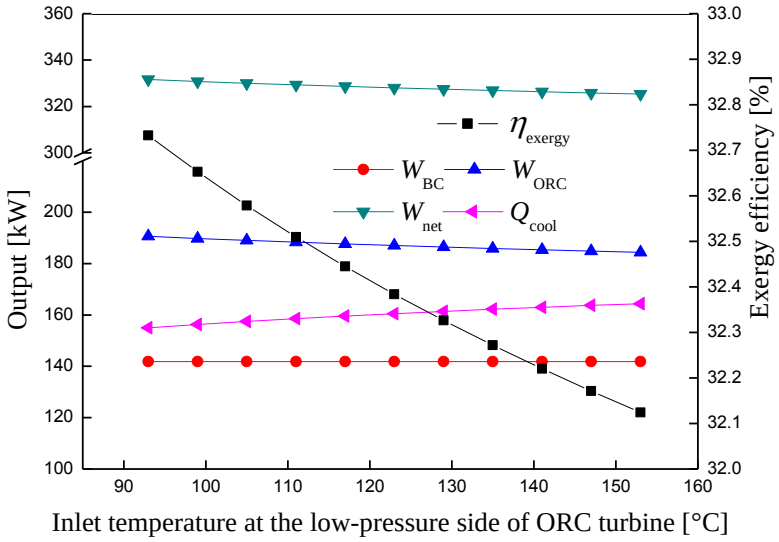

994

995 **Fig. 10.** Influences of inlet temperature at the low-pressure side of ORC turbine on the

996 output and the exergy efficiency of the system.

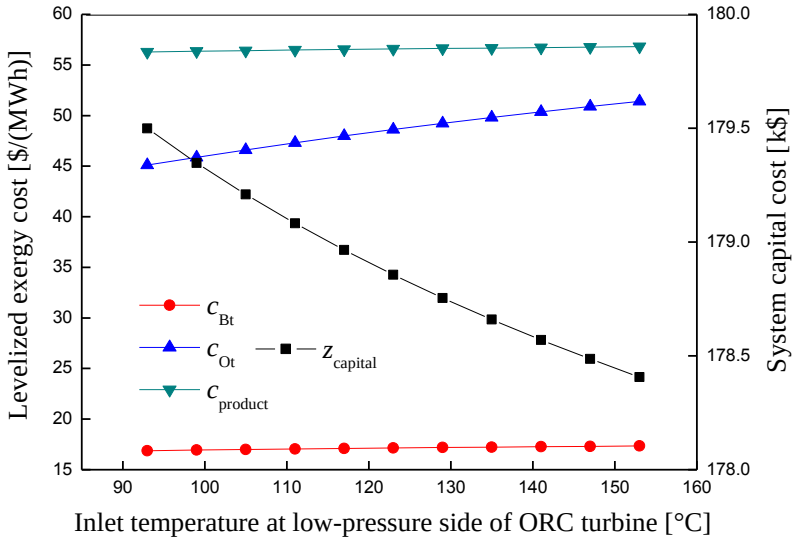

997

998 **Fig. 11.** Influences of inlet temperature at the low-pressure side of ORC turbine on

999 the levelized exergy cost and system capital cost of the system.

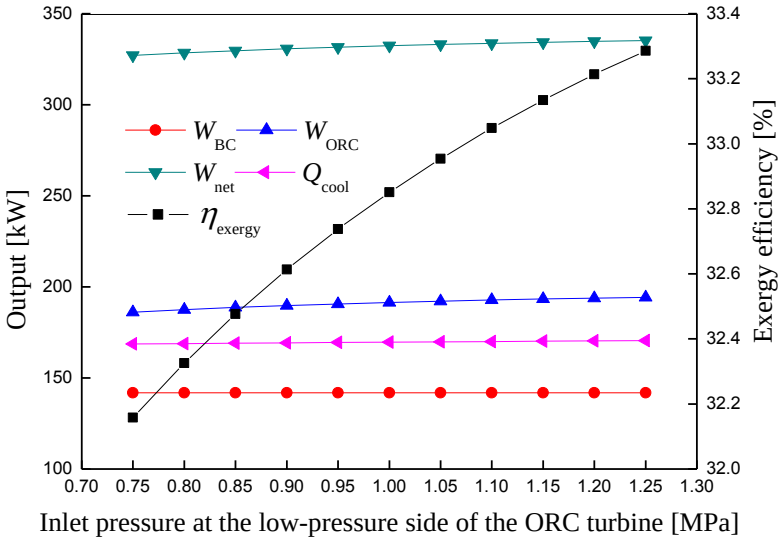

1000

1001 **Fig. 12.** Influences of inlet pressure at the low-pressure side of ORC turbine on the

1002 output and the exergy efficiency of the system.

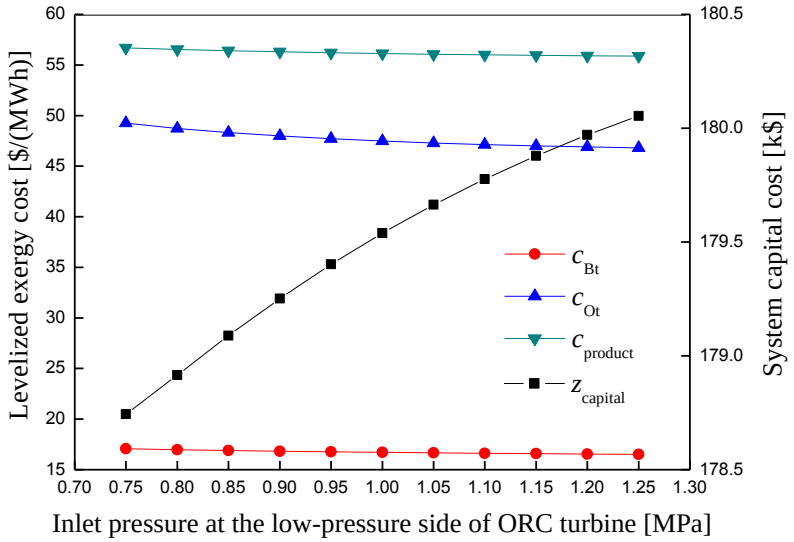

1003

1004 **Fig. 13.** Influences of the inlet pressure at the low-pressure side of ORC turbine on

1005 the levelized exergy cost and system capital cost of the system.

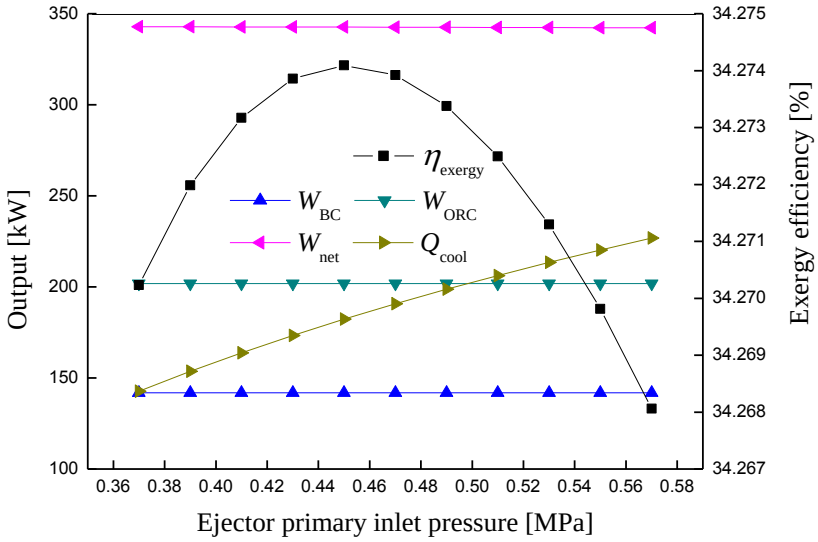

1006

1007 **Fig. 14.** Influences of ejector primary inlet pressure on the output and the exergy

1008 efficiency of the system.

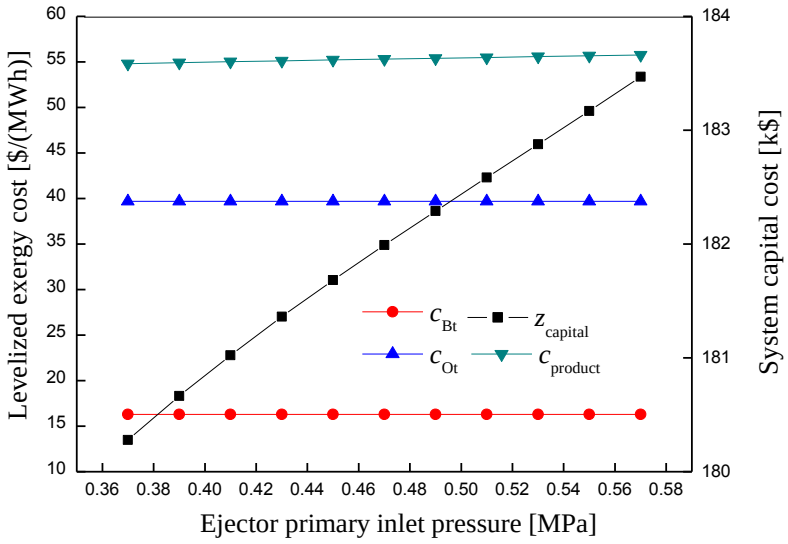

1009

1010 **Fig. 15.** Influences of ejector primary inlet pressure on the levelized exergy cost and

1011 the system capital cost of the system.

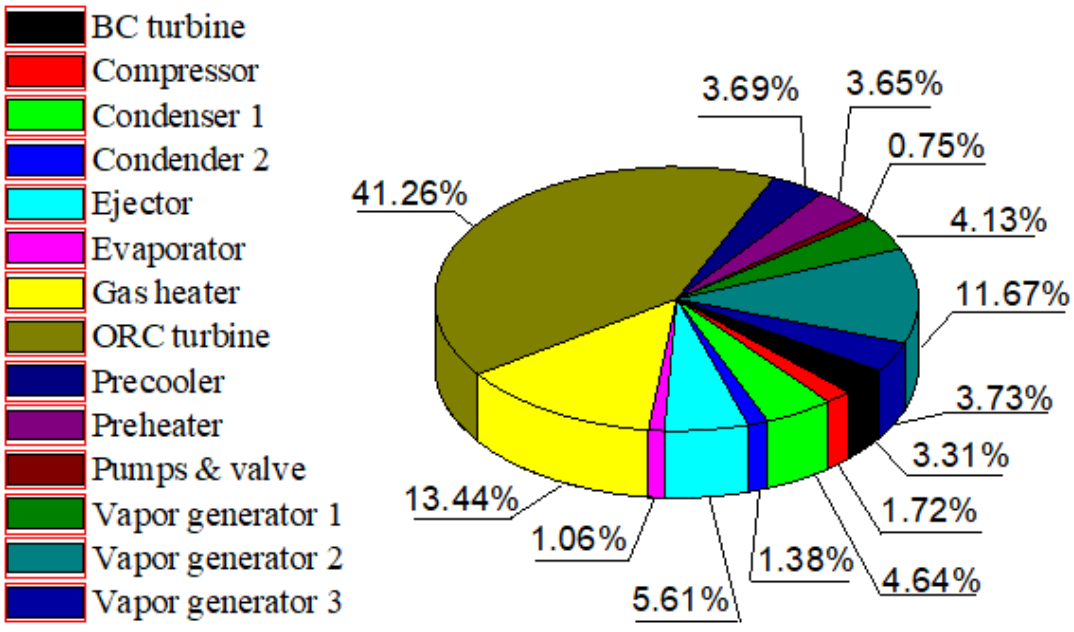

1012

1013 **Fig. 16.** Exergy destruction of different components

Response to Reviewers

Paper No. ECM-D-18-05037, Energy Conversion and Management

Title: Performance analysis and optimization of a combined cooling and power system using low boiling point working fluid driven by engine waste heat

Dear editor & reviewers,

Thank you very much for your review of our paper entitled "Performance analysis and optimization of a combined cooling and power system using low boiling working fluid driven by engine waste heat", and for your comments and recommendations. These commends and recommendations help us to make better modifications and improve the quality of the paper. We have modified the manuscript accordingly in the revised manuscript. Please find below our response and explanations for your comments and questions.

Editor Comments:

1. Avoid lumping references as in [2, 3] and all other. Instead summarize the main contribution of each referenced paper in a separate sentence. How each paper is related to the work presented in the manuscript? What is being challenged or extended?

We thank the editor for the suggestion. We have avoided the reference lumping in the revised manuscript. The lumping parts have been removed in the previous manuscript such as "~~waste heat recovery technology [2,3]~~", "~~by many researchers~~

~~[13-15]~~", "~~avoid the decomposition [17,18]~~", "~~simple layout [27,28],~~".

Research work in references were summarized to descript the present research and existing questions. Ref. [1] descripted the widely use of internal combustion engines. Ref. [2] descripted the low fuel utilization efficiency of internal combustion engines. Ref. [3] descripted the advantages of organic Rankine cycle system. Ref. [4], [5] and [6] descripted the work of selecting suitable organic working fluids for organic Rankine cycle system by three different research groups. Ref. [7] and [8] descripted the configuration improving work in single-loop organic Rankine cycle system for internal combustion engine waste heat recovery. The maximum power output of single-loop organic Rankine cycle was challenged. Ref. [9] pointed out that maximum power output of a single-loop organic Rankine cycle system was lower than that of a dual-loop organic Rankine cycle. Ref. [10], [11] and [12] descripted the configuration improving work in dual-loop organic Rankine cycle system by three different research groups. But thermal stability of the organic working fluids in these systems was neglected. To avoid this issue, Ref. [17], [18] and [19] developed thermoelectric generator and steam Rankine cycle to address the decomposition issue of the high temperature heat transfer. But the energy conversion efficiency of the thermoelectric generator and component size of steam Rankine cycle in the references were challenged. Low thermal efficiency and large component bulk might limit their application. Thus, we provided our solution: a carbon dioxide Brayton cycle. For Ref. [20], the authors didn't analysis the parameter variation of carbon dioxide Brayton cycle and they didn't utilized the energy in the jacket water. Ref. [23], [24] and [25]

descripted the utilization of jacket water in the organic Rankine cycle system for internal combustion engine waste heat recovery. But the utilization efficiency of jacket water is low. Thus, we designed a dual-pressure organic Rankine cycle to increase the mass flow rate of the working fluid preheated by jacket water. Ref. [27], [28] and [29] descripted the recent research work about multigeneration system driven by waste heat. They expressed the importance of the multigeneration. Ref. [30] and [31] descripted the combined cooling and power system driven by internal combustion engine. The authors used ammonia absorption refrigeration cycle in the systems to provide refrigeration. But the structure of the ammonia absorption refrigeration cycle is complex and it requires a relatively high driven temperature. Thus, we employed the ejector refrigeration cycle to provide refrigeration and further utilize the jacket water energy.

2. Please avoid having heading after heading with nothing in between, either merge your headings or provide a small paragraph in between.

We thank the editor for this suggestion. Heading after heading was avoided in the revised manuscript.

3. Avoid using abbreviations and acronyms in title, abstract, headings and highlights. The first time you use a chemical formula in the text, please write the full compound name and the formula in parenthesis. Do not use chemical formula in the title, abstract, chapter headings and highlights.

We thank the editor for this suggestion. Abbreviations and acronyms in abstract and headings were removed and rewritten in the revised manuscript. “(carbon dioxide)”

was used to explain CO_2 the first time it appeared in the text in Line 105: “Brayton cycle with CO_2 (carbon dioxide) as working fluid”

4. The first time you use an acronym in the text, please write the full name and the acronym in parenthesis. Do not use acronyms in the title, abstract, chapter headings and highlights.

We thank the editor for this suggestion. We have written a full name of the acronym in parenthesis the first time it appeared in the text in the revised manuscript.

The use of acronym in the text were “internal combustion engine (ICE)” in Line 44; “study of organic Rankine cycle (ORC)” in Line 51; “introduced thermoelectric generator (TEG) technology” in Line 96; “coupled with CO_2 Brayton cycle (CBC)” in Line 107; “Combined cooling and power (CCP) systems” in Line 133; “Ammonia absorption refrigeration cycle (AARC)” in Line 141; “ejector refrigeration cycle (ERC)” in Line 144; “dual-pressure organic Rankine (DORC)” in Line 150.

5. The introduction should include problem context, literature review and the hypothesis based on the gap analysis of the previously published research.

We thank the editor for this suggestion. Introduction was thoroughly rewritten in the revised manuscript. Problem context, literature review and hypothesis were included in the introduction.

6. The originality of the paper needs to be further clarified.

We thank the editor for this suggestion. Originality of the paper was further clarified in the revised manuscript.

There are three innovative features in this paper:

(1) We investigated a CO_2 Brayton cycle to prevent the risk of the decomposition of organic working fluid and provide power with high efficiency.

Organic Rankine cycles are used by many researchers to recover waste heat from internal combustion engines. Refrigerants are widely used as working in organic Rankine cycles but their decomposition temperatures are relatively low (200-300 ℃). When the high-temperature (above 450 ℃) engine exhaust gas transfers heat with these organic working fluids, there is risk of decomposition of the organic working fluids. Though organic working fluids with high decomposition temperature were investigated researchers, their flammability hindered their further applications. Some high-temperature loops for waste heat recovery were proposed by some researchers such as thermoelectric generator, steam Rankine cycle. But the thermal efficiency of the thermoelectric generator is low and the bulk of components in steam Rankine cycle is large, which might limit their application. Thus, we use a CO_2 Brayton cycle work as a high-temperature loop in the system to prevent the decomposition risks and provide power with high efficiency and compact structure.

(2) We developed a dual-pressure organic Rankine cycle to increase the utilization efficiency of the jacket water energy.

The previous internal combustion engine waste heat recovery systems, energy in jacket water was not fully utilized. In some studies, energy in jacket water was not utilized as all. Jacket water was mainly used to preheat the organic working fluid in the organic Rankine cycle based internal combustion engine waste heat recovery system. But there is mismatch of the mass flow rate of the organic working fluid in

the preheater and evaporator. Thus, only a small part of the energy in jacket water was harnessed. We developed a dual-pressure organic Rankine cycle as a bottom cycle after the CO_2 Brayton cycle. Dual-pressure organic Rankine cycle can provide a large amount of power output. Moreover, organic working fluid in both high-pressure and low-pressure are preheated by the jacket water, which increases the utilization rate of the jacket water.

(3) We developed an ejector refrigeration cycle to fully utilize the jacket water waste heat and provide refrigeration.

Combined cooling and power system driven by engine waste heat shows the advantages of high efficiency and multiple energy supply. Ammonia absorption refrigeration cycle are widely used for refrigeration in these systems. But the configuration of it is complex and it requires a high driven temperature. We coupled a ejector refrigeration cycle with the organic Rankine cycle system instead of ammonia absorption refrigeration cycle to provide refrigeration. The ejector refrigeration cycle has a simple structure and requires relatively low driven temperature. Thus, jacket water is used to drive the ejector refrigeration cycle to provide refrigeration and fully utilize the waste heat.

Reviewer #1:

This manuscript introduces the performance analysis and optimization of a combined cooling and power system using low boiling point working fluid driven by engine waste. The novelty and the impact of the present manuscript is limited and the relation to previous works is poor.

Thank the reviewer for pointing out the shortcomings of the paper. We have thoroughly rewritten the introduction section to further clarify the novelty and the relation to previous work of the paper.

There are three innovative features in this paper:

(1) We investigated a CO_2 Brayton cycle to prevent the risk of the decomposition of organic working fluid and provide power with high efficiency.

Organic Rankine cycles are used by many researchers to recover waste heat from internal combustion engines. Refrigerants are widely used as working in organic Rankine cycles but their decomposition temperatures are relatively low (200-300 ℃). When the high-temperature (above 450 ℃) engine exhaust gas transfers heat with these organic working fluids, there are risks of decomposition of the organic working fluids. Though organic working fluids with high decomposition temperature were investigated researchers, their flammability hindered their further applications. Some high-temperature loops for waste heat recovery were proposed by some researchers such as thermoelectric generator, steam Rankine cycle. But the thermal efficiency of the thermoelectric generator is low and the bulk of components in steam Rankine cycle is large, which might limit their application. Thus, we use a CO_2 Brayton cycle work as a high-temperature loop in the system to prevent the decomposition risks and provide power with high efficiency and compact structure.

(2) We developed a dual-pressure organic Rankine cycle to increase the utilization efficiency of the jacket water energy.

The previous internal combustion engine waste heat recovery systems, energy in

jacket water was not fully utilized. In some studies, energy in jacket water was not utilized as all. Jacket water was mainly used to preheat the organic working fluid in the organic Rankine cycle based internal combustion engine waste heat recovery system. But there is mismatch of the mass flow rate of the organic working fluid in the preheater and evaporator. Thus, only a small part of the energy in jacket water was harnessed. We developed a dual-pressure organic Rankine cycle as a bottom cycle after the CO_2 Brayton cycle. Dual-pressure organic Rankine cycle can provide a large amount of power output. Moreover, organic working fluid in both high-pressure and low-pressure are preheated by the jacket water, which increases the utilization rate of the jacket water.

(3) We developed an ejector refrigeration cycle to fully utilize the jacket water waste heat and provide refrigeration.

Combined cooling and power system driven by engine waste heat shows the advantages of high efficiency and multiple energy supply. Ammonia absorption refrigeration cycle are widely used for refrigeration in these systems. But the configuration of it is complex and it requires a high driven temperature. We coupled a ejector refrigeration cycle with the organic Rankine cycle system instead of ammonia absorption refrigeration cycle to provide refrigeration. The ejector refrigeration cycle has a simple structure and requires relatively low driven temperature. Thus, jacket water is used to drive the ejector refrigeration cycle to provide refrigeration and fully utilize the waste heat.

About the impact of this paper:

There are two pathways to improve the performance of the organic Rankine cycle system for engine waste heat recovery. One will be selecting organic working fluids which are suitable for the system under certain conditions. Another is to optimize the system configuration to make full use of the waste heat. In this paper, we designed a combined cooling and power system with a novel configuration which prevents the decomposition risk of organic working fluid, fully utilizes the jacket water energy and provides power and refrigeration simultaneously.

About the relation of this paper to previous work:

We have thoroughly rewritten the introduction section of this paper. More recently published papers were added to descript research conditions and existing problems. We carried out our work based on the analysis of previous work.

Reviewer #2:

Corrections mainly involve formatting points, such as English grammar, citation of references, etc.; and insufficient information regarding some equipment used in the research. Concerning the formatting and methodology the points are as follows:

1. In Nomenclature, present separately the Latin symbols, Greek symbols, Acronyms, Subscripts and Superscripts, because of the form that is presented, it is confused; include the acronym TEG - Thermoelectric generator and GA - Genetic Algorithm; if the "K" of K$" is "kilo", must be represented by "k".

Thank the reviewer for the kind suggestion. The Nomenclature section was separated as Latin symbols, Acronyms, Greek symbols and Subscripts in the revised manuscript. TEG and GA were added to the list and "K$" was changed to "k$".

2. In lines 72, 96, 97 and 203, separate the temperature values of its units, for example, 90 ºC (line 72).

In the revised manuscript, temperature values were separated with their units.

In Line 87: “low (200-300 ℃) [13], while the temperature of exhaust gas is above 450 ℃”; in Line

3. In line 104 change "to the utilize" by other word.

We have thoroughly rewritten the introduction section and the error was avoided in the revised manuscript.

4. In line 126 put comma between gas and while, and after "But" in line 127.

We have thoroughly rewritten the introduction section and the error was avoided in the revised manuscript.

5. In line 139 and 140 change the word "flew" by "flows".

We have thoroughly rewritten the introduction section and the error was avoided in the revised manuscript.

6. In lines 148, 149 and 150 put "2" of "CO2" as subscript.

We have thoroughly rewritten the introduction section and the error was avoided in the revised manuscript.

7. In line 166 change the word "consumption" by "combustion".

We have thoroughly rewritten the introduction section and the error was avoided in the revised manuscript.

8. In line 174 put comma after "Meanwhile".

We have thoroughly rewritten the introduction section and the error was avoided in

the revised manuscript.

9. From line 197 to 206 write "Several assumptions are made to simplify the simulation of the system, which are: (1) the system keeps a steady state; (2) the heat and friction ….are not considered; and so on.

We thank the reviewer for the suggestion. The system assumptions part was rewritten based on the suggestion in the revised manuscript from Line 369 to Line 337 "Several assumptions are made to simplify the simulation of the system, which are: (1) the system keeps a steady state; (2) the heat and frication in the system are not considered; (3) the pressure losses in the vapor generators, preheater, evaporator, condensers and pipes are neglected; (4) the gas temperature at the outlet of the vapor generator 1 is higher than 110 ℃ [35], considering the low gas dew point temperature; (5) the working fluids at the outlet of the condensers and the preheater are saturated liquids, and the evaporator outlet state is saturated vapor; (6) the process through the throttle valve is isenthalpic."

10. In line 228 put a comma after "thermodynamic".

We have rewritten that paragraph in the revised manuscript from line 221 to line 226. The error was avoided.

11. Begin the sentence of the line 236 by "In this study, all components in the system …" and remove "in this study" of the end of the sentence.

The sentence was rewritten in the revised manuscript in Line 235 as following:

"In this study, all the components in the system are associated directly or indirectly with fuel of other heat sources, such as exhaust as and jacket water."

12. In line 257 put comma between "expenses" and "etc."

A comma was put between "expenses" and "etc." in the revised manuscript in line 250 as following:

(like the taxes, insurance engineering expenses, etc.)

13. Indicate that equations from 11 to 21 are proposed in [33].

We have indicated in the revised manuscript as following:

Line 360: “In the following text, equations from Eq. (11) to Eq. (21) are proposed in Ref. [37].”

14. In line 265 write "where Ki,turb are the constants corresponding to the turbine type; and W is the power …."; and in similar manner in lines 276, 282 and 286.

We have rewritten the sentences in the revised manuscript in Line 259 “$K_{i,\ turb}$ are constants corresponding to”, Line 270 “$K_{i,\ pump}$ are the constants corresponding to”, Line 276 “$B_{i,\ pump}$ are the constants corresponding to”, Line 280 “$C_{i,\ pump}$ are the constants corresponding to”, Line 285 “$K_{i,comp}$ are the constants corresponding to”, Line 295 “$K_{i,he}$ are the constants corresponding to”, Line 302 “$B_{i,he}$ are the constants corresponding to” and Line 306 “$C_{i,he}$ are the constants corresponding to”.

15. In lines 297 and 784 I suggest to change the word "Tube-and-shell heat exchangers" to "Shell-and-tube heat exchangers".

It was corrected in the revised manuscript in lines 291 and 702 as following:

16. Verify in the equation (23) if the exponent of the term in brackets of the numerator is "n - 1".

Thank the reviewer for the kind suggestion. We have verified the equation. It was

"n".

17. In line 336 add the word "years" after 30.

It was corrected in the revised manuscript in line 328 as following: “being assumed as 30 years”

18. In lines 340 and 348 change the word "steams" by "streams"; and in lines 342, 343 and 349 change the word "steam" by "stream".

We have changed the expression in the revised manuscript in lines 332, 334, 335, 340 and 341 as following:

“In a steady system, there are a number of entering and outing working fluid streams and heat and work interactions with the surroundings. In exergoeconomic analysis, each flowing stream is associated with a levelized exergy cost. The equations to calculate the cost of the stream product are given as:”

“where c denotes levelized exergy cost of the streams; $E_{y,in}$ and $E_{y,out}$ are the exergy transfer rate of the stream flowing in and out of a component;”

19. In line 348 remove the space before "where" and verify if the variable "c" is the "levelized exergy cost of the system" or is the "average cost per unit of exergy" according to the Nomenclature.

Thank the reviewer for the kind suggestion. "c" is the "levelized exergy cost of the system". We have corrected the error in the Nomenclature and remove the space in line 340.

20. In line 349 add "of" after out.

We have corrected the error in the revised manuscript in line 341 as following:

“flowing in and out of a component”

21. In line 360 and 363 add the word "where" before "cfuel" and "cBt", respectively; and remove the initial space.

We have corrected the error in the revised manuscript in lines 352 and 355.

22. In line 365 add "… and the fuel-cost-related part, given by Eq. (32) and (33).

We have corrected the error in the revised manuscript in lines 357 and 358. “capital-cost-related part and the fuel-cost-related part, given by Eq. (32) and Eq. (33).”

23. I suggest that sections 4.1.1, 4.1.2 and 4.2 are inserted at the end of section 3, because they represent materials and methods and not results and discussion.

Thank the reviewer for the kind suggestion. We have put sections 4.1.1, 4.1.2 and 4.2 to the end of section 3.

24. In line 380 remove the word "gas" and maintain only "… supercharger engine."; in line 382 replace "The heat load capacity" by "The thermal load of the …" and deleted "when cooled down to the acid dew temperature".

We have rewritten the sentences in the revised manuscript in line 370.

“In this study, the engine selected [7] is a 12-cylinder 4-stroke supercharged engine. The main designed parameters of the engine are listed in Table 3. The composition of the engine exhaust gas is presented in Table 4. The thermal load of the engine exhaust gas is about 1700 kW and 1000 kW can be obtained from the engine jacket water.”

25. In line 386 express the seven key parameters by its symbols.

We have added the symbols of the key parameters in the revised manuscript from

line 376 to 380 as following:

“Seven key parameters : BC turbine inlet temperature ($T_{Bt,in}$), BC turbine inlet pressure ($P_{Bt,\ in}$), inlet temperature at the high-pressure side of ORC turbine ($T_{Ot,\ in,\ h}$), inlet pressure at the high-pressure side of ORC turbine ($P_{Ot,\ in,\ h}$), inlet temperature at the low-pressure side of ORC turbine ($T_{Ot,\ in,\ l}$), inlet pressure at the low-pressure side of ORC turbine ($P_{Ot,\ in,\ l}$) and the ejector primary inlet pressure ($P_{ej,\ in}$),”

26. In lines 392, 393, 395 and 396 express the variables "W", "Q" and "c" in italics.

We have corrected the error in the revised manuscript from line 384 to 389.

“In the thermodynamic aspect, the net power output of the CO_2 Brayton cycle (W_{BC}), net power output of the DORC (W_{ORC}), net power of the whole system (W_{net}), cooling capacity of the system (Q_{cool}) and the exergy efficiency of the system (η_{exergy}) are selected to reflect the system performance. Levelized exergy cost for the BC turbine power output (c_{Bt}), levelized exergy cost for the ORC turbine power output (c_{Ot}), levelized exergy cost the system product ($c_{product}$) and the system capital cost ($z_{capital}$) are chosen to represent the exergoeconomic performance.”

27. Start the Results and discussion section from section 4.2.1.

We have put that section at the beginning of Results and discussion.

28. In all results shown from Fig. 2 to Fig. 15 only one parameter at a time was varied, while the others were maintained constants? Clear this in the text.

We have explained this in the revised manuscript from line 381 to 383 as following:

“When one parameter is investigated to analyze the system performance, other parameters are maintained constants based on the conditions in Table 5.”

29. In line 552 change "The can be explained …" by "This can be explained …".

It was corrected in the revised manuscript.

30. Seems incomplete to me the sentence of the line 612 "Thus, the capita-cost-related …".

We have rewritten the sentence in the revised manuscript.

31. In line 641 remove the word "vapor" after "… vapor generator 2".

We have rewritten the sentence in the revised manuscript in line 575.

32. In line 658 add "of" after "Though".

We have rewritten the sentence in the revised manuscript.

33. In the sentence of line 676 I suggest to write "The cooling capacity (Qcool) increases slightly with the …" because by Figure 12 the increase is very small and, hence, should also be corrected at the end of line 680.

We have rewritten the sentence in the revised manuscript in lines 604 and 607.

34. In line 709 add a "t" after "can'".

The error was corrected in the revised manuscript in line 631.

35. Rewrite the two sentences from line 713 to 715.

We have rewritten the two sentences in the revised manuscript from line 635 to 637 as following:

"The increase of the ejector primary inlet pressure causes the increase of the entrainment ratio of the ejector. Thus, more secondary flow is entrained to the ejector from the evaporation, leading to the increase of the cooling capacity."

36. In the paragraph from line 751 to line 753 I suggest to refer to Fig. 8 and 9 where

are evidenced the highest output power, exergy efficiency and the lowest levelized exergy cost (but not the cooling capacity) at the highest inlet pressure at the high-pressure side ORC turbine.

We thank the reviewer for this kind suggestion. We compared the results of the genetic algorithm optimization results with the parameter trend in Fig. 8 and 9. The value of net power output, exergy efficiency, levelized exergy cost and the inlet pressure at the high-pressure side ORC turbine in the two parts were nearly the same. The inlet pressure at the high-pressure side ORC turbine is varied while other six parameters are kept as constants in Fig. 8 and 9. Thus, the inlet pressure at the high-pressure side ORC turbine plays a more important other six parameters. When the inlet pressure at the high-pressure side ORC turbine is close to the highest permitted pressure, the system performance is close to the optimization performance.

Note that: When the inlet pressure at the high-pressure side ORC turbine increases, the pinch point temperature difference in vapor generator 2 decreases. Thus, there would be temperature cross in the vapor generator when inlet pressure at the high-pressure side ORC turbine is larger than critical value. That's why the optimization results shows that the value of the inlet pressure at the high-pressure side ORC turbine is 1.85 MPa in stead of the maximum value 2 MPa.

We have rewritten the paragraph from Line to Line as following:

"The optimization results of GA are listed in Table 8. It can be obtained that the minimum levelized exergy cost for the system product $c_{product}$ is 53.25 $\$(MWh)^{-1}$. The net power output, exergy efficiency of the CCP system are 374.37 kW, 37.31%

respectively. The inlet pressure at the high-pressure side of ORC turbine is 1.85 MPa. Meanwhile, it can be evidenced from Fig. 8 and 9 that the highest output power (about 374.37 kW), exergy efficiency (about 37.31%) and the lowest levelized exergy cost (about 53.25 $(MWh)^{-1}$) at the highest inlet pressure at the high-pressure side ORC turbine (about 1.85 MPa). The results shown in Fig. 8 and 9 are close to the optimization results. The inlet pressure at the high-pressure side ORC turbine is varied while other six parameters are kept as constants in Fig. 8 and 9. Thus, inlet pressure at the high-pressure side ORC turbine plays a more important role than other six parameters when determining the performance of the system. When the inlet pressure at the high-pressure side ORC turbine is close to the highest permitted pressure, the system performance is close to the optimization performance."

37. The sentence of conclusion (2) is very extensive and I suggest ending it in "… for the system product.", beginning the next sentence such as, "Meanwhile, the increase of the ORC …".

We have rewritten the sentence in the revised manuscript in line 689 as following: "In the DORC, the increase of $T_{Ot,\,in}$ and $T_{Ot,\,in,\,l}$ would cause the decrease of the system exergy efficiency and the increase of the levelized exergy cost for the system product. Meanwhile, the increase of $P_{Ot,\,in,\,h}$ and $P_{Ot,\,in,\,l}$ would result in the increase of the exergy efficiency and the decrease of the levelized exergy cost."

38. In line 810 replace the word "frication" by "friction".

The error was corrected in the revised manuscript in line 728 as following: "the Darcy friction factor,"

39. In the "References" use the abbreviation names of the Journals, such as, Energy Convers Manage and the number of pages as 201-14, instead of using 201-214, for example; in the reference [14] line 863 change the number of the pages to 215-32 to differentiate from reference [12];

Thank the reviewer for the suggestion. We have rewritten the abbreviation names of Journals and the page number in the revised manuscript.

40. in reference [16] correct the names of authors to Rajabloo T, Bonalumi D, Lora P; in reference [17] add at the end of the author names, the author Zhu W; in reference [31] add at the end of the author names, the authors Liu H, Wang E, Yao B; in reference [32] correct the author names to Bejan A, Tsatsaronis G, Moran M and the first name of the publisher to John; in reference [33] add other authors, i.e., Turton R, Bailie RC, Whiting WB, Shaeiwitz JA;

We have corrected the errors in the revised manuscript in lines 816, 819, 823, 824 and 825 as following:

[34] Shu G, Zhao M, Tian H, Huo Y, Zhu W. Experimental comparison of R123 and R245fa as working fluids for waste heat recovery from heavy-duty diesel engine. Energy 2016; 115:756-69.

[35] Zhang J, Zhang H, Yang K, Yang F, Wang Z, Zhao G, Liu H, Wang E, Yao B. Performance analysis of regenerative organic Rankine cycle (RORC) using the pure working fluid and the zeotropic mixture over the whole operating range of a diesel engine. Energy Convers Manage 2014; 84:282-94.

[36] Bejan A, Tsatsaronis G, Moran M. Thermal design and optimization. New York:

John Wiley & Sons; 1996.

41. What is the reference [35]?

That reference was a website for the $CEPCI_{ref,2001}$. We have replaced it with reference [38]. In Ref. [38] $CEPCI_{ref,2001}$ is 398.

42. In table 3 replace the word "Term" by "Parameter" and the same in Table 8; in this table I suggest that the values presented be limited in two digits after comma to standardize all.

We have replaced the expression and limited the digits of the value in Table 8 in the revised manuscript.

43. In Table 6 replace "Ranges of the decision variables" by only "Parameters or Variables" and add "Operation" before "Range".

We have replaced the expression in Table 6 in the revised manuscript.

44.In Table B1 the source is [33} and not [32].

Thank the reviewer for helping us find the error. It was corrected in the revised manuscript.

Reviewer #3:

The authors have conducted a study that covers a topic of great interest: "Performance analysis and optimization of a combined cooling and power system using low boiling point working fluid driven by engine waste heat". This very important topic deserved a great deal of attention. However, many shortcomings can be identified. Therefore, I recommend that these shortcomings, as listed in the following, should be addressed before it can be considered for publication;

1. Abstract section, present in more detail and clarity

Thanks for the reviewer's kind suggestion. The abstract section was thoroughly rewritten in the revised manuscript. More details were added in the abstract.

"This paper develops a combined cooling and power system, which consists of a carbon dioxide Brayton cycle, a dual-pressure organic Rankine cycle and an ejector refrigeration cycle, to recover waste heat from exhaust gas and jacket water in internal combustion engines. Thermodynamic models of the system are performed and exergoeconomic methods are used to calculate the levelized exergy cost of the component products. Effects of seven parameters, including temperature and pressure at the Brayton cycle turbine inlet, temperature and pressure at the high-pressure and low-pressure side of the organic Rankine cycle turbine inlet and pressure at the ejector primary inlet, are evaluated. Single-objective optimization is carried out by means of genetic algorithm to obtain the minimum levelized exergy cost of system product. Results show that the increase of pressure at Brayton cycle turbine inlet and high-pressure and low-pressure side of the organic Rankine cycle turbine inlet contributes to the decrease of levelized exergy cost of the system product. Optimization results show that minimum levelized exergy cost for system product is 53.25 \$ $(MWh)^{-1}$. When levelized exergy cost is minimum, system net power output, cooling capacity and exergy efficiency are 374.37 kW, 188.63 kW and 37.31%, respectively."

2. Please, Give more numerical results about the study results in the abstract section.

Thank the reviewer for the suggestion. The abstract section was rewritten in the

revised manuscript and more numerical results were put in the abstract section.

3. Analysis of the state of the art in the introduction is insufficient, which undermines novelty of this work. An updated and complete literature review should be conducted.

The introduction section was thoroughly rewritten in the revised manuscript. More recent references were discussed and some old references were removed. The novelty of this work was further clarified.

4. Literature section should be given current papers after 2017.

We thank the reviewer for the kind suggestion. References in 2017 and 2018 were put in the introduction sections and some old references were removed in the revised manuscript.

[5] Rijpkema J, Munch K, Andersson S. Thermodynamic potential of twelve working fluids in Rankine and flash cycles for waste heat recovery in heavy duty diesel engines. Energy 2018; 160:996-1007.

[6] Su X, Shedd T A. Towards working fluid properties and selection of Rankine cycle based waste heat recovery (WHR) systems for internal combustion engines – A fundamental analysis. Appl Therm Eng 2018; 142:502-10.

[10] Wang X, Shu G, Tian H, Liu P, Jing D, Li X. Dynamic analysis of the dual-loop Organic Rankine Cycle for waste heat recovery of a natural gas engine. Energy Convers Manage 2017; 148:724-736.

[11] Wang E, Yu Z, Zhang H, Yang F. A regenerative supercritical dual-loop organic Rankine cycle system for energy recovery from the waste heat of internal combustion engines. Appl Energy 2017; 190:574-90.

[12] Huang H, Zhu J, Deng W, Ouyang T, Yan B, Yang X. Influence of exhaust heat distribution on the performance of dual-loop organic Rankine Cycle (DORC) for waste heat recovery. Energy 2018; 151:54-65.

[13] Rajabloo T, Bonalumi D, Lora P. Effect of a partial thermal decomposition of the working fluid on the performances of ORC power plants. Energy 2017; 133:1013-26.

[14] Shi L, Shu G, Tian H, Deng S. A review of modified Organic Rankine cycles (ORCs) for internal combustion engine waste heat recovery (ICE-WHR). Renew Sustain Energy Rev 2018; 92:95-110.

5. How were reference conditions (environmental pressure and temperature) considered?

In this paper, environment temperature is 20 ℃ and environment pressure is 101.3 kPa. We referenced it from the following reference:

Yang X, Zheng N, Zhao L, Deng S, Li H, Yu Z. Analysis of a novel combined power and ejector refrigeration cycle. Energy Convers Manage; 2016; 108:266-74.

6. The level of English throughout the manuscript does not meet the journal's desired standard. There are a number of grammatical errors.

Thank the reviewer for the kind suggestion. We have checked the grammatical errors and thoroughly rewrote the paper in the revised manuscript.

7. Introduction part needs to be extended by some of the recently published papers to show the importance of multigeneration systems in high-quality journals

We thank the reviewer for the kind suggestion. We have expressed the importance of the multigeneration systems with three recently published paper in the introduction

section of the revised manuscript.

[27] Li Fan, Sun Bo, Zhang C, Zhang L. Operation optimization for combined cooling, heating, and power system with condensation heat recovery. Appl Energy 2018; 230:305-16.

[28] Yari Mortaza, Ariyanfar Leyli, Aghdam EA. Analysis and performance assessment of a novel ORC based multigeneration system for power, distilled water and heat. Renew Energy 2018; 119:262-81.

[29] Bai Z, Liu T, Liu Q, Lei J, Gong L, Jin H. Performance investigation of a new cooling, heating and power system with methanol decomposition based chemical recuperation process. Appl Energy 2018; 229: 1152-63.

8. Originality of the paper should be emphasized clearly. How this study differs from related published papers?

The introduction section was rewritten in the revised manuscript. We analyzed the gaps existing in the published papers and provided our original solutions. The innovative features of the paper were summarized at the end of the introduction section.

There are three innovative features in this paper:

(1) We investigated a CO_2 Brayton cycle to prevent the risk of the decomposition of organic working fluid and provide power with high efficiency.

Organic Rankine cycles are used by many researchers to recover waste heat from internal combustion engines. Refrigerants are widely used as working in organic Rankine cycles but their decomposition temperatures are relatively low (200-300 ℃).

When the high-temperature (above 450 ℃) engine exhaust gas transfers heat with these organic working fluids, there are risks of decomposition of the organic working fluids. Though organic working fluids with high decomposition temperature were investigated researchers, their flammability hindered their further applications. Some high-temperature loops for waste heat recovery were proposed by some researchers such as thermoelectric generator, steam Rankine cycle. But the thermal efficiency of the thermoelectric generator is low and the bulk of components in steam Rankine cycle is large, which might limit their application. Thus, we use a CO_2 Brayton cycle work as a high-temperature loop in the system to prevent the decomposition risks and provide power with high efficiency and compact structure.

(2) We developed a dual-pressure organic Rankine cycle to increase the utilization efficiency of the jacket water energy.

The previous internal combustion engine waste heat recovery systems, energy in jacket water was not fully utilized. In some studies, energy in jacket water was not utilized as all. Jacket water was mainly used to preheat the organic working fluid in the organic Rankine cycle based internal combustion engine waste heat recovery system. But there is mismatch of the mass flow rate of the organic working fluid in the preheater and evaporator. Thus, only a small part of the energy in jacket water was harnessed. We developed a dual-pressure organic Rankine cycle as a bottom cycle after the CO_2 Brayton cycle. Dual-pressure organic Rankine cycle can provide a large amount of power output. Moreover, organic working fluid in both high-pressure and low-pressure are preheated by the jacket water, which increases the utilization rate of

the jacket water.

(3) We developed an ejector refrigeration cycle to fully utilize the jacket water waste heat and provide refrigeration.

Combined cooling and power system driven by engine waste heat shows the advantages of high efficiency and multiple energy supply. Ammonia absorption refrigeration cycle are widely used for refrigeration in these systems. But the configuration of it is complex and it requires a high driven temperature. We coupled an ejector refrigeration cycle with the organic Rankine cycle system instead of ammonia absorption refrigeration cycle to provide refrigeration. The ejector refrigeration cycle has a simple structure and requires relatively low driven temperature. Thus, jacket water is used to drive the ejector refrigeration cycle to provide refrigeration and fully utilize the waste heat.

This paper differs from the previous paper mainly in the following four point:

(1) We used a CO_2 Brayton cycle to prevent the risk of decomposition of the organic working fluid and comprehensively analyzed its performance.

(2) We designed a dual-pressure organic Rankine cycle as a bottom cycle to increase the utilization efficiency of the jacket water.

(3) We used jacket water to drive the ejector refrigeration cycle to fully utilize the jacket water energy and provide refrigeration.

(4) We used exergoeconomic method to analyze the system performance.

9. Discuss and elaborate more on the exergy destruction rates of system and sub-systems. They were not written in the text.

Exergy destruction rates of the components in the system were calculated and presented in the revised manuscript from line 670 to 678 as following:

"Fig. 16 shows the exergy destruction of different components of the system under the optimization conditions. The largest exergy destruction takes place in the ORC turbine (41.26%), which is mainly caused by the mixing of the high-pressure working fluid and the low-pressure working fluid. Gas heater contributes 13.44% of the total exergy destruction. Three vapor generators take up 4.13%, 11.67% and 3.73% of the exergy destruction, respectively. The exergy destruction for the ejector is 5.61%, which is also caused by the working fluid mixing. For BC turbine, condenser 1, precooler and preheater, the exergy destruction are 3.31%, 4.64%, 3.69% and 3.65%, respectively. Other components contribute to the rest 4.87% of the exergy destruction."

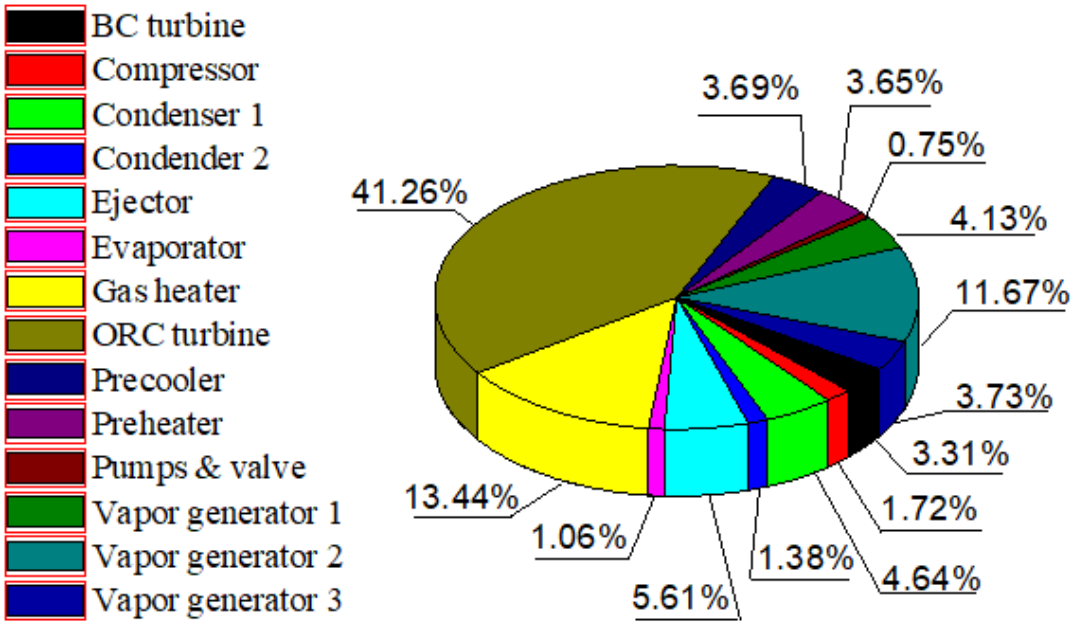

Fig. 16. Exergy destruction of different components

Performance analysis and optimization of a combined cooling and power system using low boiling point working fluid driven by engine waste heat

Wenge Huang, Jiangfeng Wang*, Jiaxi Xia, Pan Zhao, Yiping Dai

Institute of Turbomachinery, Shaanxi Engineering Laboratory of Turbomachinery and Power Equipment, State Key Laboratory of Multiphase Flow in Power Engineering, School of Energy and Power Engineering, Xi'an Jiaotong University, Xi'an 710049, China

Corresponding author: Jiangfeng Wang

Mailing address:

Institute of Turbomachinery, Shaanxi Engineering Laboratory of Turbomachinery and Power Equipment, State Key Laboratory of Multiphase Flow in Power Engineering, School of Energy and Power Engineering

Xi'an Jiaotong University, Xi'an 710049, China

E-mail address: jfwang@mail.xjtu.edu.cn (JF Wang).

Performance analysis and optimization of a combined cooling and power system using low boiling point working fluid driven by engine waste heat

Wenge Huang, Jiangfeng Wang*, Jiaxi Xia, Pan Zhao, Yiping Dai

Institute of Turbomachinery, Shaanxi Engineering Laboratory of Turbomachinery and Power Equipment, State Key Laboratory of Multiphase Flow in Power Engineering, School of Energy and Power Engineering, Xi'an Jiaotong University, Xi'an 710049, China

Abstract

This paper develops a combined cooling and power system, which consists of a carbon dioxide Brayton cycle, a dual-pressure organic Rankine cycle and an ejector refrigeration cycle, to recover waste heat from exhaust gas and jacket water in internal combustion engines. Thermodynamic models of the system are performed and exergoeconomic methods are used to calculate the levelized exergy cost of the component products. Effects of seven parameters, including Brayton cycle turbine inlet temperature and inlet pressure, organic Rankine cycle turbine high-pressure side and low-pressure side inlet temperature and ejector primary inlet pressure, are evaluated. Single-objective optimization is carried out by means of genetic algorithm to obtain the minimum levelized exergy cost of system product. Results show that the increase of pressure at Brayton cycle turbine inlet and high-pressure and low-pressure side of the organic Rankine cycle turbine inlet contributes to the decrease of levelized

exergy cost of the system product. Optimization results show that minimum levelized exergy cost for system product is 53.25 $ (MWh)$^{-1}$. When system product levelized exergy cost is minimum, system net power output, cooling capacity and exergy efficiency are 374.37 kW, 188.63 kW and 37.31%, respectively.

Nomenclature

Latin symbols		ρ	density, kg m^{-3}
A	area, m^2	μ	dynamic viscosity, m^2 s^{-1}
B_o	boiling number	η	efficiency, %
c	levelized average cost, $ (MWh)$^{-1}$	δ	thickness, m
c_p	specific heat, kJ kg^{-1} K^{-1}	*Subscribes*	
C	cost rate, $ year^{-1}	1-31	state points
D	diameter, m	g1-g3	state points
e	exergy, kJ kg^{-1}	w1-w3	state points
E	exergy flow rate, kJ s^{-1}	Bt	Brayton cycle turbine
E_y	exergy flow rate per year, kJ year^{-1}	BM	bare module
F	multiplying factor	cond	condenser
f	friction factor	comp	compressor
G	mass flow rate, kg s^{-1}	D	destruction
h	enthalpy, kJ kg^{-1}	elec	electricity
H	depth, m	es	equivalent diameter
i_{eff}	interest rate	ev	evaporation/evaporator
l	length, m	ex	exergy

M	mass flow rate, kg s^{-1}	F	fuel
n	lifetime, year	g	exhaust gas
Nu	Nusselt number	gh	gas heater
P	pressure, MPa	he	heat exchanger
Pr	Prandtl number	L	loss
Pt	center distance between tubes, m	l	liquid
P_r	reduced pressure	M	material
Q	heat transfer rate, kW	Ot	ORC turbine
Q_{cool}	cooling capacity, kW	P	product
q_m	average imposed wall heat flux, W m^{-2}	p1	pump 1
r_f	enthalpy of vaporization, kJ kg^{-1}	p2	pump 2
T	temperature, K	p3	pump 3
U	overall heat transfer coefficient, W m^{-2} K^{-1}	p4	pump 4
W	power, kW	pf	primary flow
W_y	annually power, MWh $year^{-1}$	prec	precooler
x	vapor quality	preh	preheater
Z	annually levelized cost value, \$ $year^{-1}$	s	shell
z	capital cost, k\$	t	tube
Acronyms		th	thermal
BC	Brayton cycle	turb	turbine
CBC	CO_2 Brayton cycle	vg	vapor generator
CCP	combined cooling and power	w	tube wall

CRF	capital recovery factor
CEPCI	chemical engineering plant cost index
DORC	dual-pressure organic Rankine cycle
ERC	ejector refrigeration cycle
GA	genetic algorithm
TEG	thermoelectric generator
AARC	ammonia absorption refrigeration cycle
Greek symbols	
α	convection heat transfer coefficient, W m^{-2} K^{-1}
λ	heat conductivity, W m^{-1} K^{-1}

1. Introduction

Nowadays, internal combustion engine (ICE) is the major motive power source in energy field, which are widely used in transport, construction, agriculture, etc. Over 50 % of the total transportation fuel is consumed by ICEs [1]. However, only 30-45% of the fuel energy is converted into effective power output, while the remaining energy is discharged to the environment via exhaust gas, jacket water and charge air, causing a large amount of waste fuel energy [2]. Thus, technology for waste heat recovery from ICEs has drawn much interest of researchers in the last decade. Much effort has been devoted to the study of organic Rankine cycle (ORC) based ICE waste heat recovery system for its advantages of high efficiency and simple structure [3].

There are two important pathways that will lead to the improvement of the ORC

system for ICE waste heat recovery. One will be selecting organic working fluids which are suitable for the system under certain conditions. Another is to optimize the system configuration to make full use of the waste heat.

The work of selecting suitable organic working fluids for ORC was carried out by many researchers to improve the efficiency of the ICE waste heat recovery. Tian et al. [4] evaluated the performance of 20 different working fluids in an ORC system for ICE waste heat recovery. Rijpkema et al. [5] compared the performance of twelve working fluids in an ORC-based ICE waste heat recovery system to find the suitable candidate. Su et al. [6] developed a theoretical efficiency model about working fluids selecting for ORC-based ICE waste heat recovery system via strict mathematical derivation.

Configuration optimization in ORC-based ICE waste heat recovery system mainly focuses on reducing the system irreversible rate to fully utilize the engine waste heat. Vaja and Gambarotta [7] added a preheater and a recuperator separately to a simple ORC system to improve the performance for the ICE waste heat recovery. Kim et al. [8] proposed a novel single-loop ORC system to recovery engine waste heat. They employed two recuperators in series to heat the working fluid. Comparison showed that the net power output of the system was 35.6% more than simple ORC system. Because that the maximum power output of single-loop ORC is lower than that of the dual-loop ORC system [9], more attention has been focused on dual-loop ORC based ICE waste heat recovery system in recent years. Wang et al. [10] modeled a dual-loop ORC system for engine waste heat recovery. The high-temperature loop absorbed heat

from exhaust gas and its residual heat acted as heat source for the low-temperature loop. Wang et al. [11] investigated a dual-loop ORC system for ICE waste heat recovery. The high-temperature loop absorbed heat from exhaust gas for the first time. Then the low-temperature loop absorbed heat from the residual heat of the exhaust gas to realize the cascading utilization of the waste heat. Huang et al. [12] proposed a complex dual-loop ORC system for engine waste heat recovery. The high-temperature loop absorbed heat from the exhaust gas and residual heat from both the exhaust gas and the high-temperature loop provided heat for the low-temperature loop.

When referring to heat transfer in the high-temperature loop, thermal stability of organic working fluid is necessary to be considered. In previous studies, refrigerants were most selected as working fluids. The decomposition temperatures of refrigerants are relatively low (200-300 ℃) [13], while the temperature of exhaust gas is above 450 ℃[14]. Direct heat transfer between high-temperature exhaust gas and refrigerant caused the risk of working fluid decomposition. Though high decomposition temperature working fluids such as siloxanes and alkanes were adopted by some researchers, their flammability hindered their further applications [15]. Though placing a heat transfer oil intermediate loop between the exhaust gas and the ORC system could address this issue [16], it would cause a large amount of the high-temperature waste heat unharnessed. Therefore, some other high-temperature loops for waste heat recovery were employed by researchers to couple with the ORC. Miller et al. [17] introduced thermoelectric generator (TEG) technology. High-temperature exhaust gas was first exploited by the TEG, then the cooled exhaust

gas could drive the ORC safely. But the energy conversion capacity of TEG is low because of the material limitation. Steam Rankine for its high efficiency and stable operation attracted much attention of researchers. Shu et al. [18] placed a steam Rankine cycle between the ORC and the exhaust gas. Yu et al. [19] coupled a steam Rankine cycle with an ORC for the ICE waste heat recovery. However, the large bulk of the components in steam Rankine cycle limits further applications (such as application in vehicles) [20]. Considering the requirement of high thermal efficiency and compact configuration, Brayton cycle could be a compromise solution. Brayton cycle with CO_2 (carbon dioxide) as working fluid has the advantage of low environmental impact and good thermodynamic performance [21]. Few studies about ORC system coupled with CO_2 Brayton cycle (CBC) for ICE waste heat recovery have been published. Though Zhang et al. [20] carried out some relevant studies, their attention was focused on comparing the performance of CBC, TEG and steam Rankine cycle when coupled with the same bottom ORC. Detailed analysis of the CBC was not given and the energy in jacket water was not harnessed.

Jacket water, though containing large amounts of energy [22], obtained little attention in the previous studies. For its relatively low temperature, jacket water was mainly used to preheat the organic working fluid in the ORC system. In the ORC-based ICE waste heat recovery system designed by Zhang et al. [23] jacket water was used to preheat the organic working fluid. Then the organic working fluid was heat by the high-temperature exhaust gas to vapor state and expanded in the ORC turbine. In Yang's [24] ICE waste heat recovery system, jacket water and secondary

exhaust gas were used to preheat the organic working fluids in ORC. In the dual-loop ORC based ICE waste heat recovery system investigated by Song et al. [25], jacket water was used to preheat the low-temperature-loop. Yu et al. [26] calculated the energy recovery efficiency from an ORC-based ICE waste heat recovery system. 75% waste heat could be recovered from the exhaust gas, while only 9.5% waste heat was recovery from jacket water. The relatively low utilization rate of jacket water energy in the ORC system is caused by the mismatch of working fluid mass flow rate in the preheater and the evaporator. Thus, the utilization of energy in jacket water could be further explored.

Multigeneration system driven by waste heat has drawn increasing interest of researchers in light of the trend towards reducing emissions, increasing the efficiency of energy use and providing variable energy. Li et al. [27] modeled a combined cooling, heating and power system to highly utilize the waste heat. Yari et al. [28] proposed a waste heat recovery system to provide power, distilled water and heat. Bai et al. [29] investigated a cooling, heating and power system driven by exhaust gas to recovery the waste heat. Combined cooling and power (CCP) systems driven by ICE waste heat were also investigated by some researchers. Chen et al. [30] designed an ammonia-water combined cooling and power system using the waste heat from the ICEs. Ammonia-water was heated by exhaust gas and jacket water. One part of the ammonia-water vapor flew into the turbine to provide power and the other part flew into the evaporator to provide refrigeration. Salek et al. [31] coupled an ammonia absorption refrigeration cycle and a bottoming Rankine cycle with internal

combustion engine to produce power and cooling capacity.

Ammonia absorption refrigeration cycle (AARC) were widely used in the combined cooing and power system for its large refrigeration output. However, the complex cycle structure and high driven temperature requirement of AARC might sometimes limit its applications. On the contrary, ejector refrigeration cycle (ERC) exhibits the advantages of easy maintenance and high reliability [32] and it can be driven by low-temperature heat source such as the jacket water. Thus, ICE waste heat recovery system with ERC driven by jacket water not only simultaneously generate power and refrigeration but also fully utilized the jacket water waste heat.

In this study, a combined cooling and power system is developed, which comprises a CO_2 Brayton cycle, a dual-pressure organic Rankine (DORC) cycle and an ejector refrigeration cycle. The CO_2 Brayton cycle absorbs heat from the high-temperature exhaust gas directly to prevent the decomposition risk. The turbine exhaust in the CO_2 Brayton cycle and the engine exhaust gas after heat transfer are respectively regarded as the heat sources for the high-pressure side and low-pressure side of the dual-pressure ORC, realizing the cascading utilization of exhaust gas. Meanwhile, organic working fluids in high-pressure side and low-pressure side are both preheated by jacket water which increases the mass flow rate of the organic working fluid preheated by jacket water. What's more, the ejector refrigeration cycle is adopted to produce refrigeration and fully utilize waste heat in jacket water. Thermodynamic and exergoeconomic analysis is carried out to examine the effects of key parameters on system performance. Then a system optimization is conducted to obtain the minimum

levelized exergy cost for the system product by means of genetic algorithm (GA).

The innovative features of this paper are as follow:

- A CO_2 Brayton cycle is investigated to prevent the risk of decomposition of organic working fluid and provide power.
- A novel dual-pressure ORC system is developed to cascading utilize the waste heat in exhaust gas and jacket water and provide large amounts of power output.
- An ejector refrigeration cycle driven by jacket water is designed to provide refrigeration and fully utilize the jacket water waste heat.

2. System description

The combined cooling and power system is shown in Fig. 1. The system integrates a dual-pressure organic Rankine cycle with a CO_2 Brayton cycle and an ejector refrigeration, which can produce power and refrigeration simultaneously. High-temperature gas heat from the ICE enters the gas heater to provide heat for the CBC. In the CBC, compressor compresses the CO_2 to a supercritical state. The high-pressure CO_2 flows into the gas heater to absorb heat. Then CO_2 with high temperature and high pressure expands through the BC turbine to produce power.

After expanding in the BC turbine, the high-temperature exhaust CO2 flows into vapor generator 2 to heat the organic working fluid. High-pressure side organic working fluid heated by the CO2 then flows into the ORC turbine to produce power. Meanwhile low-pressure side organic working fluid absorbs heat from the secondary engine exhaust gas in vapor generator 1 and then enters ORC turbine to produce

power.

Exhaust vapor from the ORC turbine is cooled by condenser 1 to liquid state and pressured by pump 1. Jacket water with large mass flow rate is used to preheat the organic working fluid in the preheater. The preheated organic working fluid then separates. One part of the fluid is pumped by pump 3 to the vapor generator 1 to cycle in the low-pressure side. The other part is pumped by pump 2 to the vapor generator 2 to cycle in the high-pressure side.

The jacket water then flows into vapor generator 3 to provide heat for the ejector refrigeration cycle. After the condensation process in condenser 2, liquid working fluid is divided into two separated parts. One part of the fluid is pumped to the vapor generator 3 to absorb heat from jacket water and then becomes superheated vapor. The other part of the working fluid flows through the throttle valve to become low-pressure vapor-liquid mixture. The low-pressure mixture enters the evaporator to produce cooling capacity when absorbing heat from the environment and become low-pressure vapor. After that, the superheated vapor mixes with the low-pressure vapor in the ejector. The mixed working fluid enters the condenser 2 to be condensed to liquid.

R245fa is selected as the working fluid for the organic Rankine cycle and the ejector refrigeration cycle because of the great thermodynamic performance [33] and the low environment effects [34].

3. System model

Several assumptions are made to simplify the simulation of the system, which are: (1) the system keeps a steady state; (2) the heat and frication in the system are not considered; (3) the pressure losses in the vapor generators, preheater, evaporator, condensers and pipes are neglected; (4) the gas temperature at the outlet of the vapor generator 1 is higher than 110 ℃ [35], considering the low gas dew point temperature; (5) the working fluids at the outlet of the condensers and the preheater are saturated liquids, and the evaporator outlet state is saturated vapor; (6) the process through the throttle valve is isenthalpic.

3.1.Energy model

The net power of the CO_2 Brayton cycle is expressed as:

$$W_{BC} = W_{Bt} - W_{comp} \tag{1}$$

The net power of the DORC is given as:

$$W_{ORC} = W_{Ot} - W_{p1} - W_{p2} - W_{p3} \tag{2}$$

The cooling capacity of the ERC is given as:

$$Q_{cool} = M_{cool} \cdot (h_{21} - h_{20}) \tag{3}$$

The net power output of the whole system is calculated as:

$$W_{net} = W_{ORC} + W_{BC} - W_{p4} \tag{4}$$

The thermal efficiency of the system is given as:

$$\eta_{th} = \frac{W_{net} + Q_{cool}}{M_{g1} \cdot (h_{g1} - h_{g3}) + M_{w1} \cdot (h_{w1} - h_{w3})} \tag{5}$$

The detailed energy model equations of each component are list in Table 1. Note

that there are two expanding processes in the ORC turbine. The high-pressure vapor expands in the turbine and then mixes with the vapor from vapor generator 1. After that, the mixed vapor expands in the turbine for the second time.

3.2.Exergy model

The energy model of the system is based on the first law of thermodynamics. From the viewpoint of the first law, it is equivalent for work and heat. Nevertheless, according to the second law of the thermodynamics, the irreversibility of work and heat is different. The exergy is used to quantifies the difference between them. The exergy model of the system is based on a dead state (the ambient condition in this study). Definition of exergy is given as:

$$e = (h - h_0) - T_0 \cdot (s - s_0) \tag{6}$$

where h_0, T_0 and s_0 are the parameters under the ambient conditions.

The exergy flow rate in this study is given by:

$$E = M \cdot e \tag{7}$$

In this study, all the components in the system are associated directly or indirectly with fuel of other heat sources, such as exhaust as and jacket water. The heat sources provide exergy for the components to operate. For each component, there is an exergy balance equation, being expressed as [36]:

$$E_F = E_P + E_D + E_L \tag{8}$$

where E_F, E_P, E_D, E_L donate the rate of exergy for the component fuel, the rate of exergy for component product, the rate of component exergy destruction and the rate of component exergy loss, respectively.

The details of the exergy balance equations for each component are listed in Table 1.

The exergy efficiency represents the degree of the utilization of the waste heat in the system, being expressed as:

$$\eta_{ex} = \frac{W_{net} + E_{cool}}{E_{g1} - E_{g3} + E_{w1} - E_{w3}} \tag{9}$$

where E_{cool} is the exergy rate of the cooling process, being expressed as:

$$E_{cool} = E_{25} - E_{24} \tag{10}$$

3.3.Capital cost calculation

A method of modeling the capital costs of main components is used in this study. According to Ref. [37], the bare module cost of the components is calculated as the basic cost. The basic cost of the components includes the direct project cost (such as component cost, material cost of the installation, etc.) and the indirect project cost (like the taxes, insurance engineering expenses, etc.). The bare module cost of the components is calculated under basic conditions. For deviations from the based conditions, multiplying factors (the specific component type, the specific system pressure and the specific material of construction) are added in the calculation to correct the results. In the following text, equations from Eq. (11) to Eq. (21) are proposed in Ref. [37].

Axial turbines (BC turbine and ORC turbine) are used in this study. The bare module cost equation of the turbine is:

$$\log_{10} C_{\text{turb}}^{0} = K_{1,\text{turb}} + K_{2,\text{turb}} \cdot \log_{10} W + K_{3,\text{turb}} \cdot (\log_{10} W)^2 \quad (11)$$

where $K_{\text{i, turb}}$ are constants corresponding to the turbine type; and W is the power output of the turbine.

Turbines used in this study are made of carbon steel (CS) and operate under high pressure. Thus, a multiplying factor is used to correct the result. The capital cost of the turbine is given as:

$$C_{\text{turb}} = F_{\text{BM,turb}} \cdot C_{\text{turb}}^{0} \quad (12)$$

where $F_{\text{BM,turb}}$ is the multiplying factor corresponding to the working conditions of the turbine.

Reciprocating pumps are used in this study. The bare module cost equation of the pumps is given as:

$$\log_{10} C_{\text{pump}}^{0} = K_{1,\text{pump}} + K_{2,\text{pump}} \cdot \log_{10} W + K_{3,\text{pump}} \cdot (\log_{10} W)^2 \quad (13)$$

where $K_{\text{i, pump}}$ are the constants corresponding to the pump type; and W is the power input of the pump.

Pumps used in this study are made of stainless steel (SS) and work under high pressure. Thus, multiplying factors are used to correct the bare module cost. The capital cost of the pump is given as:

$$C_{\text{pump}} = \left(B_{1,\text{pump}} + B_{2,\text{pump}} \cdot F_{\text{M,pump}} \cdot F_{\text{P,pump}}\right) \cdot C_{\text{pump}}^{0} \quad (14)$$

where $B_{i,\,pump}$ are the constants corresponding to the type of the pump; $F_{M,pump}$ is the material factor of the pump and $F_{P,pump}$ is the pressure factor of the pump. The equation of the pressure factor is given as:

$$\log_{10} F_{P,pump} = C_{1,pump} + C_{2,pump} \cdot \log_{10} P_{pump} + C_{3,pump} \cdot (\log_{10} P_{pump})^2 \quad (15)$$

where $C_{i,\,pump}$ are the constants corresponding to the type of the pump; and P_{pump} is the pressure of the pump under working conditions.

Axial compressor is used in this study. The bare module cost equation of the compressor is given as:

$$\log_{10} C_{comp}^0 = K_{1,comp} + K_{2,comp} \cdot \log_{10} W + K_{3,comp} \cdot (\log_{10} W)^2 \quad (16)$$

where $K_{i,comp}$ are the constants corresponding to the type of the compressor; W is the power input of the compressor.

The compressor is made of carbon steel (CS) and works under high pressure. Correction equation of the bare module cost is given as:

$$C_{comp} = F_{BM,comp} \cdot C_{comp}^0 \quad (17)$$

where $F_{BM,comp}$ is the constant corresponding to the type of the compressor.

Shell-and-tube heat exchangers (gas heater, vapor generators, precooler, preheater, evaporator and condensers) are used in this study. The bare module cost equation of the heat exchanger is given as:

$$\log_{10} C_{he}^0 = K_{1,he} + K_{2,he} \cdot \log_{10} A + K_{3,he} \cdot (\log_{10} A)^2 \quad (18)$$

where $K_{i,he}$ are the constants corresponding to the type of the heat exchanger; A is the heat transfer area of the heat exchanger. The calculation of the heat exchanger areas is presented in Appendix A.

Heat exchangers used in this study are made of carbon steel (CS) and work under different pressure. Multiplying factors are needed to correct the results, the equation is given as:

$$C_{\mathrm{he}} = \left(B_{1,\mathrm{he}} + B_{2,\mathrm{he}} \cdot F_{\mathrm{M,he}} \cdot F_{\mathrm{P,he}}\right) \cdot C_{\mathrm{he}}^{0} \quad (19)$$

where $B_{\mathrm{i,he}}$ are the constants corresponding to the type of the heat exchanger. $F_{\mathrm{M,he}}$ and $F_{\mathrm{P,he}}$ are the material factor and pressure factor, respectively. The pressure factor is obtained from the following equation:

$$\log_{10} F_{\mathrm{P,he}} = C_{1,\mathrm{he}} + C_{2,\mathrm{he}} \cdot \log_{10} P_{\mathrm{he}} + C_{3,\mathrm{he}} \cdot (\log_{10} P_{\mathrm{he}})^{2} \quad (20)$$

where $C_{\mathrm{i,he}}$ are the constants corresponding to the type of the heat exchanger; P_{he} is the designed working pressure for the heat exchanger.

The values of the constants mentioned above for the main components are listed in Appendix B.

The calculation of the bare module cost depends on past records or published correlations for price information. It is necessary to update the costs because of the inflation. This can be achieved by the following equation:

$$C_2 = C_1 \cdot \left(\frac{I_2}{I_1}\right) \quad (21)$$

where C is the purchased cost and I is the cost index. The subscript 1 refers to base time when cost is known and subscript 2 refers to time when cost is desired. The *CEPCI* (Chemical Engineering Plant Cost Index) is employed to calculate the inflation. The values of $CEPCI_{2016}$ and $CEPCI_{\mathrm{ref},2001}$ are 541.7 and 397, respectively [38].

3.4.Exergoeconomic model

Exergoeconomic is a branch of engineering which combines the thermodynamic analysis and economic principles. Thermodynamic performance and economic cost of the system are all taken into consideration.

To find the relationship between the present value of the expenditure and the equivalent annually levelized costs, the capital recovery factor (CRF) is employed, being expressed as [36]:

$$Z_{\mathrm{i}} = CRF \cdot C_{\mathrm{i}} \tag{22}$$

$$CRF = \frac{i_{\mathrm{eff}} \cdot (1+i_{\mathrm{eff}})^{n}}{(1+i_{\mathrm{eff}})^{n}-1} \tag{23}$$

where i_{eff} is the effective discount rate with a value of 0.05 [39]; and n is the lifetime of the CCP system, being assumed as 30 years [40].

In order to calculate the equivalent annually levelized costs, the annual working time of the system is assumed as 8000 h [41]. Then the annual exergy rates and annual power output or consumption are obtained.

In a steady system, there are a number of entering and outing working fluid streams and heat and work interactions with the surroundings. In exergoeconomic analysis, each flowing stream is associated with a levelized exergy cost. The equations to calculate the cost of the stream product are given as:

$$C_{\mathrm{in}} = c_{\mathrm{in}} \cdot E_{\mathrm{y,in}} \tag{24}$$

$$C_{\mathrm{out}} = c_{\mathrm{out}} \cdot E_{\mathrm{y,out}} \tag{25}$$

$$C_{\mathrm{work}} = c_{\mathrm{work}} \cdot W_{\mathrm{y}} \tag{26}$$

$$C_{heat} = c_{heat} \cdot E_{y,heat} \quad (27)$$

where c denotes levelized exergy cost of the streams; $E_{y,in}$ and $E_{y,out}$ are the exergy transfer rate of the stream flowing in and out of a component; W_y and $E_{y,heat}$ are the power and the heat transfer rate of the components considering the annual working time.

The cost balance equation applied to the kth system component is given as:

$$\sum_{out} C_{out,k} + C_{w,k} = C_{heat,k} + \sum_{in} C_{in,k} + Z_k \quad (28)$$

Details of the cost balance equation are listed in Table 2.

The levelized exergy cost for system product is chosen to indicate the exergoeconomic performance, being expressed as [42,43]:

$$c_{product} = c_{capital} + c_{fuel} \quad (29)$$

where $c_{capital}$ is the capital-cost-related part of the levelized exergy cost for the system product, being expressed as:

$$c_{capital} = \frac{Z_{total}}{W_{net} + E_{cool}} \quad (30)$$

where c_{fuel} is the fuel-cost-related part of the levelized exergy cost for the system product, being expressed as:

$$c_{fuel} = \frac{c_{Bt} \cdot W_{y,comp} + c_{Ot} \cdot W_{y,pump1} + c_{Ot} \cdot W_{y,pump2} + c_{Ot} \cdot W_{y,pump3} + c_{Ot} \cdot W_{y,pump4}}{W_{net} + E_{cool}} \quad (31)$$

where c_{Bt} and c_{Ot} are the levelized exergy cost for the BC turbine power output and the ORC turbine power output, which are calculated in Table 3. Likewise, they can be expressed as the capital-cost-related part and the fuel-cost-related part, given by Eq. (32) and Eq. (33).

$$c_{Bt} = \frac{Z_{Bt}}{W_{y,Bt}} + \frac{c_3 \cdot \left(E_{y,3} - E_{y,4}\right)}{W_{y,Bt}} \quad (32)$$

$$c_{Ot} = \frac{Z_{Ot}}{W_{y,Ot}} + \frac{c_{10} \cdot \left(E_{y,10} + E_{y,11} - E_{y,12}\right)}{W_{y,Ot}} \quad (33)$$

In addition, the levelized exergy cost for the condensers and the precooler is equal to zero, being given by:

$$c_{26}=c_{28}=c_{30}=0 \quad (34)$$

The levelized exergy cost for the exhaust gas as well as the jacket water is zero, being expressed as:

$$c_{g1}=c_{w1}=0 \quad (35)$$

3.5.Internal combustion engine

In this study, the engine selected [7] is a 12-cylinder 4-stroke supercharged engine. The main designed parameters of the engine are listed in Table 3. The composition of the engine exhaust gas is presented in Table 4. The thermal load of the engine exhaust gas is about 1700 kW and 1000 kW can be obtained from the engine jacket water.

3.6.Simulation conditions for the system

The thermodynamic parameters of the working fluid are calculated under the environment of MATLAB with the help of REFPROP 9.1 [44]. The basic conditions of simulation for the CCP system are listed in Table 5.

Seven key parameters : BC turbine inlet temperature ($T_{Bt,in}$), BC turbine inlet pressure ($P_{Bt,\,in}$), inlet temperature at the high-pressure side of ORC turbine ($T_{Ot,\,in,\,h}$), inlet pressure at the high-pressure side of ORC turbine ($P_{Ot,\,in,\,h}$), inlet temperature at

392 the low-pressure side of ORC turbine ($T_{Ot,\,in,\,l}$), inlet pressure at the low-pressure side
393 of ORC turbine ($P_{Ot,\,in,\,l}$) and the ejector primary inlet pressure ($P_{ej,\,in}$), are chosen to
394 analyze the thermodynamic and exergoeconomic performance of the system. When
395 one parameter is investigated to analyze the system performance, other parameters are
396 maintained constants based on the conditions in Table 5.

397 In the thermodynamic aspect, the net power output of the CO_2 Brayton cycle (W
398 $_{BC}$), net power output of the DORC (W_{ORC}), net power of the whole system (W_{net}),
399 cooling capacity of the system (Q_{cool}) and the exergy efficiency of the system (η_{exergy})
400 are selected to reflect the system performance. Levelized exergy cost for the BC
401 turbine power output (c_{Bt}), levelized exergy cost for the ORC turbine power output
402 (c_{Ot}), levelized exergy cost the system product ($c_{product}$) and the system capital cost
403 ($z_{capital}$) are chosen to represent the exergoeconomic performance.

404 **4. Results and discussion**

405 The influence of the BC turbine inlet temperature ($T_{Bt,in}$) on the output and the
406 exergy efficiency of the system are shown in Fig. 2. The net power output of the CBC
407 increases with the rise of $T_{Bt,in}$. That can be explained by the large decrease of the
408 compressor power consumption. With the increase of the CO_2 temperature at the BC
409 turbine inlet, the mass flow rate of CO_2 decreases, leading to the decrease of the
410 compressor power consumption. Although the drop of CO_2 mass flow rate would cut
411 down the BC turbine power output, the decrease quantity of compressor power
412 consumption is larger than the decrease of the BC turbine power output. Thus, the

large decrease of the compressor power consumption determines the increase trend of the CBC net power output.

It is presented that the net power output of the DORC increases with the rise of the BC turbine inlet temperature. Since the residual heat in exhaust CO_2 acts as the heat source for the high-pressure side of DORC, the temperature rise of the exhaust CO_2, caused by the rise of $T_{Bt,in}$, would offer more heat for the bottom cycle, which causes the increase of the mass flow rate of the organic working fluid in the high-pressure side of DORC . Hence, the power output of the ORC turbine increases, leading to the increase of the net power output of the DORC.

With the increase of $T_{Bt,in}$, the cooling capacity of the ERC decreases, as shown in Fig. 2. The increase of the organic working fluid mass flow rate in DORC would absorb more heat from jacket water, resulting in the decrease of energy available for the ERC. As a result, less secondary flow working fluid from the evaporator is entrained to the ejector, resulting the decrease of the cooling capacity of the CCP system.

The increase of the CBC net power output and the DORC net power output account for the increase of the net power output of the whole CCP system. Though the cooling capacity of the ERC is large, it produces only a small amount of exergy. The decrease of the exergy output caused by the cooling capacity drop can be made up by the increase of the power exergy output. Thus, the exergy efficiency of the system increases.

The influences of the BC turbine inlet temperature on the levelized exergy cost and

435 the system capital cost of the system are shown in Fig. 3. The levelized exergy cost
436 for the BC turbine power output (c_{Bt}) drops with the rise of the BC turbine inlet
437 temperature ($T_{Bt,in}$). That can be explained by the decrease of the capital-cost-related
438 part of c_{Bt}. The capital-cost-related part of c_{Bt} decreases with the decrease of cost of
439 compressor, which is cut down by the drop of the compressor power consumption.
440 The increase of the ORC turbine power output causes the decrease of both the
441 capital-cost related part and the fuel-cost-related part of c_{Ot}, resulting in the decrease
442 of c_{Ot}.

443 The system capital cost ($z_{capital}$) rises with the rise of $T_{Bt,in}$. The large increase of the
444 ORC turbine power output increases the cost of the ORC turbine. Moreover, the
445 increase of the mass flow rate of the organic working fluid in the DORC causes the
446 increase of cost for the vapor generator 2 and the preheater. Though the cost of
447 compressor decreases, it can't change the ascending trend of the total system capital.

448 It can be obtained in Fig. 3 that the levelized exergy cost for the system product
449 ($c_{product}$) decreases with the rise of $T_{Bt,in}$. The decline in levelized exergy cost for the
450 BC turbine and ORC turbine power output, according to Eq. (31), would cause the
451 decrease of the fuel-cost related part of $c_{product}$. Though the increase of $z_{capital}$ would cut
452 down the capital-cost-related part of $c_{product}$, the impact of levelized exergy cost for the
453 BC turbine and ORC turbine is greater, which leads to the descending trend of $c_{product}$.

454 The influence of the BC turbine inlet pressure ($P_{Bt,\,in}$) on the output and the exergy
455 efficiency of the system are shown in Fig. 4. The net power output of the CBC
456 increases with the increase of $P_{Bt,\,in}$, which can be explained by the rise of enthalpy

drop of the CO_2 in the BC turbine. Though the rise of $P_{Bt,\ in}$ requires more compressor power consumption, the increase of the BC turbine power output is larger in quantity than the consumption, which leads to the increase of the CBC net power output.

The net power output of the DORC decreases with the rise of $P_{Bt,\ in}$. On the one hand, the temperature of the exhaust CO_2 at the BC turbine outlet decreases with the increase of $P_{Bt,\ in}$. Thus, less heat is offered to the high-pressure cycle of DORC, resulting in the decrease of the high-pressure cycle power output. On the other hand, the increase of $P_{Bt,\ in}$ causes the increase of the compressor power consumption, which results in the rise of the CO_2 temperature at the compressor outlet. Thus, less heat is released in the gas heater and more heat is provided to the low-pressure cycle of DORC, which leads to the increase of the low-pressure cycle power output. However, the increase of the power output in low-pressure side is smaller than the decrease of the power output in the high-pressure side. Thus, the net power of the DORC decreases slightly.

The cooling capacity of the system increases with the increase of $P_{Bt,\ in}$. Just like the variation of the power output, the decrease of the mass flow rate in the high-pressure side of DORC is larger than the increase of mass flow rate in the low-pressure side. Therefore, the total mass flow rate in the DORC decreases, resulting in the reduction of heat provided for the ejector refrigeration cycle. Thus, the cooling capacity of the ERC decreases.

The net power output of the whole system increases with the increase of the BC turbine inlet pressure. Though the net power output of the DORC decreases, the

increase of CBC net power output is much larger. Thus, the net power output of the CCP system increases with the increase of $P_{Bt,\,in}$. The exergy efficiency of the system likewise has the same rising trend.

The influences of the BC turbine inlet pressure ($P_{Bt,\,in}$) on the levelized exergy cost and the system capital cost of the system are depicted in Fig. 5. The levelized exergy cost for the BC turbine output c_{Bt} increases with the rise of the $P_{Bt,\,in}$, which can be explained by the variations of the capital-cost-related part and the fuel-cost-related part. The increase of $P_{Bt,\,in}$ causes the increase of cost for both the BC turbine and the compressor, which lead to the rise of the two related parts.

The levelized exergy cost for the ORC turbine product (c_{Ot}) increases with the rise of $P_{Bt,in}$. The decrease of the mass flow rate in the DORC causes that less exergy is produced in vapor generator 2, causing the increase of the fuel-related part of c_{Ot}. Therefore, the levelized exergy cost for the ORC turbine (c_{Ot}) increases.

The system capital cost ($z_{capital}$) increases with the rise of ($P_{Bt,\,in}$). The increase of the mass flow rate in the ERC causes the rise of capital cost for the evaporator and vapor generator 3, which combined with the rise of the BC turbine cost and compressor cost accounts for the system capital cost rise.

The levelized exergy cost for the system product decreases with the rise of $P_{Bt,\,in}$ as presented in Fig. 5. According to Eq. (31), the rise of the c_{Ot}, c_{Bt} would cause the rise of the fuel-cost-related part of $c_{product}$. However, because of the large increase of the system net power output, the capital-cost-related part and the fuel-cost-related part decrease actually, which determines the decrease of $c_{product}$.

The influence of inlet temperature at the high-pressure side of ORC turbine ($T_{Ot,\,in,\,h}$) on the output and the exergy efficiency of the system are shown in Fig. 6. The net power output of the CBC remains unchanged since thermal parameters in dual-pressure ORC are irrelevant to the thermodynamic performance of the CBC.

The net power output of the DORC decreases with the increase of $T_{Ot,\,in,\,h}$. Though the increase of the vapor temperature could lead to the rise of the enthalpy drop in the ORC turbine, it would also cause the decrease of the mass flow rate in the high-pressure side, whose impact is greater than that of the enthalpy drop. Therefore, the power output of the DORC decreases.

The cooling capacity of the ejector refrigeration cycle increases with the rise of $T_{Ot,\,in,\,h}$. More heat is provided for the ERC because of the decrease of the mass flow rate in the DORC, leading to the increase of the mass flow rate in vapor generator 3. Thus, more secondary flow from the evaporator is entrained into the ejector, resulting in the increase of the cooling capacity.

The net power output of the CCP system decreases with the rise of $T_{Ot,\,in,\,h}$. The unchanged CBC power output and the drop of the DORC power output determine the decrease of the net power output of the CCP system. The exergy efficiency of the system as well drops with the increase of the increase of $T_{Ot,\,in,\,h}$.

The influences of inlet temperature at the high-pressure side of ORC turbine on the levelized exergy cost and the system capital cost of the system are presented in Fig. 7. The levelized exergy cost for the ORC turbine output (c_{Ot}) increases with the increase of $T_{Ot,\,in,\,h}$. The reason is that the two related parts of c_{Ot} increase with the drop of the

ORC turbine power output.

The levelized exergy cost for the BC turbine power output (c_{Bt}) increases with the rise the $T_{Ot,\,in,\,h}$. Since the decrease of the mass flow rate in the high-pressure side of DORC, the exergy generated in the vapor generator 2 decreases, causing the increase of the levelized exergy cost of the vapor. Thus, the increase levelized exergy cost of the vapor, which is heated by the BC turbine residual heat, causes the increase of the levelized exergy cost for the exhaust CO_2. According to Eq. (32), the fuel-cost-related part of c_{Bt} increases, leading to the increase of c_{Bt}.

The system capital cost ($z_{capital}$) decreases with the increase of $T_{Ot,\,in,\,h}$. The decrease of the DORC power output causes the drop of the ORC turbine cost, which leads to the descending trend of $z_{capital}$.

The levelized exergy cost for the system product ($c_{product}$) increases with the rise of $T_{Ot,\,in,\,h}$, as shown in Fig. 7. The increase of the levelized exergy cost for the BC turbine and ORC turbine power output cause the rise of fuel-cost-related part of $c_{product}$. Meanwhile, the large decrease of the net power of the CCP system causes the increase of the capital-cost-related part. The two increase parts determine the rise of $c_{product}$.

The influences of the inlet pressure at the high-pressure side of ORC turbine ($P_{Ot,\,in,\,h}$) on the output and exergy efficiency of the system are presented in Fig. 8. The net power of the CBC keeps unchanged because of the unchanged thermal parameters in the cycle.

The net power output of the DORC increase with the rise of $P_{Ot,\,in,\,h}$. The increase of the evaporation pressure cuts down the latent heat of the organic working fluid,

545 which causes the increase of the mass flow rate in the high-pressure side of DORC.
546 As a result, the net power output of the ORC turbine increases, leading to the increase
547 of the net power output of the DORC.

548 Considering the increase of the DORC net power output and the unchanged CBC
549 net power output, the net power output of the whole system increases. Also, the
550 exergy efficiency of the system increases.

551 The increase of the mass flow rate in the DORC absorbs more heat from the jacket
552 water in the preheater. Thus, less heat is released in the vapor generator 3, causing the
553 decrease of the mass flow rate of the working fluid in the ERC. As a result, the
554 cooling capacity of the system decreases.

555 The influence of the inlet pressure at the high-pressure side of the ORC turbine ($P_{Ot,}$
556 $_{in,\,h}$) on the levelized exergy cost and system capital cost of the system are presented
557 in Fig. 9. The large increase of the ORC turbine power output accounts for the
558 decrease of the levelized exergy cost for the ORC turbine power output (c_{Ot}). The
559 increase of the mass flow rate in the high-pressure side of DORC means that more
560 exergy in the vapor is generated by the vapor generator 2, which leads to the decrease
561 of its levelized exergy cost. Thus, the levelized exergy cost for the BC turbine exhaust
562 CO_2, which provides heat for the vapor, decreases with the vapor levelized exergy
563 cost. Moreover, the drop of the CO_2 levelized exergy cost causes the decrease of the
564 fuel-cost-related part of c_{Bt}, which further results in the decrease of c_{Bt}.

565 The increase of the ORC turbine power output and the increase of mass flow rate in
566 the DORC cause the increase of cost for the turbine and the vapor generator 2, leading

567 to the rise of the system capital cost.

568 The levelized exergy cost for the system product (c_{product}) decreases with the
569 increase of $P_{\text{Ot, in, h}}$. The decrease of c_{Ot} and c_{Bt} account for the decrease of the
570 fuel-cost-related part of the levelized exergy for the system product. The impact of c_{Ot}
571 and c_{Bt} is greater than that of the system capital cost whose rise would result in the
572 increase of the capital-cost-related part of c_{product}. Thus, the levelized exergy cost of the
573 system product (c_{product}) shows a descending trend.

574 The influences of the inlet temperature at the low-pressure side of ORC turbine ($T_{\text{Ot,}}$
575 $_{\text{in, l}}$) on the output and the exergy efficiency of the system are presented in Fig. 10.
576 Parameters changes in the DORC are irrelevant to the thermodynamic performance of
577 the CBC. Thus, the net power of the CBC remains unchanged.

578 The net power output of the DORC decreases with the increase of $T_{\text{Ot, in, l}}$. The
579 increase of the inlet temperature causes the decrease of the mass flow rate in the
580 low-pressure side of the DORC, leading to the decrease of the DORC net power
581 output.

582 Considering the decrease of the DORC net power output and the unchanged CBC
583 net power output, the net power output of the whole system deceases. Likewise, the
584 exergy efficiency of the system decreases.

585 The cooling capacity of the ejector refrigeration cycle increases with the increase of
586 $T_{\text{Ot, in, l}}$. The decrease of the mass flow rate in the low-pressure side means that more
587 heat is offered to the ERC. Thus, the mass flow rate of the working fluid in the vapor
588 generator 3 increases and more working fluid is entrained to the ejector from the

evaporator, which leads to the increase of the refrigeration cycle.

The influence of inlet temperature at the low-pressure side of the ORC turbine ($T_{Ot,\ in,\ l}$) on the levelized exergy cost and system capital cost of the system are presented in Fig. 11. The levelized cost for the BC turbine power output increase with the increase of $T_{Ot,\ in,\ l}$. The decrease of the mass flow rate in the vapor generator 1 leads to the drop of the vapor exergy output, which results in the increase of the levelized exergy cost for the vapor. The levelized exergy cost for vapor in vapor generator 2, which is the equal to that of the vapor in vapor generator 1, increases as a result, causing the increase of the levelized exergy cost of the exhaust CO_2 after the BC turbine. Thus, the fuel-cost-related part of c_{Bt} increases, resulting in the rise of c_{Bt}.

The levelized exergy cost for the ORC turbine (c_{Ot}) increases with the increase of $T_{Ot,\ in,\ l}$. That can be explained by the increase of the levelized exergy cost of the ORC low-pressure inlet vapor and the decrease of the power output of the ORC turbine power output. Both the fuel-cost-related part and the capital-cost-related part of c_{Ot} increases.

The decrease of the mass flow rate and the ORC turbine power output cause the decrease of the vapor generator 1 cost and the turbine cost. Thus, the capital cost of the system decreases.

The levelized exergy cost for the system product increases with the increase of $T_{Ot,\ in,\ l}$. The increase of c_{Bt} and c_{Ot} cause the increase of the fuel-cost-related part of the levelized exergy cost for the system product. Though, the decease of the system capital cost causes the decrease of the capital-cost-related part, its effect is less

611 important. Thus, the increase of the fuel-cost-related part determines the increase of
612 the levelized exergy cost for the system product.

613 The influences of the inlet temperature of the low-pressure side of the ORC turbine
614 ($P_{\mathrm{Ot,\ in,\ l}}$) on the output of the exergy efficiency of the system are shown in Fig. 12.
615 The net power of the CBC keeps unchanged with the increase of the increase of the
616 low evaporation pressure. The reason is that the thermodynamic of the CBC is
617 irrelevant to the thermal parameters in DORC.

618 The net power output of the DORC increases with the rise of $P_{\mathrm{Ot,\ in,\ l}}$. The increase
619 of enthalpy drop of the organic working fluid in the low-pressure side, which is
620 caused by the rise of $P_{\mathrm{Ot,\ in,\ l}}$, results in the increase of the power output of the
621 low-pressure side. Though mass flow rate in the low-pressure side would decrease, its
622 impact is less important than that of the enthalpy drop. Thus, the net power output of
623 DORC increases.

624 The unchanged CBC power output and the increase of the DORC power accounts
625 for the increase of the system net power output and exergy efficiency of the system.

626 The cooling capacity increases slightly with the increase of $P_{\mathrm{Ot,\ in,\ l}}$. Because of the
627 decrease of the mass flow rate in DORC, less heat is released in the preheater and
628 more heat is provided in vapor generator 3. Thus, the mass flow rate of the working
629 fluid in the ERC increases, resulting in the slight increase of the cooling capacity.

630 The influences of inlet pressure at the low-pressure side of the ORC turbine ($P_{\mathrm{Ot,\ in,\ l}}$)
631 on the levelized exergy cost and system capital cost of the system are shown in Fig.
632 13. The levelized exergy cost for the ORC turbine power output decreases with the

633 increase of $P_{Ot,\,in,\,l}$. That can be explained by the decrease of the vapor generator 1
634 cost, caused by the decrease of the mass flow rate in DORC, and the increase of the
635 DORC power output. Both the capital-cost-related part and the fuel-cost-related part
636 of c_{Ot} decrease.

637 The levelized exergy cost for the BC turbine power output decreases with of $P_{Ot,\,in,\,l}$.
638 The decrease of the c_{Ot} causes the drop of levelized exergy cost for the vapor in vapor
639 generator 2, which is heated by the residual heat in the BC turbine exhaust CO_2. Thus,
640 the levelized exergy cost of the exhaust CO_2 decreases, which further leads to the drop
641 of the fuel-cost-related part of c_{Bt}. Therefore, the levelized exergy cost for the BC
642 turbine power output (c_{Bt}) decreases, as shown in Fig. 13.

643 The increase of the ORC turbine power output causes the increase of the ORC
644 turbine cost. Meanwhile, the increase of the cooling capacity causes the increase of
645 the heat transfer area in the evaporator which requires the rise of the evaporator cost.
646 Thus, the capacity cost of the system increases.

647 The levelized exergy cost for the system product decreases with the increase of $P_{Ot,}$
648 $_{in,\,l}$. The decrease of the levelized exergy cost for the BC turbine power output and
649 ORC turbine power cause the decrease of the fuel-cost-related part of the system
650 levelized exergy cost, which determined the decrease of the levelized exergy cost for
651 the system product.

652 The influence of ejector primary inlet pressure ($P_{ej,\,in}$) on the output and the exergy
653 efficiency of the system are shown in Fig. 14. Thermal parameter changes in the ERC
654 can't affect the thermodynamic performance of the CBC and DORC. Thus, the net

power output of the two cycles remain unchanged. With the increase of the ejector primary inlet pressure, the power consumption of pump 4 increases, leading to the slight decrease of the power output of the whole system.

The increase of the ejector primary inlet pressure causes the increase of the entrainment ratio of the ejector. Thus, more secondary flow is entrained to the ejector from the evaporation, leading to the increase of the cooling capacity.

With the increase of the ejector primary inlet pressure, the power consumption of pump 4 increases gradually. At first, the exergy loss in pump 4 is smaller than the exergy produced by the cooling capacity. Then, with the increase of the pump power consumption, the exergy loss in pump 4 becomes larger than the cooling exergy increase. Thus, the exergy efficiency for the system increases at first and then decreases with the increase of the ejector primary inlet pressure.

The influence of the ejector primary inlet pressure on the levelized exergy cost and the system capital cost of the system are presented in Fig. 15. The increase of the ejector primary inlet pressure can’t affect the power output of the BC turbine and the ORC turbine. Thus, the levelized exergy cost for the BC turbine and the ORC power output remain unchanged.

The increase of the pump power consumption results in the increase of the pump 4 cost. The increase of the mass flow rate in the evaporator causes the increase of the evaporator cost. Thus, the system capital cost increases, which leads to the increase of the capital-cost-related part of c_{product}. As a result, the levelized exergy cost for the system increases.

The parametric analysis reveals the potential of optimization for the CCP system. With the increase of the BC turbine inlet temperature, the net power output of the system increases while the cooling capacity decreases. With the increase of the inlet temperature at the high-pressure side of ORC turbine, the net power output of the system decreases while the cooling capacity increases. In this study, seven key parameters (BC turbine inlet temperature, BC turbine inlet pressure, inlet temperature at the high-pressure side of ORC turbine, inlet pressure at the high-pressure side of ORC turbine, inlet temperature at the low-pressure side of ORC turbine, inlet pressure at the low-pressure side of ORC turbine and the ejector primary inlet pressure) are chosen as the variables to optimize the system. The ranges of these parameters are listed in Table 6.

Considering that the levelized exergy cost reflects the thermodynamic and the exergoeconomic aspect of the system, the levelized exergy cost for the system product is selected as the objective function and genetic algorithm is selected to conduct the single-objective optimization.

Genetic algorithm (GA) is an optimization method based on the natural biological evaluation. [45] It simulates the natural genetic rules and searches the optimization result in all the generation. The control parameters of the GA are listed in Table 7.

The optimization results of GA are listed in Table 8. It can be obtained that the minimum levelized exergy cost for the system product $c_{product}$ is 53.25 \$(MWh)$^{-1}$. The net power output, exergy efficiency of the CCP system are 374.37 kW, 37.31% respectively. The inlet pressure at the high-pressure side of ORC turbine is 1.85 MPa.

Meanwhile, it can be evidenced from Fig. 8 and 9 that the highest output power (about 374.37 kW), exergy efficiency (about 37.31%) and the lowest levelized exergy cost (about 53.25 $(MWh)^{-1}$) at the highest inlet pressure at the high-pressure side ORC turbine (about 1.85 MPa). The results shown in Fig. 8 and 9 are close to the optimization results. The inlet pressure at the high-pressure side ORC turbine is varied while other six parameters are kept as constants in Fig. 8 and 9. Thus, inlet pressure at the high-pressure side ORC turbine plays a more important role than other six parameters when determining the performance of the system. When the inlet pressure at the high-pressure side ORC turbine is close to the highest permitted pressure, the system performance is close to the optimization performance.

Fig. 16 shows the exergy destruction of different components of the system under the optimization conditions. The largest exergy destruction takes place in the ORC turbine (41.26%), which is mainly caused by the mixing of the high-pressure vapor and the low-pressure vapor. Gas heater contributes 13.44% of the total exergy destruction. Three vapor generators take up 4.13%, 11.67% and 3.73% of the exergy destruction, respectively. The exergy destruction for the ejector is 5.61%, which is also caused by the working fluid mixing. For BC turbine, condenser 1, precooler and preheater, the exergy destruction are 3.31%, 4.64%, 3.69% and 3.65%, respectively. Other components contribute to the rest 4.87% of the exergy destruction.

5. Conclusion

In this paper, a combined cooling and power system is developed. Seven

parameters are selected to analyze the thermodynamic and exergoeconomic performance of the system. Single-objective optimization is carried out with the help of GA. The conclusions of the study are presented as follows:

(1) In the CBC, the increase of $T_{Bt,in}$ and $P_{Bt,\ in}$ contribute to the increase of the system exergy efficiency and the decrease of the levelized exergy cost for the system product.

(2) In the DORC, the increase of $T_{Ot,\ in}$ and $T_{Ot,\ in,\ l}$ would cause the decrease of the system exergy efficiency and the increase of the levelized exergy cost for the system product. Meanwhile, the increase of $P_{Ot,\ in,\ h}$ and $P_{Ot,\ in,\ l}$ would result in the increase of the exergy efficiency and the decrease of the levelized exergy cost.

(3) In the ERC, the increase of $P_{ej,\ in}$ would cause the increase of the refrigeration capacity and the decrease of the system net power output.

(4) Single -objective optimization results show that the minimum levelized exergy cost for the system product is obtain as 53.25 $\$(MWh)^{-1}$ with net power output of 374.37 kW, cooling capacity of 188.63 kW and system exergy efficiency of 37.31%.

Acknowledgement

The authors gratefully acknowledge the financial support by the National Natural Science Foundation of China (Grant No. 51476121)

Appendix A

This section shows the calculation of the heat transfer area in the heat exchangers

741 used in this study.

742 All the heat exchangers used in this study are shell-and-tube heat exchanger. The
743 thermodynamic properties of the working fluid vary with the heat transfer process.
744 Thus, to calculate the heat transfer area actually, the heat transfer processes are
745 discretized into a lot of small sections. In each section, the heat transfer area is small
746 and the thermodynamic properties are assumed to be constant.

747 For each section the heat transfer area is calculated as:

748 $$A_i = Q_i \Big/ \left(\Delta T_i \cdot U_i\right) \tag{B1}$$

749 where ΔT_i is the log-mean temperature difference (LMTD) and U_i is the overall heat
750 transfer coefficient.

751 $$\frac{1}{U_i} = \frac{1}{\alpha_{t,i}} + \frac{\delta}{\lambda} + \frac{1}{\alpha_{s,i}} \tag{B2}$$

752 In Eq. (B2) δ and λ represent the thickness of the tube and the thermal conductivity
753 of the tube wall, respectively. $\alpha_{t,i}$ is the convection heat transfer coefficient in the tube
754 side and $\alpha_{s,i}$ is the convection heat transfer coefficient in the shell side.

755 For different heat transfer process, the convection heat transfer coefficient has
756 different format. We classify the heat transfer processes into single-phase heat transfer
757 process and two-phase heat transfer process. In gas heater, precooler and the preheater,
758 single-phase heat transfer process happens. In evaporator, two-phase heat transfer
759 process occurs. In vapor generators and the condensers, both the single-phase and the
760 two-phase heat transfer process happen.

761 In the single-phase heat transfer process, the convection heat transfer coefficient in

the tube side and the shell side are expressed as [46]:

$$\alpha_{t,i} = \frac{\lambda \cdot Nu}{D_i} \tag{B3}$$

$$\alpha_{s,i} = 0.36\left(\frac{\lambda}{D_{es}}\right)\cdot\left(\frac{D_{es}\cdot G_s}{\mu}\right)^{0.55}\cdot \mathrm{Pr}^{\frac{1}{3}}\cdot\left(\frac{\mu}{\mu_w}\right)^{0.14} \tag{B4}$$

In Eq. (B3), the Nusselt number is calculated as [47,48]:

$$Nu = \left[\frac{(f/8)\cdot \mathrm{Re}\cdot \mathrm{Pr}}{12.7(f/8)^{0.5}\cdot\left(\mathrm{Pr}^{2/3}-1\right)+1.07}\right],\ for\ \mathrm{Re}<10^4 \tag{B5}$$

$$Nu = \left[\frac{(f/8)\cdot(\mathrm{Re}-1000)\cdot \mathrm{Pr}}{12.7(f/8)^{0.5}\cdot\left(\mathrm{Pr}^{2/3}-1\right)+1.07}\right],\ for\ 10^4<\mathrm{Re}<5\times10^6 \tag{B6}$$

where f is the Darcy friction factor, Re is the Reynolds and Pr is the Prandtl number.

In Eq. (B4), D_{es} is the equivalent diameter of the shell, being expressed as:

$$D_{es} = \frac{1.10\mathrm{Pt}^2}{D_{out,i}} - D_{out,i} \tag{B7}$$

where Pt is the center distance between the tubes.

Evaporation and condensation are two different two-phase heat transfer processes. In this study, the cold organic working fluid flows in the tubes of the heat exchangers. The convection heat transfer coefficient of evaporation and condensation are expressed as [49,50]:

$$\alpha_{ev,i} = 0.023\left[\frac{G(1-x)}{\mu_l}\right]^{0.8}\cdot \mathrm{Pr}_l^{0.4}\cdot\frac{\lambda_l}{d}\cdot\left[1+3000Bo^{0.86}+1.12\left(\frac{x}{1-x}\right)^{0.75}\cdot\left(\frac{\rho_l}{\rho_v}\right)^{0.41}\right] \tag{B8}$$

$$\alpha_{cond,i} = 0.023\left[\frac{G(1-x)}{\mu_l}\right]^{0.8}\cdot \mathrm{Pr}_l^{0.4}\cdot\frac{\lambda_l}{d}\cdot\left[(1-x)^{0.8}+\frac{3.8x^{0.76}(1-x)0.04}{P_r^{0.38}}\right] \tag{B9}$$

In Eq. (B9), P_r is the reduced pressure. In Eq. (B8) Bo is the boiling number, being expressed as:

$$Bo = \frac{q_m}{G \cdot r_f} \quad \text{(B10)}$$

Appendix B

The constants for component capital cost calculation are list in Table B1.

Reference

[1] Abdul-Wahhab H, Al-Kayiem H, Aziz A, Nasif M. Survey of invest fuel magnetization in developing internal combustion engine characteristics. Renew Sustain Energy Rev 2017; 79:1392-99.

[2] Heywood J. B. Internal combustion engine fundamentals. New York: McGraw-Hill; 1988.

[3] Chao H, Chao L, Hong G, Hui X, You L, Shuang W. The optimal evaporation temperature and working fluids for subcritical Organic Rankine Cycle. Energy 2012; 38: 136-143.

[4] Tian H, Shu G, Wei H, Liang X, Liu L. Fluids and parameters optimization for the organic Rankine cycles (ORCs) used in exhaust heat recovery of Internal Combustion Engine (ICE). Energy 2012; 47: 125-136.

[5] Rijpkema J, Munch K, Andersson S. Thermodynamic potential of twelve working fluids in Rankine and flash cycles for waste heat recovery in heavy duty diesel engines. Energy 2018; 160:996-1007.

[6] Su X, Shedd T A. Towards working fluid properties and selection of Rankine cycle based waste heat recovery (WHR) systems for internal combustion engines – A

800 fundamental analysis. Appl Therm Eng 2018; 142:502-10.
801 [7] Vaja I, Gambarotta A. Internal Combustion Engine (ICE) bottoming with Organic
802 Rankine Cycles (ORCs). Energy 2010; 35(2):1084-93.
803 [8] Kim M, Shin G, Kim G, Cho B. Single-loop organic Rankine cycle for engine
804 waste heat recovery using both low-and high-temperature heat sources. Energy 2016;
805 96:482-94.
806 [9] Ringer J, Seifert M, Guyotot V, Hübner W. Rankine cycle for waste heat recovery
807 of IC engines. SAE. 2009. 2009-01-0174.
808 [10] Wang X, Shu G, Tian H, Liu P, Jing D, Li X. Dynamic analysis of the dual-loop
809 Organic Rankine Cycle for waste heat recovery of a natural gas engine. Energy
810 Convers Manage 2017; 148:724-736.
811 [11] Wang E, Yu Z, Zhang H, Yang F. A regenerative supercritical dual-loop organic
812 Rankine cycle system for energy recovery from the waste heat of internal combustion
813 engines. Appl Energy 2017; 190:574-90.
814 [12] Huang H, Zhu J, Deng W, Ouyang T, Yan B, Yang X. Influence of exhaust heat
815 distribution on the performance of dual-loop organic Rankine Cycle (DORC) for
816 waste heat recovery. Energy 2018; 151:54-65.
817 [13] Rajabloo T, Bonalumi D, Lora P. Effect of a partial thermal decomposition of the
818 working fluid on the performances of ORC power plants. Energy 2017; 133:1013-26.
819 [14] Shi L, Shu G, Tian H, Deng S. A review of modified Organic Rankine cycles
820 (ORCs) for internal combustion engine waste heat recovery (ICE-WHR). Renew
821 Sustain Energy Rev 2018; 92:95-110.

822 [15] EI-Harbawi M, Shaaran S, Ahmad F, Wahi M, Abdul A, Larid D, Yin C.
823 Estimating the flammability of vapours above refinery wasterwater laden with
824 hydrocarbon mixtures. Fire Safety J 2012; 51:61-67.
825 [16] Wang X, Tian H, Shu G. Part-load performance prediction and operation strategy
826 design of organic Rankine cycles with a medium cycle used for recovering waste heat
827 from gaseous fuel engines. Energies 2016; 9: 527.
828 [17] Miller E, Hendricks T, Wang H, Peterson R. Integrated dual-cycle energy
829 recovery using thermoelectric conversion and an organic Rankine bottoming cycle.
830 Proceedings of the Institution of Mechanical Engineers, Part A: J Power Energy 2011;
831 225:33-43.
832 [18] Shu G, Wang X, Tian H. Theoretical analysis and comparison of Rankine cycle
833 and different organic Rankine cycles as waste heat recovery system for a large
834 gaseous fuel internal combustion engine. Appl Therm Eng 2016; 108:525-37.
835 [19] Yu G, Shu G, Tian H, Huo Y, Zhu W. Experimental investigations on a cascaded
836 steam-/organic-Rankine-cycle (RC/ORC) system for waste heat recovery (WHR)
837 from diesel engine. Energy Convers Manage 2016; 129:43-51.
838 [20] Zhang C, Shu G, Tian H, Wei H, Liang X. Comparative study of alternative
839 ORC-based combined power systems to exploit high temperature waste heat. Energy
840 Convers Manage 2015; 89:541-54.
841 [21] Galindo J, Guardiola C, Dolz V, Kleut P. Further analysis of a
842 compression-expansion machine for a Brayton Waste Heat Recovery cycle on an IC
843 engine. Applied Thermal Engineering 2018; 128: 345-356.

844 [22] Ma J, Liu L, Zhu T, Zhang T. Cascade utilization of exhaust gas and jacket water
845 waste heat from an Internal Combustion Engine by a single loop Organic Rankine
846 Cycle system. Appl Therm Eng 2016; 107:218-26.
847 [23] Zhang H G, Wang E H, Fan B Y. A performance analysis of a novel system of a
848 dual loop bottoming organic Rankine cycle (ORC) with a light-duty diesel engine.
849 Applied Energy 2013;102: 1504-1513.
850 [24] Yang F, Cho H, Zhang H, Zhang J. Thermoeconomic multi-objective
851 optimization of a dual loop organic Rankine cycle (ORC) for CNG engine waste heat
852 recovery. Applied Energy 2017; 205: 1100-1118.
853 [25] Song J, Gu C. Parametric analysis of a dual loop Organic Rankine cycle (ORC)
854 system for engine waste heat recovery. 2015; 105:995-1005.
855 [26] Yu G, Shu G, Tian H, Wei H, Liu L. Simulation and thermodynamic analysis of a
856 bottoming Organic Rankine Cycle (ORC) of diesel engine (DE). Energy 2013;
857 51:281-90.
858 [27] Li Fan, Sun Bo, Zhang C, Zhang L. Operation optimization for combined cooling,
859 heating, and power system with condensation heat recovery. Appl Energy 2018;
860 230:305-16.
861 [28] Yari Mortaza, Ariyanfar Leyli, Aghdam EA. Analysis and performance
862 assessment of a novel ORC based multigeneration system for power, distilled water
863 and heat. Renew Energy 2018; 119:262-81.
864 [29] Bai Z, Liu T, Liu Q, Lei J, Gong L, Jin H. Performance investigation of a new
865 cooling, heating and power system with methanol decomposition based chemical

recuperation process. Appl Energy 2018; 229: 1152-63.

[30] Chen Y, Han W, Jin H. Investigation of an ammonia-water combined power and cooling system driven by the jacket water and exhaust gas heat of an internal combustion engine. International Journal of Refrigeration 2017; 82: 174-188.

[31] Salek F, Moghaddam A, Naserian M. Thermodynamic analysis of diesel engine coupled with ORC and absorption refrigeration cycle. Energy Conversion and Management 2017; 140: 240-246.

[32] Wang J, Dai Y, Sun Z. A theoretical study on a novel combined power and ejector refrigeration cycle. Int J Refrig 2009; 32(6):1186-94.

[33] Dai Y, Wang J, Gao L. Parametric optimization and comparative study of organic Rankine cycle (ORC) for low grade waste heat recovery. Energy Convers Manage 2009; 50:576-82.

[34] Shu G, Zhao M, Tian H, Huo Y, Zhu W. Experimental comparison of R123 and R245fa as working fluids for waste heat recovery from heavy-duty diesel engine. Energy 2016; 115:756-69.

[35] Zhang J, Zhang H, Yang K, Yang F, Wang Z, Zhao G, Liu H, Wang E, Yao B. Performance analysis of regenerative organic Rankine cycle (RORC) using the pure working fluid and the zeotropic mixture over the whole operating range of a diesel engine. Energy Convers Manage 2014; 84:282-94.

[36] Bejan A, Tsatsaronis G, Moran M. Thermal design and optimization. New York: John Wiley & Sons; 1996.

[37] Turton R, Bailie RC, Whiting WB, Shaeiwitz JA. Analysis, synthesis, and design

888 of chemical processes. 3rd ed. Upper Saddle River, N.J: Prentice Hall; 2009.
889 [38] Li J, Ge Z, Liu Q, Duan Y, Yang Z. Thermo-economic performance analyses and
890 comparison of two turbine layouts for organic Rankine cycles with dual-pressure
891 evaporation. Energy Conversion and Management, 2018; 164: 603-614.
892 [39] Sheng Z, Huai W, Tao G. Performance comparison and parametric optimization
893 of subcritical organic Rankine cycle (ORC) and transcritical power cycle system for
894 low-temperature geothermal power generation. Appl Energy 2011;88(8):2740-54.
895 [40] Tempesti D, Fiaschi D. Thermo-economic assessment of a micro CHP system
896 fueled by geothermal and solar energy. Energy 2013; 58: 45-51.
897 [41] Velez F, Segovia JJ, Martin MC, Antonlin G, Chejne F, Quijano A. A technical,
898 economical and market review of organic Rankine cycles for the conversion of
899 low-grade heat for power generation. Renew Sustain Energy Rev 2012; 16:4175-89.
900 [42] Akbari D, Mahmoudi M. Thermoeconomic analysis & optimization of the
901 combined supercritical CO2 (carbon dioxide) recompression Brayton/ organic
902 Rankine cycle. Energy 2014; 78:501-12.
903 [43] Zare V, Mahmoudi M, Yari M. An exergoeconomic investigation of waste heat
904 recovery from the Gas Turbine-Modular Helium Reactor (GT-MHR) employing an
905 ammonia–water power/cooling cycle. Energy 2013;61. 397-409.
906 [44] Lemmon EW, Huber ML, McLinden MO. NIST standard reference database 23,
907 reference fluid thermodynamic and transport properties (REFPROP). Version 9.1.
908 National Institute of Standards and Technology; 2010
909 [45] Wang J, Dai Y, Gao L. Parametric analysis and optimization for a combined

power and refrigeration cycle. Appl Energy 2008;85(11):1071-85.

[46] Kern DQ. Process heat transfer. New York: McGraw-Hill; 1950

[47] Kandylas IP, Stamatelos AM. Engine exhaust system design based on heat transfer computation. Energy Convers Manage 1999; 40:1057-72.

[48] Incropera FP, DeWitt DP. Fundamentals of heat and mass transfer. New York: Wiley; 2002

[49] Gungor KE, Winterton RHS. Simplified general correlation for saturated flow boiling and comparisons of correlations with data. Chem Eng Res and Des, 1987; 65:148-56.

[50] Shah MM. A general correlation for heat transfer during film condensation inside pipes. Int J Heat Mass Transf 1979; 22:547-56.

Figure captions

Fig. 1. Schematic diagram of the CCP system

Fig. 2. Influences of BC turbine inlet temperature on the output and the exergy efficiency of the system.

Fig. 3. Influences of BC turbine inlet temperature on the levelized exergy cost and the system capital cost of the system.

Fig. 4. Influences of BC turbine inlet pressure on the output and the exergy efficiency of the system.

Fig. 5. Influences of BC turbine inlet pressure on the levelized exergy cost and the system capital cost of the system.

Fig. 6. Influences of inlet temperature at the high-pressure side of ORC turbine on the output and the exergy efficiency of the system.

Fig. 7. Influences of inlet temperature at the high-pressure side of ORC turbine on the levelized exergy cost and the system capital cost of the system.

Fig. 8. Influences of inlet pressure at the high-pressure side of ORC turbine on the output and the exergy efficiency of the system.

Fig. 9. Influences of inlet pressure at the high-pressure side of ORC turbine on the levelized exergy cost and the system capital cost of the system.

Fig. 10. Influences of inlet temperature at the low-pressure side of ORC turbine on the output and the exergy efficiency of the system.

Fig. 11. Influences of inlet temperature at the low-pressure side of ORC turbine on the levelized exergy cost and system capital cost of the system.

Fig. 12. Influences of inlet pressure at the low-pressure side of ORC turbine on the output and the exergy efficiency of the system.

Fig. 13. Influences of inlet pressure at the low-pressure side of ORC turbine on the levelized exergy cost and system capital cost of the system.

Fig. 14. Influences of ejector primary inlet pressure on the output and the exergy efficiency of the system.

Fig. 15. Influences of ejector primary inlet pressure on the levelized exergy cost and the system capital cost of the system.

Fig. 16. Exergy destruction of different components

954 **Table 1** Energy and exergy models for each component in CCP system

Component	Energy equation	E_F	E_P	E_D	E_L
Gas heater	$M_{g1}\cdot(h_{g1}-h_{g2})=M_2\cdot(h_3-h_2)$	$E_{g1}-E_{g2}$	E_3-E_2	$E_{g1}+E_2-E_3-E_{g2}$	/
BC turbine	$W_{Bt}=M_3\cdot(h_3-h_4)=M_3\cdot(h_3-h_{4s})\cdot\eta_{Bt}$	E_3-E_4	W_{Bt}	$E_3-E_4-W_{Bt}$	/
Vapor generator 2	$M_4\cdot(h_4-h_5)=M_9\cdot(h_{10}-h_9)$	E_4-E_5	$E_{10}-E_9$	$E_4+E_9-E_5-E_{10}$	/
Precooler	$M_1\cdot(h_5-h_1)=M_{26}\cdot(h_{27}-h_{26})$	/	/	$E_5+E_{26}-E_1-E_{27}$	$E_{27}-E_{26}$
Compressor	$W_{comp}=M_1\cdot(h_2-h_1)=M_1\cdot(h_{2s}-h_1)/\eta_{comp}$	W_{comp}	E_2-E_1	$E_1-E_2+W_{comp}$	/
Vapor generator 1	$M_{g2}\cdot(h_{g2}-h_{g3})=M_8\cdot(h_{11}-h_8)$	$E_{g2}-E_{g1}$	$E_{11}-E_8$	$E_{g2}+E_8-E_{11}-E_{g3}$	/
ORC turbine	$W_{Ot}=M_{10}\cdot(h_{10}-h_{12})+M_{11}\cdot(h_{11}-h_{12})$	$E_{10}+E_{11}-E_{12}$	W_{Ot}	$E_{10}+E_{11}-E_{12}-W_{Ot}$	/
Condenser 1	$M_{12}\cdot(h_{12}-h_{13})=M_{28}\cdot(h_{29}-h_{28})$	/	/	$E_{12}+E_{28}-E_{13}-E_{29}$	$E_{29}-E_{28}$
Pump 1	$W_{p1}=M_{13}\cdot(h_{14}-h_{13})=M_{13}\cdot(h_{14s}-h_{13})/\eta_{p1}$	W_{p1}	$E_{14}-E_{13}$	$E_{13}-E_{14}+W_{p1}$	/
Preheater	$M_{15}\cdot(h_{15}-h_{14})=M_{w1}\cdot(h_{w1}-h_{w2})$	$E_{w1}-E_{w2}$	$E_{15}-E_{14}$	$E_{w1}+E_{14}-E_{15}-E_{w2}$	/
Pump 2	$W_{p2}=M_7\cdot(h_9-h_7)=M_7\cdot(h_{9s}-h_7)/\eta_{p2}$	W_{p2}	E_9-E_7	$E_7-E_9+W_{p2}$	/
Pump 3	$W_{p3}=M_6\cdot(h_8-h_6)=M_6\cdot(h_{8s}-h_6)/\eta_{p3}$	W_{p3}	E_8-E_6	$E_6-E_8+W_{p3}$	/
Vapor generator 3	$M_{23}\cdot(h_{23}-h_{22})=M_{w2}\cdot(h_{w2}-h_{w3})$	$E_{w2}-E_{w3}$	$E_{23}-E_{22}$	$E_{w2}+E_{22}-E_{23}-E_{w3}$	/
Condenser 2	$M_{16}\cdot(h_{16}-h_{17})=M_{30}\cdot(h_{31}-h_{30})$	/	/	$E_{16}+E_{30}-E_{17}-E_{31}$	$E_{31}-E_{30}$
Valve	$h_{19}=h_{20}$	/	/	$E_{19}-E_{20}$	/
Pump 4	$W_{p4}=M_{22}\cdot(h_{22}-h_{18})=M_{22}\cdot(h_{22s}-h_{18})/\eta_{p4}$	W_{p4}	$E_{22}-E_{18}$	$E_{18}-E_{22}+W_{p4}$	/
Ejector	$M_{16}\cdot h_{16}=M_{23}\cdot h_{23}+M_{21}\cdot h_{21}$	$E_{23}+E_{21}$	E_{16}	$E_{23}+E_{21}-E_{16}$	/
Evaporator	$M_{20}\cdot(h_{21}-h_{20})=M_{24}\cdot(h_{24}-h_{25})$	$E_{20}-E_{21}$	$E_{25}-E_{24}$	$E_{20}+E_{24}-E_{21}-E_{25}$	/

955 **Table 2** Cost balance and auxiliary relation [30] for each component of CCP system

Component	Cost balance	Auxiliary relation

Gas heater	$c_{g2} \cdot E_{y,g2} + c_3 \cdot E_{y,3} = c_{g1} \cdot E_{y,g1} + c_2 \cdot E_{y,2} + Z_{gh}$	c_{g1}=c_{g2}=0
Vapor generator 2	$c_5 \cdot E_{y,5} + c_{10} \cdot E_{y,10} = c_4 \cdot E_{y,4} + c_9 \cdot E_{y,9} + Z_{vg,2}$	c_4=c_5
BC turbine	$c_4 \cdot E_{y,4} + c_{Bt} \cdot W_{y,Bt} = c_3 \cdot E_{y,3} + Z_{Bt}$	c_4=c_3
Precooler	$c_1 \cdot E_{y,1} + c_{26} \cdot E_{y,26} = c_5 \cdot E_{y,5} + c_{27} \cdot E_{y,27} + Z_{prec}$	c_1=c_5
Compressor	$c_2 \cdot E_{y,2} = c_1 \cdot E_{y,1} + c_{elec,1} \cdot W_{y,comp} + Z_{comp}$	$c_{elec,1}$=c_{Bt}
Vapor generator 1	$c_{g3} \cdot E_{y,g3} + c_{11} \cdot E_{y,11} = c_{g2} \cdot E_{y,g2} + c_8 \cdot E_{y,8} + Z_{vg,1}$	c_{g2}=c_{g3}
ORC turbine	$c_{12} \cdot E_{y,12} + c_{Ot} \cdot W_{y,Ot} = c_{11} \cdot E_{y,11} + c_{10} \cdot E_{y,10} + Z_{Ot}$	c_{10}=c_{11}=c_{12}
Pump 1	$c_{14} \cdot E_{y,14} = c_{13} \cdot E_{y,13} + c_{elec,3} \cdot W_{y,pump1} + Z_{pump1}$	$c_{elec,3}$=c_{Ot}
Condenser 1	$c_{13} \cdot E_{y,13} + c_{29} \cdot E_{y,29} = c_{28} \cdot E_{y,28} + c_{12} \cdot E_{y,12} + Z_{cond1}$	c_{13}=c_{12}
Preheater	$c_{w2} \cdot E_{y,w2} + c_{15} \cdot E_{y,15} = c_{w1} \cdot E_{y,w1} + c_{14} \cdot E_{y,14} + Z_{preh}$	c_{w1}=c_{w2}=0
Pump 2	$c_9 \cdot E_{y,9} = c_7 \cdot E_{y,7} + c_{elec,2} \cdot W_{y,pump2} + Z_{pump2}$	$c_{elec,2}$=c_{Ot}
Pump 3	$c_8 \cdot E_{y,8} = c_6 \cdot E_{y,6} + c_{elec,3} \cdot W_{y,pump3} + Z_{pump3}$	$c_{elec,3}$=c_{Ot}
Vapor generator 3	$c_{w3} \cdot E_{y,w3} + c_{23} \cdot E_{y,23} = c_{w2} \cdot E_{y,w2} + c_{22} \cdot E_{y,22} + Z_{vg,3}$	c_{w3}=c_{w2}
Valve	/	c_{19}=c_{20}
Pump 4	$c_{22} \cdot E_{y,22} = c_{18} \cdot E_{y,18} + c_{elec,3} \cdot W_{y,pump4} + Z_{pump4}$	$c_{elec,4}$=c_{Ot}
Condenser 2	$c_{17} \cdot E_{y,17} + c_{31} \cdot E_{y,31} = c_{30} \cdot E_{y,30} + c_{16} \cdot E_{y,16} + Z_{cond2}$	c_{16}=c_{17}
Ejector	$c_{16} \cdot E_{y,16} = c_{23} \cdot E_{y,23} + c_{21} \cdot E_{y,21}$	/
Evaporator	$c_{21} \cdot E_{y,21} + c_{25} \cdot E_{y,25} = c_{20} \cdot E_{y,20} + c_{24} \cdot E_{y,24} + Z_{ev}$	c_{20}=c_{21}

956 **Table 3** Main parameters of the engine [7]

Parameters	Value
Power output (kW)	2928
Rotation (r(min)$^{-1}$)	1000

Exhaust gas temperature (℃)	470
Exhaust gas mass flow rate (kg s^{-1})	4.35
Temperature of jacket water (℃)	90/79
Mass flow rate of jacket water (kg s^{-1})	25

957 **Table 4** Composition of the exhaust gas [7]

Composition	Molecular $(g(mol)^{-1})$	Fraction (%)
O_2	32.00	9.3
CO_2	44.00	9.1
H_2O	18.01	7.4
N_2	28.01	74.2

958 **Table 5** Condition of simulation for the CCP system

Parameter	Value
Ambient temperature (℃)	20
Ambient pressure (MPa)	0.101
Compressor inlet temperature (℃)	35
BC turbine inlet temperature (℃)	400
BC turbine inlet pressure (MPa)	18
BC turbine outlet pressure (MPa)	8
Inlet temperature at the high-pressure side of ORC turbine (℃)	150
Inlet pressure at the high-pressure side of ORC turbine (MPa)	1.6
Inlet temperature at the low-pressure side of ORC turbine (℃)	100
Inlet pressure at the low-pressure side of ORC turbine (MPa)	1.0

Outlet pressure of pump 1 (MPa)	0.9
Ejector primary inlet pressure (MPa)	0.4
Terminal temperature difference at gas heater outlet (℃)	100
Pinch point temperature difference in vapor generator 1 (℃)	30
Pinch point temperature difference in vapor generator 2 (℃)	30
Pinch point temperature difference in vapor generator 3 (℃)	25
Condensation temperature of condenser 1 (℃)	30
Condensation temperature of condenser 2 (℃)	30
Evaporation temperature of evaporator (℃)	5
Isentropic efficiency of BC turbine (%)	80
Isentropic efficiency of ORC turbine (%)	80
Isentropic efficiency of compressor (%)	80
Isentropic efficiency of pump 1 (%)	75
Isentropic efficiency of pump 2 (%)	75
Isentropic efficiency of pump 3 (%)	75
Inlet temperature of cooling water (℃)	20

959 **Table 6** Parameters for GA

Parameter	Operation range
BC turbine inlet temperature (℃)	330-440
BC turbine inlet pressure (MPa)	15-20
Inlet temperature at the high-pressure side of ORC turbine (℃)	130-180
Inlet pressure at the high-pressure side of ORC turbine (MPa)	1.4-2

Inlet temperature at the low-pressure side of ORC turbine (℃)	90-150
Inlet pressure at the low-pressure side of ORC turbine (MPa)	0.9-1.3
Ejector primary inlet pressure (MPa)	0.3-1

960 **Table 7** Control parameters of GA

Tuning parameters	Value
Population size	20
Mutation probability	0.01
Crossover probability	0.8
Stop generation	200

961 **Table 8** Single-objective optimization results

Parameter	Value
BC turbine inlet temperature (℃)	425.46
BC turbine inlet pressure (MPa)	20.00
Inlet temperature at the high-pressure side of ORC turbine (℃)	144.32
Inlet pressure at the high-pressure side of ORC turbine (MPa)	1.85
Inlet temperature at the low-pressure side of ORC turbine (℃)	100.03
Inlet pressure at the low-pressure side of ORC turbine (MPa)	1.26
Ejector primary inlet pressure (MPa)	0.54
Net power output (kW)	374.37
Cooling capacity (kW)	188.63
Exergy efficiency (%)	37.31
Levelized exergy cost ($ (MWh)$^{-1}$)	53.25

962 **Table B1** Constants for component costs [37]

Constant	Value	Constant	Value	Constant	Value
$B_{1,he}$	1.63	$K_{3,pump}$	0.1538	$C_{3,he}$	0.08183
$B_{2,he}$	1.66	$K_{1,turb}$	2.7051	$C_{1,pump}$	-0.3635
$B_{1,pump}$	1.89	$K_{2,turb}$	1.4398	$C_{2,pump}$	0.3957
$B_{2,pump}$	1.35	$K_{3,turb}$	-0.1776	$C_{3,pump}$	-0.0026
$K_{1,he}$	4.3247	$K_{1,comp}$	2.2897	$F_{M,he}$	1.0
$K_{2,he}$	-0.3030	$K_{2,comp}$	1.3604	$F_{BM,turb}$	3.5
$K_{3,he}$	0.1634	$K_{3,comp}$	-0.1027	$F_{BM,comp}$	2.7
$K_{1,pump}$	3.3892	$C_{1,he}$	0.03881	$F_{M,pump}$	2.2
$K_{2,pump}$	0.0536	$C_{2,he}$	-0.11272		

963
964

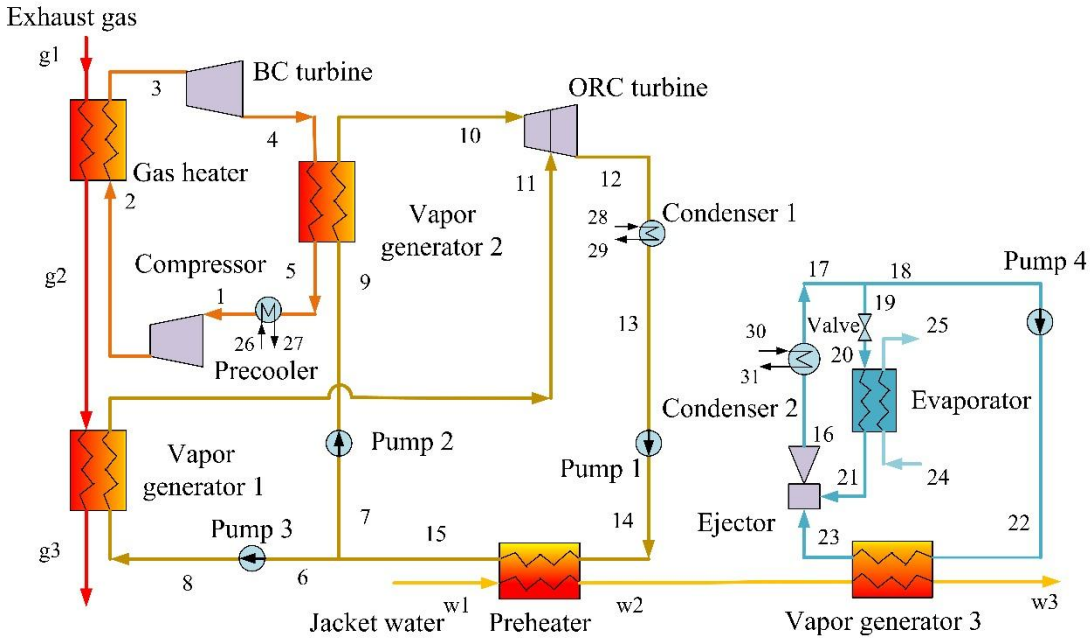

965

966 **Fig. 1.** Schematic diagram of the CCP system

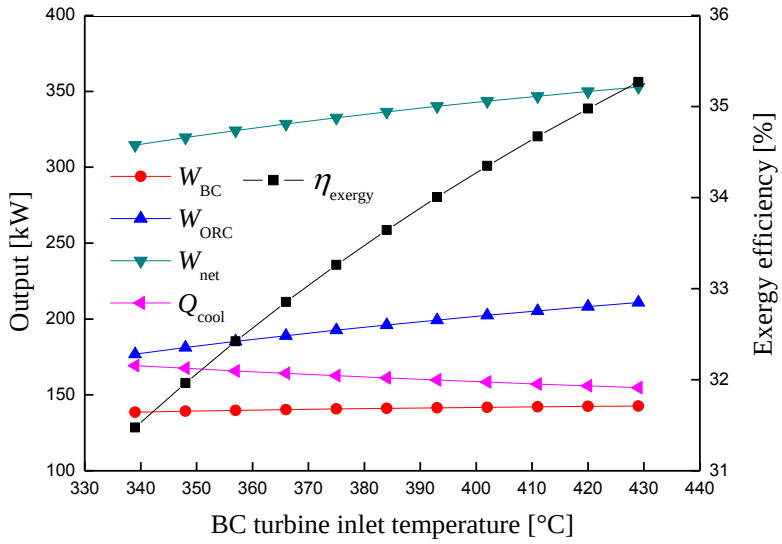

967

968 **Fig. 2.** Influences of BC turbine inlet temperature on the output and the exergy

969 efficiency of the system.

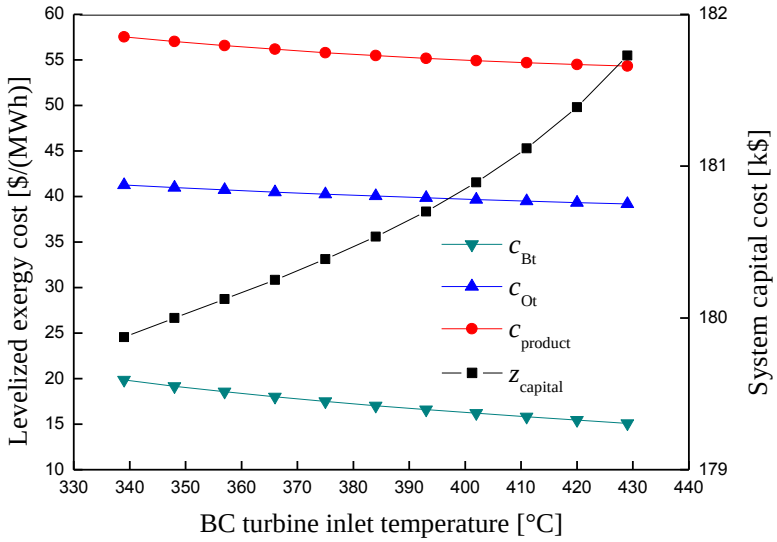

970

971 **Fig. 3.** Influences of BC turbine inlet temperature on the levelized exergy cost and the

972 system capital cost of the system.

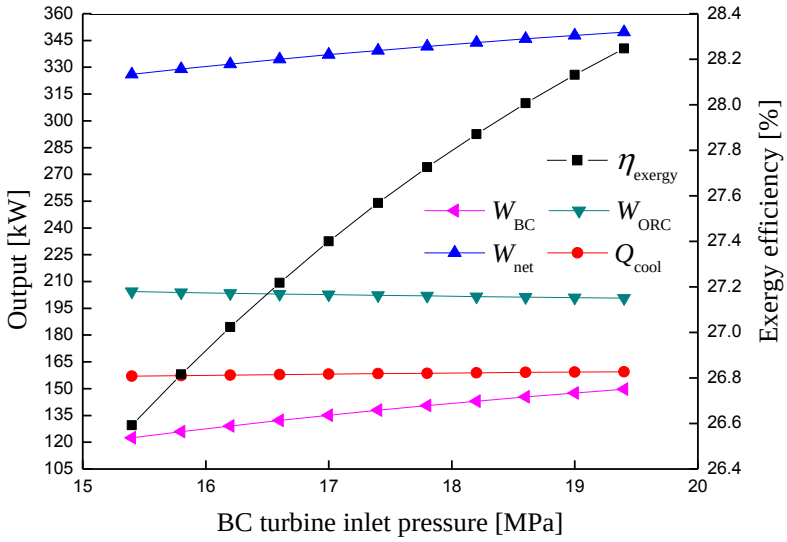

973

974 **Fig. 4.** Influences of BC turbine inlet pressure on the output and the exergy efficiency

975 of the system.

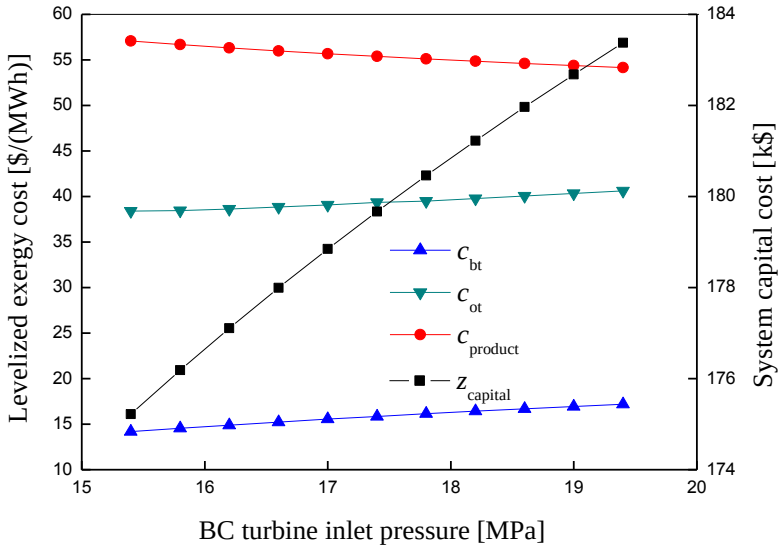

976

977 **Fig. 5.** Influences of BC turbine inlet pressure on the levelized exergy cost and the

978 system capital cost of the system.

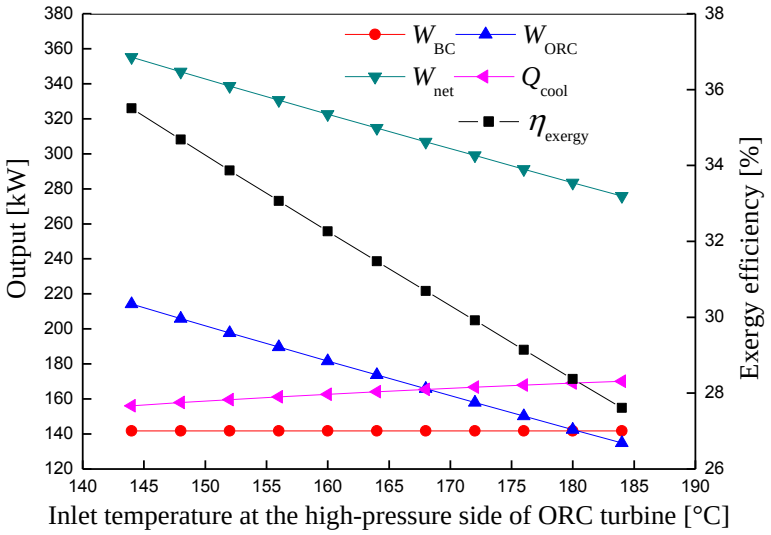

979

980 **Fig. 6.** Influences of inlet temperature at the high-pressure side of ORC turbine on the

981 output and the exergy efficiency of the system.

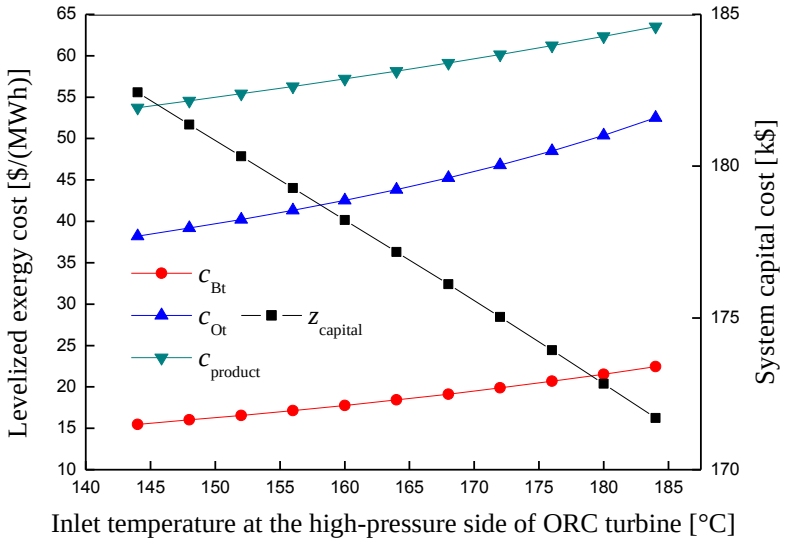

982

983 **Fig. 7.** Influences of inlet temperature at the high-pressure side of ORC turbine on the

984 levelized exergy cost and the system capital cost of the system.

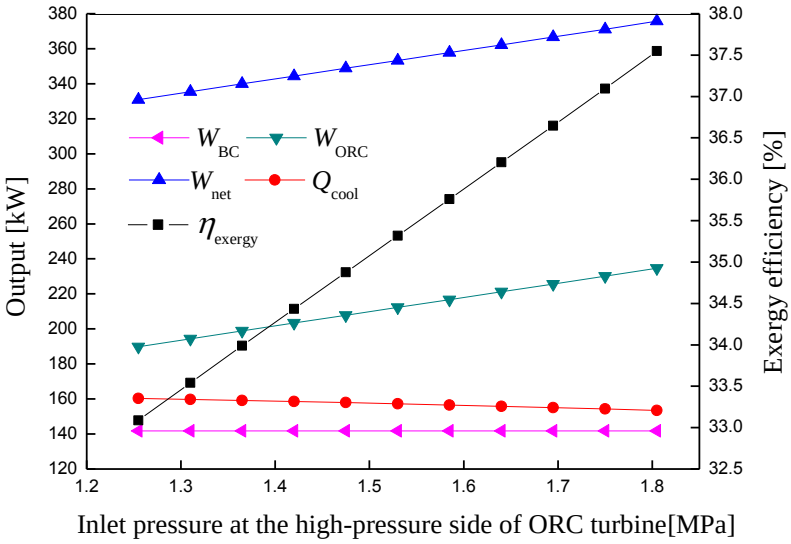

985

986 **Fig. 8.** Influences of inlet pressure at the high-pressure side of ORC turbine on the

987 output and the exergy efficiency of the system.

988

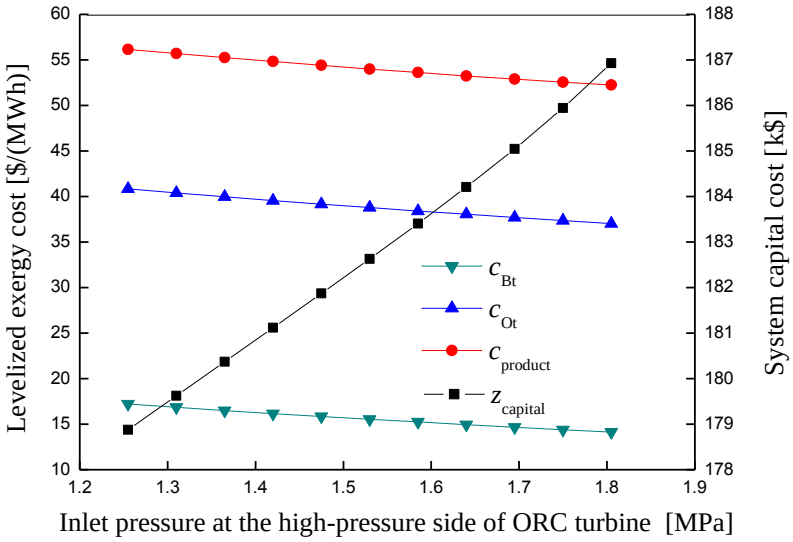

989

990 **Fig. 9.** Influences of inlet pressure at the high-pressure side of ORC turbine on the

991 levelized exergy cost and the system capital cost of the system.

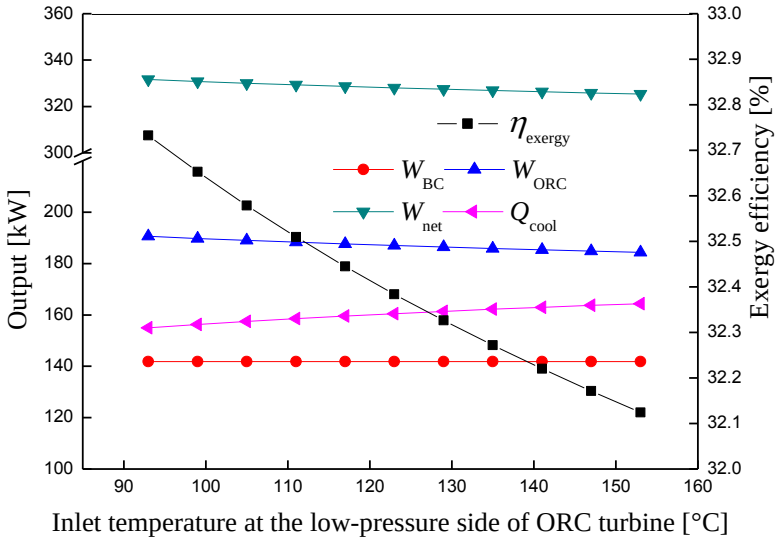

992

993 **Fig. 10.** Influences of inlet temperature at the low-pressure side of ORC turbine on the

994 output and the exergy efficiency of the system.

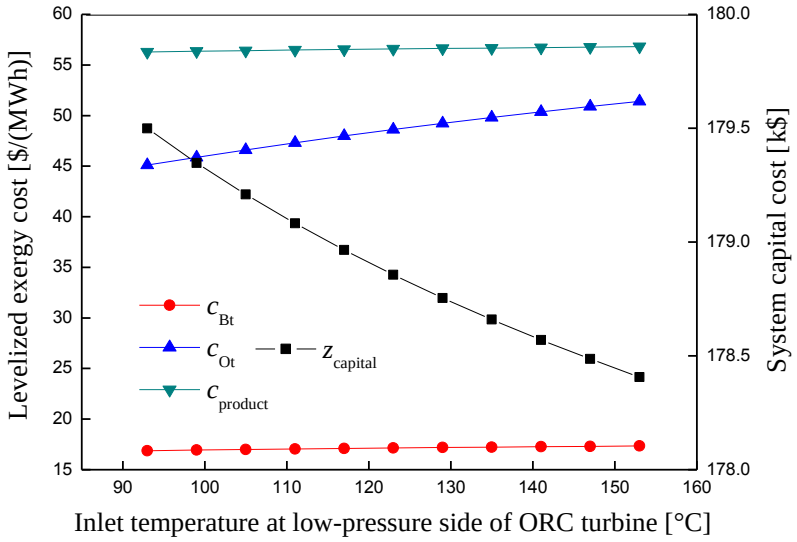

995

996 **Fig. 11.** Influences of inlet temperature at the low-pressure side of ORC turbine on

997 the levelized exergy cost and system capital cost of the system.

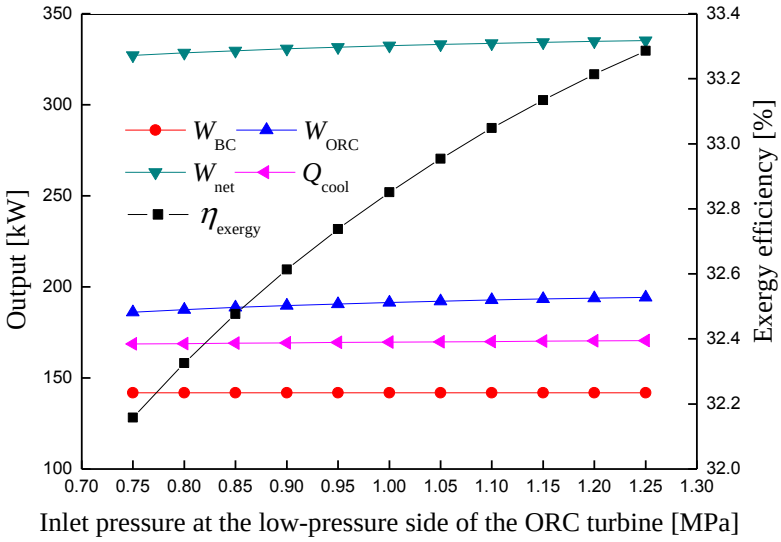

998

999 **Fig. 12.** Influences of inlet pressure at the low-pressure side of ORC turbine on the

1000 output and the exergy efficiency of the system.

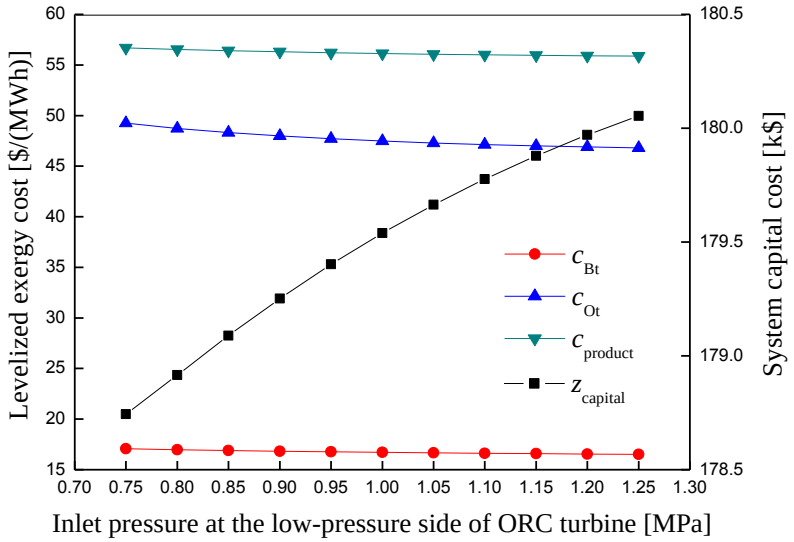

1001

1002 **Fig. 13.** Influences of the inlet pressure at the low-pressure side of ORC turbine on

1003 the levelized exergy cost and system capital cost of the system.

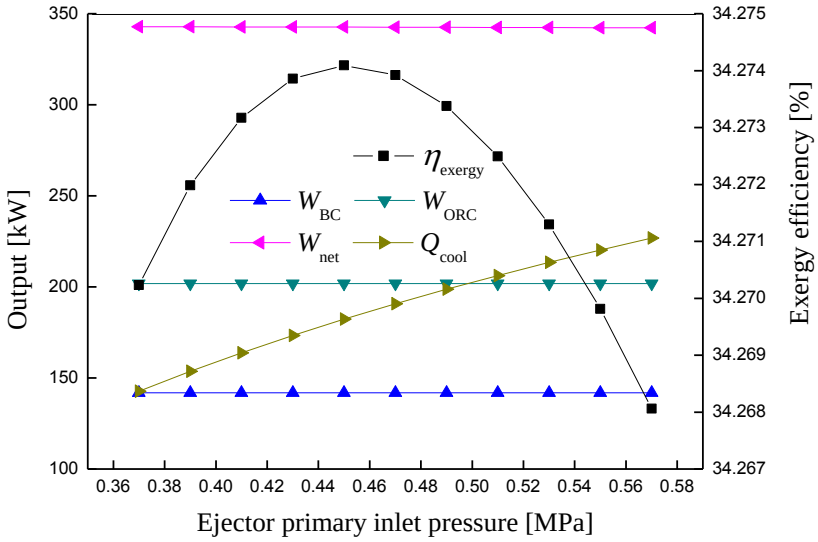

1004

1005 **Fig. 14.** Influences of ejector primary inlet pressure on the output and the exergy

1006 efficiency of the system.

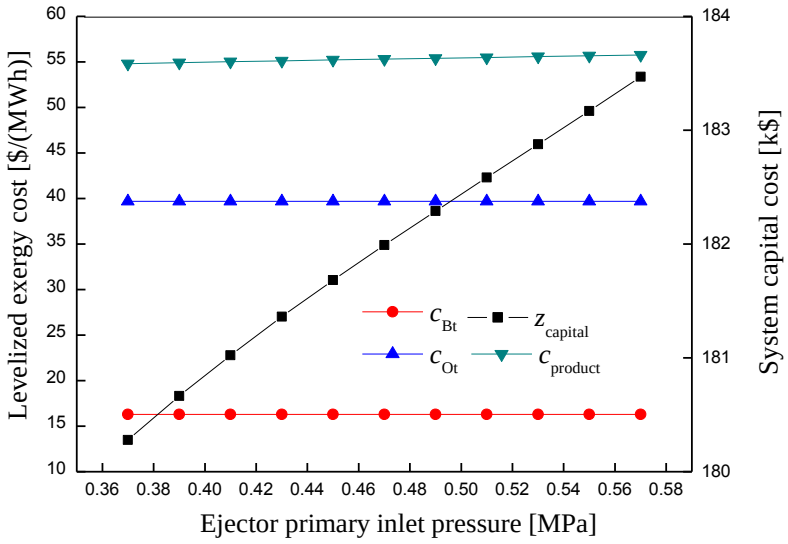

1007

1008 **Fig. 15.** Influences of ejector primary inlet pressure on the levelized exergy cost and

1009 the system capital cost of the system.

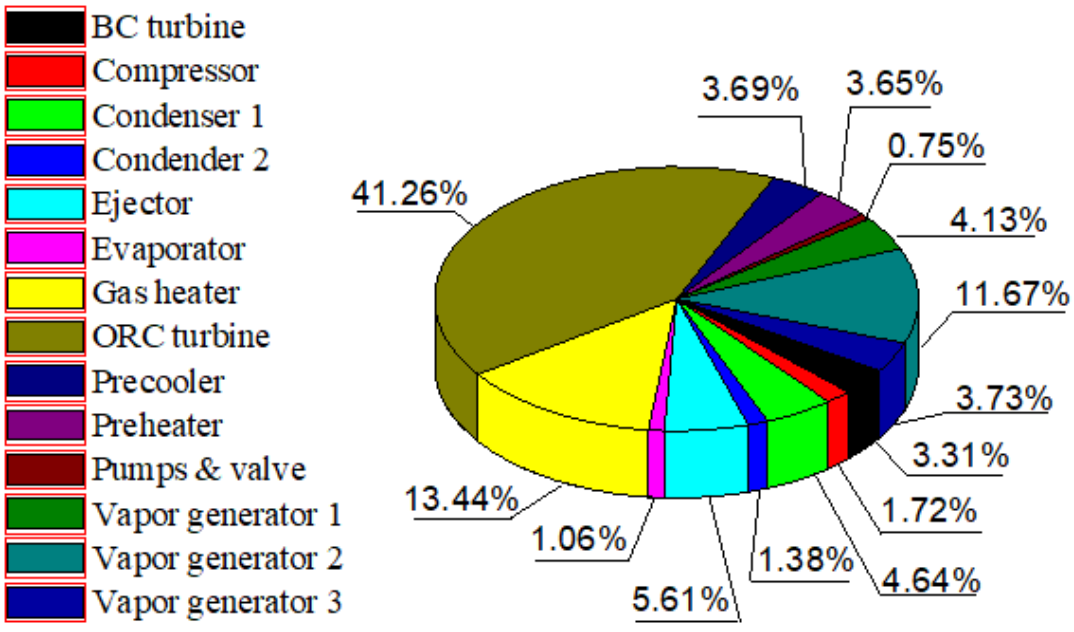

1010

1011 **Fig. 16.** Exergy destruction of different components